SCIENCE CHINA
Chemistry

•REVIEWS•

May 2024 Vol.67 No.5: 1397–1441
https://doi.org/10.1007/s11426-024-1971-4

# Supramolecular systems for bioapplications: recent research progress in China

Yue-Yang Liu[1,2†], Xiao-Yong Yu[3†], Yu-Chen Pan[3†], Hang Yin[4†], Shuang Chao[5†], Yujie Li[5†], He Ma[6†], Minzan Zuo[7†], Kun-Xu Teng[8†], Jun-Li Hou[2*], Yong Chen[3], Dong-Sheng Guo[3], Ruibing Wang[4*], Yuxin Pei[5*], Zhichao Pei[5*], Jiang-Fei Xu[6*], Xiao-Yu Hu[7*], Chunju Li[9*], Qing-Zheng Yang[8*], Leyong Wang[10], Yu Liu[3*] & Zhan-Ting Li[1,2*]

[1]*State Key Laboratory of Organometallic Chemistry, Key Laboratory of Synthetic and Self-Assembly Chemistry for Organic Functional Molecules, Shanghai Institute of Organic Chemistry, Chinese Academy of Sciences, University of Chinese Academy of Sciences, Shanghai 200032, China;*

[2]*Department of Chemistry, Fudan University, Shanghai 200438, China;*

[3]*College of Chemistry, State Key Laboratory of Elemento-Organic Chemistry, Collaborative Innovation Center of Chemical Science and Engineering, Nankai University, Tianjin 300071, China;*

[4]*State Key Laboratory of Quality Research in Chinese Medicine, Institute of Chinese Medical Sciences, University of Macau, Macau 999078, China;*

[5]*College of Chemistry & Pharmacy, Northwest A&F University, Yangling 712100, China;*

[6]*Key Lab of Organic Optoelectronics & Molecular Engineering, Department of Chemistry, Tsinghua University, Beijing 100084, China;*

[7]*College of Materials Science and Technology, Nanjing University of Aeronautics and Astronautics, Nanjing 211106, China;*

[8]*Key Laboratory of Radiopharmaceuticals, Ministry of Education, College of Chemistry, Beijing Normal University, Beijing 100875, China;*

[9]*Tianjin Key Laboratory of Structure and Performance for Functional Molecules, College of Chemistry, Tianjin Normal University, Tianjin 300387, China;*

[10]*State Key Laboratory of Analytical Chemistry for Life Science, Jiangsu Key Laboratory of Advanced Organic Materials, School of Chemistry and Chemical Engineering, Nanjing University, Nanjing 210023, China*

Received January 29, 2024; accepted February 15, 2024; published online March 22, 2024

Supramolecular systems feature dynamic, reversible and stimuli-responsive characteristics, which are not easily achieved by molecular entities. The last decade has witnessed tremendous advances in the investigations of supramolecular systems for various bioapplications, which include drug delivery, anticancer therapy, antibacterial therapy, photodynamic therapy, photothermal therapy, combination therapy, antidotes for residual drugs or toxins, and bioimaging and biosensing. Host-guest chemistry has played a key role in the development of such bioactive supramolecular systems, and natural macrocycles (such as cyclodextrins), synthetic macrocycles (such as calixarenes, cucurbit[*n*]urils, and pillararenes), and porous framework polymers (such as supramolecular organic frameworks and flexible organic frameworks) have been most successfully used as hosts to build different kinds of host-guest systems for attaining designed biofunctions. The self-assembly of rationally designed amphiphilic molecules, macromolecules and polymers represent another important approach for the construction of supramolecular architectures with advanced biofunctions. In this review, we summarize the important contributions made by Chinese researchers in this field, with emphasis on those reported in the past five years.

**host-guest chemistry, drug delivery, anticancer and antibacterial, photodynamic therapy, photothermal therapy, antidote, transmembrane channel, bioimaging and biosensing**

†These authors contributed equally to this work.
*Corresponding authors (houjl@fudan.edu.cn; rwang@um.edu.mo; peiyx@nwafu.edu.cn; peizc@nwafu.edu.cn; xujf@mail.tsinghua.edu.cn; huxy@nuaa.edu.cn; cjli@shu.edu.cn; qzyang@bnu.edu.cn; yuliu@nankai.edu.cn; ztli@mail.sioc.ac.cn)

**Citation:** Liu YY, Yu XY, Pan YC, Yin H, Chao S, Li Y, Ma H, Zuo M, Teng KX, Hou JL, Chen Y, Guo DS, Wang R, Pei Y, Pei Z, Xu JF, Hu XY, Li C, Yang QZ, Wang L, Liu Y, Li ZT. Supramolecular systems for bioapplications: recent research progress in China. *Sci China Chem*, 2024, 67: 1397–1441, https://doi.org/10.1007/s11426-024-1971-4

## CONTENTS



## 1 Introduction

Supramolecular chemistry originated from the finding of Pedersen for the selective binding of crown ethers for alkaline metals [1]. In supramolecular chemistry, host-gest chemistry has been the central topic [2–14], through which rationally designed molecular or macromolecular hosts complex guest molecules or ions with high stability and selectivity [15,16]. In the past decades, advances in host-guest chemistry have been tremendous, and some systems reach binding affinity that rivals or even surpasses that of the natural biotin-avidin system [17–20]. With highly stable host-guest systems available, supramolecular chemists have made a great effort to explore their functions or applications in various research areas, including separation and purification [21], pollutant removal [22], sensing and probing [23], bioimaging [24–26], drug delivery [27], drug sequestration or antagonism as antidotes [28–31]. Among others, studies on the bioapplications of host-guest systems have received increasing attention [32–38], since such applications well make use of the binding or entrapment of synthetic hosts for discrete drugs or bioactive species. In addition to the direct inclusion of drugs by synthetic hosts, where drugs may be regarded as "special target spots" in blood and binding constants between hosts and drugs provide high predictability for the activity of the hosts, especially in the presence of clinically used drugs for comparison [28,30,31,39], host-guest chemistry has also been applied for constructing advanced supramolecular architectures, which allows for easy preparations, high tunability and stimuli-responsiveness [27,33]. Many of these investigations have been performed with the aim of developing their biofunctions [37,40–42], for which host-guest systems play a key role in holding molecular monomers to form well-established assemblies.

Although crown ether-ion binding has been the proto-

typical host-guest system [43], natural cyclodextrins (CDs) have been studied with a much longer history for the inclusion of hydrophobic organic molecules to improve their performance in biomedical, food, and daily chemical industries [44–47]. In the past decades, supramolecular chemists have also developed a large number of macrocyclic hosts for complexing various guest ions or molecules. In this context, calix[*n*]arenes (*n* = 3–6) [48–50], (acyclic) cucurbit[*n*]urils (CB[*n*], *n* = 4–8, 10) [51–55], and pillar[*n*]arenes (*n* = 5–7) [51,56–58] have been demonstrated as the most versatile and useful macrocyclic hosts for exploring new molecular recognition chemistry and recognition-based biofunctions. To a considerable extent, the host-guest chemistry of these kinds of macrocycles has played a key role in promoting the development of supramolecular chemistry as an important subdiscipline of comprehensive chemical science. The great potential of supramolecular systems as biofunctional materials has also continuously attracted chemists to design new (acyclic) macrocycles [59–65] and self-assembled architectures. In the latter category, supra-amphiphiles [66,67] and framework-based porous polymers [31,42,68] have been demonstrated to be important kinds of supramolecular structures as biomedical materials. Since all bioactivities are investigated *in vitro* and/or *in vivo*, hydrophobicity has played a central role in the formation of host-guest systems and supramolecular architectures assembled through host-guest complexation [6]. Other noncovalent interactions, such as hydrogen bonding, ion-pair electrostatic attraction, coordination, and van der Waals force, are also important in providing directionality and enhanced stability and ordering for both kinds of systems.

The bioapplications of supramolecular systems are diverse, which include drug delivery, antibacterial, photodynamic and photothermal therapy, drug solubilization and activity enhancement, and drug sequestration and antagonism. In many cases, supramolecular systems are designed to directly gain a specific biofunction [28,30]. In most other cases, discrete functions of improving or modulating the activity of drugs are realized directly through the complexation of drugs by rationally designed hosts. The key feature of this supramolecular strategy is that the design of new biofunctional systems or architectures is generally based on their selective complexation or entrapment of drugs that enables the activity enhancement of the corresponding drugs through different manners. Moreover, the reversibility of the complexation also allows for the construction of supramolecular systems that exhibit responsiveness to disease microenvironments *in vivo* or outside photo-, electro- or magnetic stimulus [12], which is usually unavailable for conventional small molecule or macromolecular drugs.

In recent years, Chinese researchers have made great contributions to the construction of supramolecular systems that display specific biofunctions. This review summarizes the major advances, in particular those made in the past five years. We first exemplify the representative biofunctional systems generated on the basis of the host-guest interactions between CDs, calixarenes, (acyclic) CB[*n*], pillararenes or other kinds of macrocycles and cages, and various guests including drugs. We then highlight the applications of single molecule and self-assembled macrocycles or tubes as ion, water or molecular channels with specific bioactivity [69], supra-amphiphiles for drug delivery [70], and framework-styled porous polymers as drug carriers or sequestration agents. We further sum up advances in supramolecular photodynamic and photothermal therapies which can be realized through efficient host-guest inclusion or the self-assembly of rationally designed organic molecules. Finally, we present our opinions on the perspectives of biofunctional supramolecular systems and their potentials for preclinical studies and challenges that need to be addressed for promoting the advance towards this aim.

## 2 Cyclodextrin- and calixarene-based supramolecular systems

### 2.1 Co-assembled systems for near-infrared bioimaging

The supramolecular assembly mediated by macrocyclic molecules, especially the co-assembly of different kinds of macrocycles, has been a feasible strategy for constructing organic room temperature phosphorescence (RTP) and biomacromolecular recognition systems [71–74]. In the aspect of biological applications, the study of fluorescent probes for cell imaging has valuable application potential due to the great significance of tumor cell imaging for the diagnosis of cancer [75]. However, many components in human tissues, such as cytochrome, melanin, and hemoglobin, exhibit a large degree of background absorption or scattering in the visible light band, which greatly limits the application of visible light fluorescence in cell imaging. Attributed to the fact that, when used for cell optical imaging, near-infrared (NIR) dyes have less background fluorescence interference, lower absorption and scattering of biomolecules, and weaker damage to cells, the research on NIR fluorescent dyes has attracted increasing attention in recent years [76–78].

To further develop efficient NIR fluorescent dyes, a number of methods have been established to obtain intracellular NIR emission [79]. Among them, the construction of long-lived NIR-delayed fluorescent dye systems based on host-guest coordination mediated by macrocyclic molecules and cascade energy transfer has been extensively studied [80–83]. Stable host-guest complexes can provide a rigid microenvironment for guest molecules to inhibit the nonradiative transitions caused by molecular rotation [84–86]. Moreover, hydrophobic cavities can protect the phosphor-

escence from being quenched by external water or oxygen [87,88]. A variety of self-assembly strategies based on macrocycles have been used to effectively combine discrete interactions, including hydrophobicity, hydrogen bonding, and electrostatic interactions, forming tightly packed structures that fix the phosphor to limit non-radiative relaxation pathways and further prevent the influence of quenching agents on phosphorescence [89–91]. In addition, microenvironments for effective energy transfer of loaded fluorescent dyes can be created by various macrocycles, which bring the donor and acceptor molecules together to meet the requirements of energy transfer (Figure 1) [92].

Liu *et al*. [93] conducted extensive research on the enhancement of phosphor emission by multivalent self-assembly strategy for tumor cell imaging. In the case of β-CD derivatives, they prepared dodecyl-chain-bridged 6-bromoisoquinoline derivative and revealed that originally non-phosphorescent guest molecule emitted significant phosphorescence at 540 nm after forming a dumbbell-like inclusion compound with CB[7] (Figure 2a). *Via* the secondary confinement with hyaluronic acid-modified β-CD to form a binary assembly, the phosphor intensity of the polymer increased by 8 times, whereas the lifetime of polymer increased from 59 μs to 0.58 ms. Furthermore, by introducing NIR dye Nile blue (NiB) or tetrasodium 5,10,15,20-tetrakis (4-sulfophenyl)porphyrin (TPPSS) as acceptor into the assembly, a long-lived NIR luminescence system can be obtained. The presence of hyaluronic acid enabled the assembled system to effectively target cancer cells and achieve lysosomes NIR imaging. Similarly, Liu *et al*. [94] further constructed a three-photon NIR-delayed fluorescence supramolecular assembly based on 4-bromophenyl pyridinium 12C for bioimaging (Figure 2b). By forming a 2:1 supramolecular complex with CB[8], the optically silent guest molecule presented obvious green phosphorescent emission. After secondary assembly with sulfonated β-CD SCD, the intensity of phosphorescence further enhanced. More importantly, the supramolecular system also exhibited a three-photon absorption and could be excited at both 320 and 840 nm, which could be applied in the three-photon imaging of HeLa cells.

In addition to cyclodextrins, amphiphilic calixarenes are also able to exhibit excellent performance in self-assembly. Hydrophilic and hydrophobic groups can be conveniently introduced on their upper and lower ports to impart amphiphilicity [97]. In the related co-assembled architectures, the amphiphilic calixarenes can effectively fix the phosphor and constrain its non-radiative transition by tightly-packed structures. For example, Liu *et al*. [95] showed that, in a supramolecular multivalent phosphorescence-capturing aggregate formed by CB[7], sulfonated calix[4]arene SC4AD, and dibromophthalimide derivative G (Figure 2c), the addition of SC4AD and CB[7] to the solution of guest G resulted in the formation of spherical nanoparticles with a 40-fold increase in the intensity of its phosphorescence emission and an extended lifetime of 1.13 ms. Subsequently, due to the matched overlap between the emission bands of the assembly and the absorption bands of Rhodamine B (RhB) and benzothiadiazole (DBT) dyes, the dye molecules were successfully loaded into the hydrophobic layer of the assembly and used as receptors for the first step of energy transfer. At the same time, NIR organic dyes NiB and Cy5 were selected as the second energy acceptors to successfully achieve the cascade energy transfer, leading to a long-range effect from 425 to 800 nm and the long-lived photoluminescence for multicolor cell imaging. Similarly, using CB[7] and amphiphilic calixarene SC4AD as cascades, NIR phosphorescence harvesting system could also be constructed from racemic 1,2-diaminocyclohexan-derived 6-bromoisoquinoline (BQ) (Figure 2d) [96]. Initially, BQ interacted with CB[8] through 1:1 foldamer-like dislocation stacking to generate weak phosphorescence emission at 555 nm. Afterwards, SC4AD further reassembled with BQ⊂CB[8] complex to form homogeneously spherical nanoparticles with a phosphorescence lifetime of 0.364 ms and a 30-fold increase in emission intensity. The enhancement of phosphorescence property was attributed to the assembly of two macrocycles and the guest, which effectively protected the fluorescent molecules from being quenched by external quenching agents. The phosphorescence harvesting system was further conducted by the introduction of organic dyes Cy5 and NiB as the primary energy transfer acceptor and heptamethine cyanine IR780 as the secondary acceptor. After the two-step cascade energy transfer, a long-lived NIR photoluminescence was finally obtained at 825 nm.

Liu *et al*. [98,99] further demonstrated that introducing optical switches to self-assembled systems can better regulate their luminescent performance. From dicationic

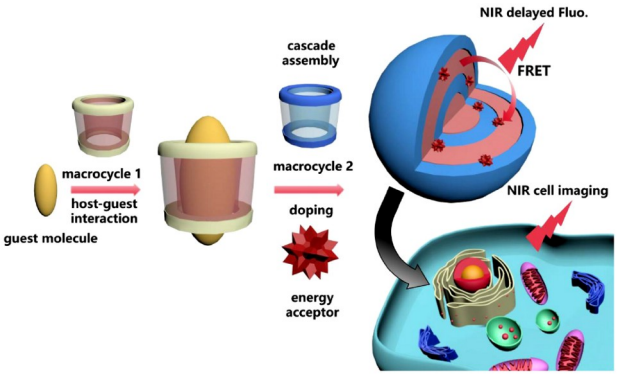


**Figure 1** Schematic diagram of the supramolecular NIR long-lived delayed fluorescence system constructed by cascade assembly and synergistic energy transfer used in cell optical imaging [92] (color online).

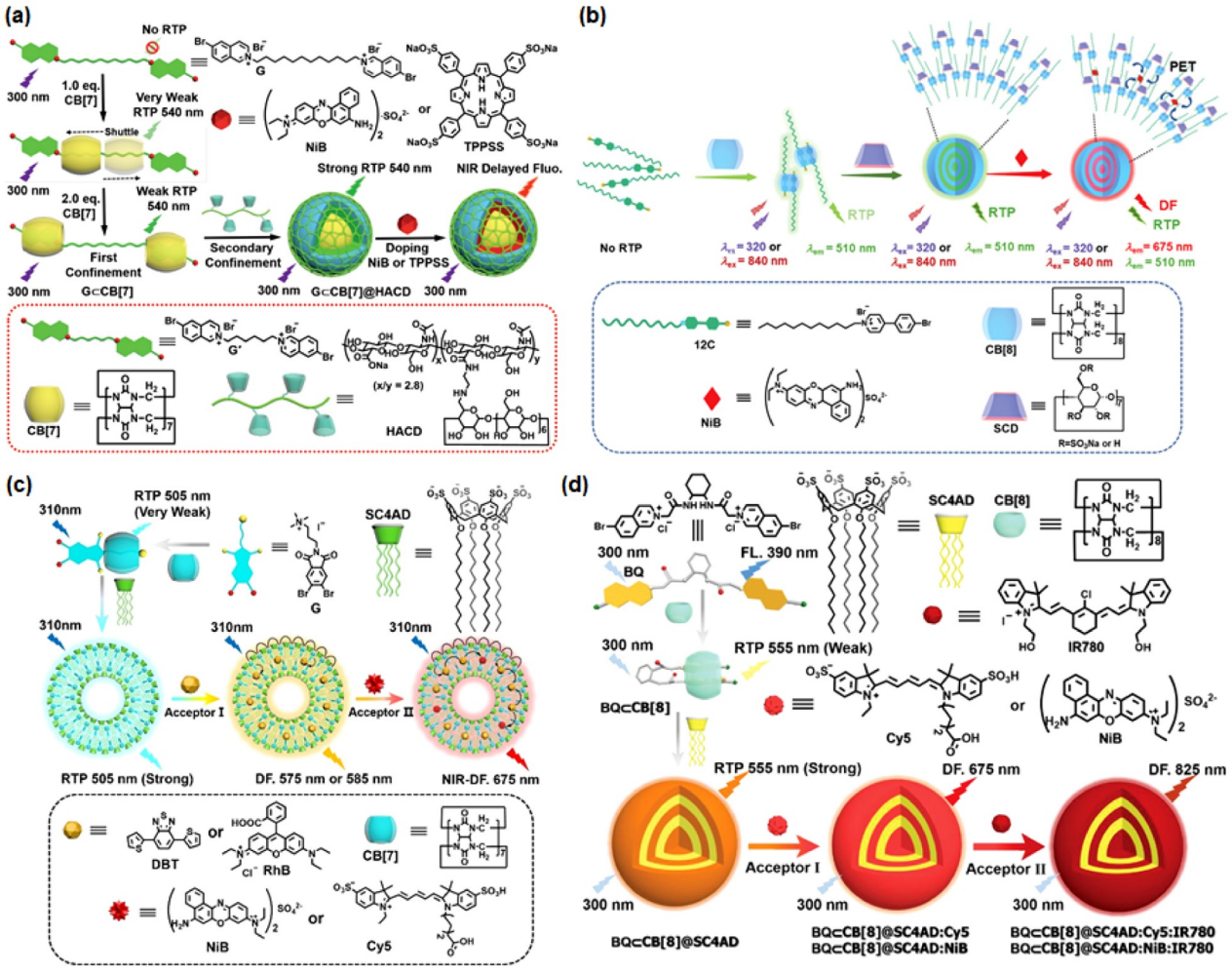


**Figure 2** (a) Construction of polysaccharide supramolecular RTP-harvesting system with NIR emission by β-CD and CB[7] [93]. (b) NIR-delayed fluorescence *via* phosphorescent energy transfer of three-photon absorption supramolecular assembly [94]. (c) Supramolecular aggregate for cascade RTP-capturing system with delayed NIR emission [95]. (d) Two-step sequential phosphorescence harvesting system with long-lived NIR emission [96] (color online).

6-bromoisoquinolinium derivative G, CB[8], SC4AD, fluorescence dyes Cy5 and NiB, and diarylethylene OF-1 (Figure 3a) [100], an efficient light-harvesting supramolecular switching system could be readily constructed. For this aim, dicationic guest G assembled with CB[8], to form a supramolecular foldamer, which bound to SC4AD to afford supramolecular nanoparticles accompanied by the blue-shift of the phosphorescence emission and significant enhancement of the phosphorescence intensity. By utilizing their hydrophobic microenvironment, the NIR dyes were successfully loaded as receptors, and subsequently OF-1 was added as molecular switch. Under the irradiation of 365 nm light, the photoluminescence of the assembly at 678 nm gradually weakened, but could be partially recovered under the irradiation of >450 nm light. Accordingly, a supramolecular phosphorescence harvesting system that was switched through different irradiation light was constructed and used for anti-counterfeiting and cell imaging.

Using photo-controlled supramolecular switching, Liu *et al.* [101] further developed a supramolecular switch from 6-bromoisoquinoline derivatives, CB[7], SC4A4, and photochromic spiropyran derivative SP (Figure 3b). The supramolecular switch enabled the reversible optical conversion between RTP and delayed fluorescence, thereby achieving an adjustable long-lived multicolor emission. After inclusion with CB[7], the non-phosphorescent guest $G_2$ generated RTP at 540 nm. Then supramolecular nanoparticles were formed after the secondary assembly with SC4A4, and the phosphorescence intensity was significantly enhanced, adding SP caused the topological shape of the nanoparticle to change to doughnut shape. Under the ultraviolet (UV) irradiation of 365 nm, the original closed-loop spiropyran converted into open-loop form, and the original phosphorescence at 540 nm changed to the NIR long-lived fluorescence at 635 nm after energy transfer. Under prolonged exposure to UV light, the aqueous solution gradually changed from bright green to

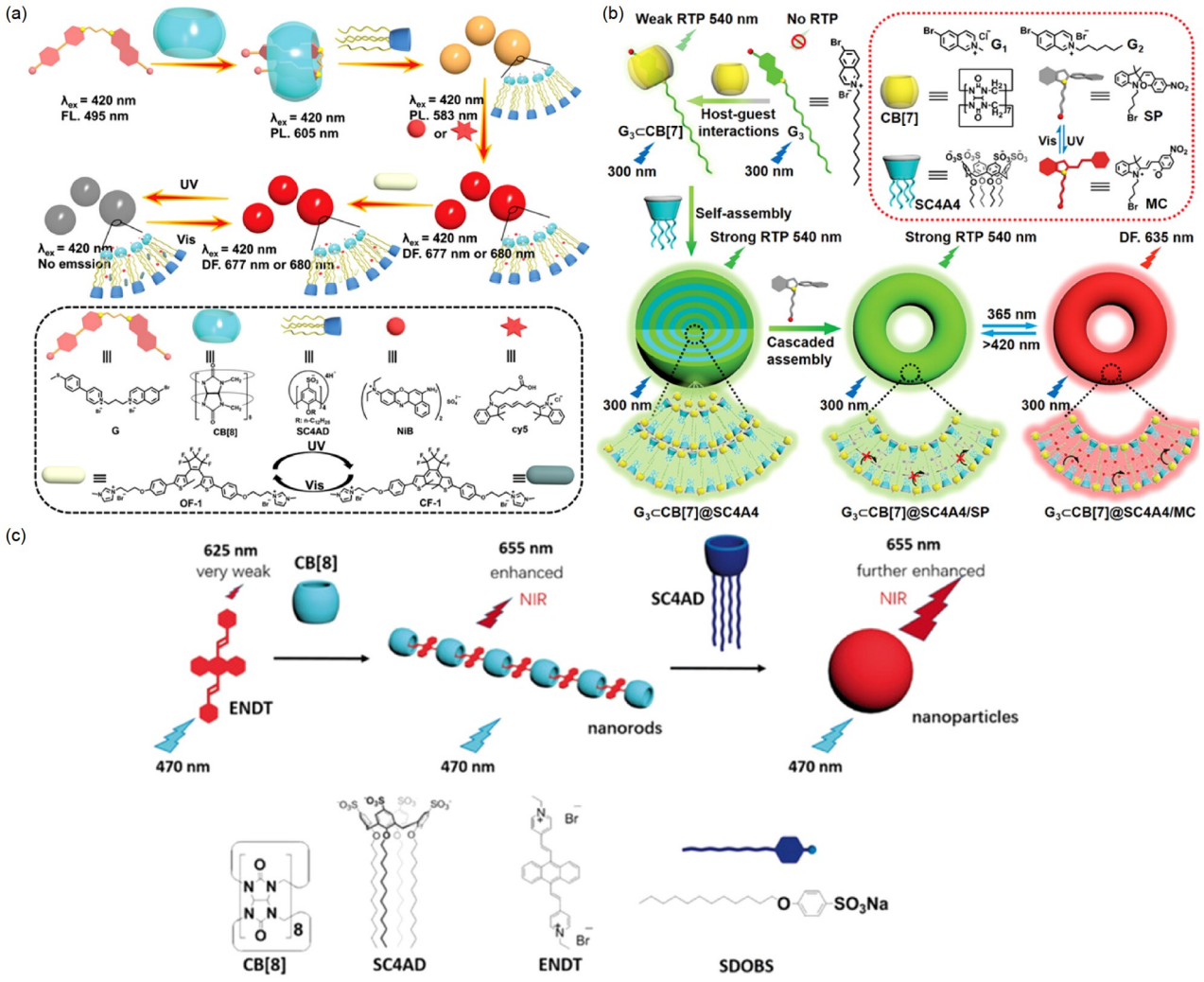


**Figure 3** (a) Generation of supramolecular switchable phosphorescent light-harvesting vesicle (FL: fluorescent luminescence, PL: phosphorescent luminescence, DF: delayed fluorescence) [100]. (b) Reversible phosphorescence/fluorescence photo-switch based on cascade supramolecular assembly [101]. (c) NIR fluorescent supramolecular assemblies constructed by cascade process [102] (color online).

yellow and finally to red, achieving an adjustable multicolor emission. Meanwhile, the assembly gradually returned to the original bright green under the visible light irradiation. A549 cells treated with the assembly could emit a bright green signal under visible light irradiation, but emitted a red signal under UV light, therefore achieving light-controlled multicolor cell labeling.

Liu *et al*. [102] also showed that, in addition to obtaining NIR fluorescence by incorporating NIR dyes into cascade assemblies for energy transfer, NIR system that red-shifted the fluorescence emission of organic dyes to NIR could also be obtained (Figure 3c). After firstly assembled with CB[8] to form nanorods, the fluorescence emission of 4,4′-anthracene-9,10-diylbis(ethene-2,1-diyl)bis(1-ethylpyridin-1-ium) bromide (ENDT) red-shifted from 625 nm to the NIR region of 655 nm, and the fluorescence intensity became obviously enhanced. Subsequently, a secondary cascade assembly was carried out with lower-rim dodecyl-modified sulfonatocalix [4] to form nanoparticles, further enhancing the NIR emission. Subsequent cell imaging experiments demonstrated that the supramolecular cascade assembly can be successfully applied to NIR lysosomal targeting imaging.

## 2.2 Co-assembled systems for diagnosis and therapy

The recognition of biomacromolecules is of great significance for the regulation and intervention of life processes. Hetero-multivalency, which involves simultaneous interactions of more than one ligand and receptor, represents a powerful strategy for this aim. For instance, Guo *et al*. [103–105] proposed a supramolecular approach to hetero-multivalent recognition *via* the co-assembly of amphiphilic β-CDs and calix[5]arenes into one ensemble (Figure 4). Developed as surfactants containing host-guest recognition sites, amphiphilic macrocycles can spontaneously assemble into aggregates and provide surfaces with multiple binding

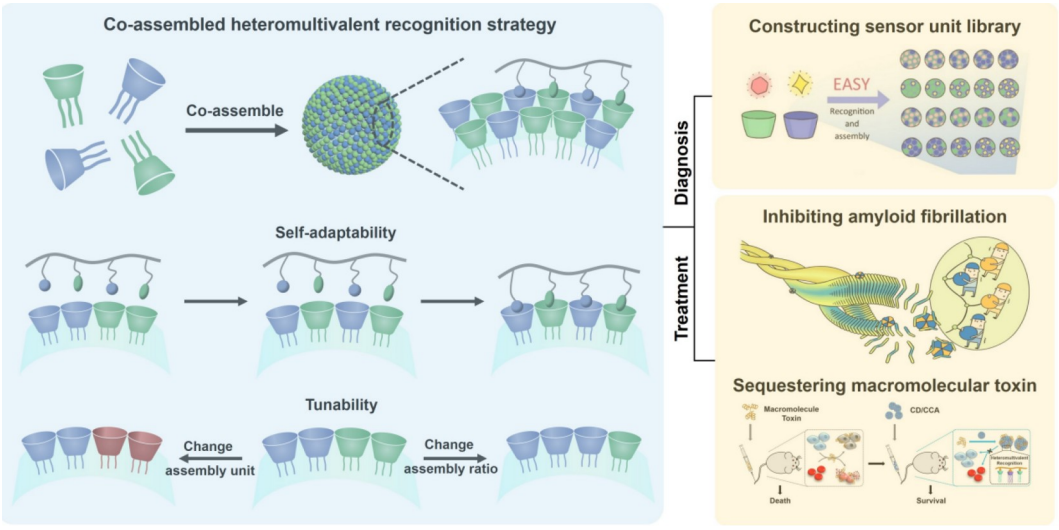


**Figure 4** The construction and characteristics of co-assembled heteromultivalent recognition strategy and its biomedical applications (color online).

sites (homo-multivalency). Co-assembling two different macrocyclic amphiphiles yielded surfaces with multiple and diverse binding sites, enabling the desired hetero-multivalency. The authors have employed a series of model peptides and verified that the CD/calixarene co-assembly indeed achieved the hetero-multivalent recognition. More importantly, the dynamic reversibility of self-assembly endows the platform with self-adaptability, which means that the co-assembly can optimize itself to better match the complex ligand sequences of biomacromolecules. The platform also displays tunability, which means the co-assembled components and ratios can be easily tuned on demand. Moreover, complex syntheses and site mismatching in covalent synthesis can also be avoided.

Co-assemblies have also been engaged in diagnosis and treatment of diseases *via* recognition of biomacromolecules (Figure 4). In terms of diagnosis, Guo *et al*. [106] took advantage of tunability and superior recognition ability toward biomacromolecules of co-assemblies to construct a sensor unit library for differential sensing, without incurring a high synthetic workload. Increasing the number of sensor units was revealed to provide more information of analytes, leading to a higher differentiating index. Upon replacing the co-assembly macrocycles and indicators, adjusting the macrocycle/macrocycle co-assembly and receptor/indicator complexation ratios, and changing the environment, Guo *et al*. [107] constructed 32 sensor units for 10 supramolecular sensor arrays to successfully distinguish normal cell lines, different cancer cell lines, and cross-contaminated cells. In terms of therapy, Guo *et al*. [108] designed the co-assembly of amphiphilic β-CD and guanidinium-modified calix[5]arene GCA for the recognition of β-amyloid Aβ-peptide, whose fibrillation is critical in Alzheimer's disease (AD) pathogenesis. β-CD is a receptor of tyrosine and phenylalanine, and GCA binds strongly to aspartic acid and glutamic acid. The Aβ is rich in these four amino acid residues; therefore, the co-assembly CD/GCA showed extremely strong binding to Aβ ($3.3 \times 10^{13}$ $M^{-1}$). Benefiting from the strong binding, CD/GCA achieved almost complete inhibition of Aβ fibrillation and quick disintegration of preformed fibrils. CD/GCA was further applied as a novel anti-Aβ therapeutic agent of AD, and significantly improved the cognitive deficit of 5xFAD mice. Additionally, Guo *et al*. [109] also applied co-assemblies to detoxify macromolecular toxins.

### 2.3 Co-assembled systems for drug ratiometric delivery

Combination therapies represent the frontier of modern treatment for addressing the heterogeneity and complexities of diseases. In combination therapies, the ratio of the combined drugs is crucial, as different ratios may lead to different treating indexes (synergism or antagonism). However, precise control and regulation of the loading and delivery ratio of drugs with repeatability remains a formidable challenge for drug delivery systems. Guo *et al*. [110] established a ratiometric delivery model based on amphiphilic macrocycles (Figure 5). Host-guest recognition was used to provide a quantitative loading strategy, which benefits from the well-defined macrocycle structures, exact cavity-loading patterns, and quantifiable association constants [111,112]. Amphiphilic macrocycles can spontaneously assemble into supramolecular nanocarriers, providing surfaces containing multiple recognition sites and thereby enabling the precise loading of diverse drugs. Accordingly, the ratio of drugs loaded can be predicted and regulated. Moreover, the supramolecular drug loading is thermodynamically controlled,

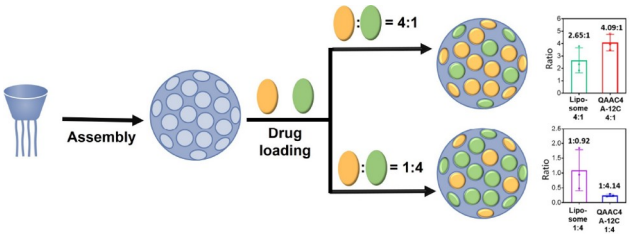


**Figure 5** Illustration of a host-guest ratiometric drug delivery system based on amphiphilic macrocycles [110] (color online).

which ensures an excellent batch-to-batch consistency. To design a practically operational host-guest ratiometric drug delivery system, the macrocycles were designed to display high binding affinities for drugs to ensure that the loaded drugs could be delivered to the lesion site as expected ratio. For example, Guo *et al*. [113,114] synthesized amphiphilic azocalixarene QAAC4A-12C, which has a deep cavity and binds tightly with guests. Two drugs in different molar ratios (1:4 and 4:1) were mixed with QAAC4A-12C nanocarriers. The calculated loading ratios were 1:4.09 and 3.91:1, and the drug ratios detected in the tumor were 1:4.14 and 4.09:1, indicating the prediction and maintenance of the drug ratios of QAAC4A-12C nanoparticles. Conversely, liposome-based nanocarriers, which mainly rely on physical embedding of drugs, exhibited unpredictable molar ratios. Thus, host-guest drug delivery systems provide a new platform for effective combination therapy involving multiple drugs.

## 3 Cucurbituril-based systems

### 3.1 Cucurbit[5]uril derivatives

Cucurbit[*n*]urils (CB[*n*]s, *n* = 5–8, 10, 13–15) have undergone rapid development since 2000 [115–119]. Renowned for their exceptional binding properties and favorable biocompatibility, CB[*n*]s have gained recognition for their potential applications in biomedicine [39]. Notably, recent advance in CB[*n*] functionalization has yielded numerous derivatives with diverse functions, enriching the CB[*n*] family and expanding their applications in biomedicine [120], which encompass imaging, sensing, detection, drug delivery and therapy, and cellular regulation. Among the CB[*n*] family, CB[5] stands out for its compact cavity size (2.4 Å), which limits its ability to accommodate typical organic molecules and form complexes. The modest cavity size of CB[5] poses challenges for hosting common organic molecules. Consequently, its portals become crucial sites for supramolecular self-assembly. Even so, Xiao *et al*. [121] have utilized hexamethyl CB[5] (HmeCB[5]) and 1,4-diaminobenzene to craft a novel low-molecular-weight supramolecular hydrogel. Upon incorporating phosphor 6-bromo-2-naphthol (BrNp), this hydrogel exhibits fluorescence-phosphorescence dual emission, which allows for cytoplasmic staining of HeLa cells through the red channel.

### 3.2 Cucurbit[6]uril and its derivatives

#### *3.2.1 Bioimaging and detection*

With a cavity size (3.9 Å), CB[6] exhibits increased potential for biomedical applications by accommodating linear organic molecules, such as spermine, to form supramolecular complexes. Although the intrinsic limitation of low water solubility hinders broad utilization of unmodified CB[6], the evolution of functionalized CB[6]s has significantly broadened the scope of its biomedical applications. Given the small cavity and poor water solubility of CB[6], its direct utilization for imaging, sensing, or detection functions poses challenges. Thus, recent studies have predominantly utilized CB[6] as a building block in nanostructure formation for enhanced applications. For instance, Guo *et al*. [122,123] reported that CB[6] could co-assemble with various molecules to create supramolecular architectures for detecting dyes and antibiotics. Additionally, CB[6] has been coated onto gold nanoparticles or electrodes for electrochemical detection. Liang *et al*. [124] utilized this system to detect metformin, achieving a low detection limit of 1.35 pmol/L. Xiao *et al*. used CB[6] to synthesize carbon dots. Through the addition of various co-components [125,126], these carbon dots can acquire multifunctionality, including optical bioimaging of human prostate cancer (PC-3) cells and the sensing of L-tryptophan and capecitabine. Moreover, Ni *et al*. [127] also explored the application of CB[6]-derived supramolecular organic framework for drug delivery.

#### *3.2.2 Drug delivery and therapy*

Due to its limited cavity size and poor water solubility, CB[6] was not initially favored for drug delivery and therapy. However, functionalized CB[6] allows further polymerization to create nanocapsules as a platform for bioimaging [128]. These nanocapsules have abundant surface slots and spacious interior, exhibiting significant potential in drug delivery and therapy. For example, Wang *et al*. [129] employed a ditopic linker to facilitate the synthesis of CB[6]-based nanocapsules. Loading photodynamic agent (PDA) Chlorin e6 (Ce6) into the nanocapsules and decorating their surface with folic acid-spermine (FA-SP) resulted in effective *in vitro* photodynamic therapy (PDT) activity. By replacing linkers with azobenzene units, the resulting nanocapsules acquired the ability to release cargos for therapy both *in vitro* and *in vivo*, either through light-induced distortion or hypoxia-induced breakdown of the nanocapsules (Figure 6a) [130,131]. This modification strategy is general. For instance, Chen *et al*. [132] reported that functionalizing

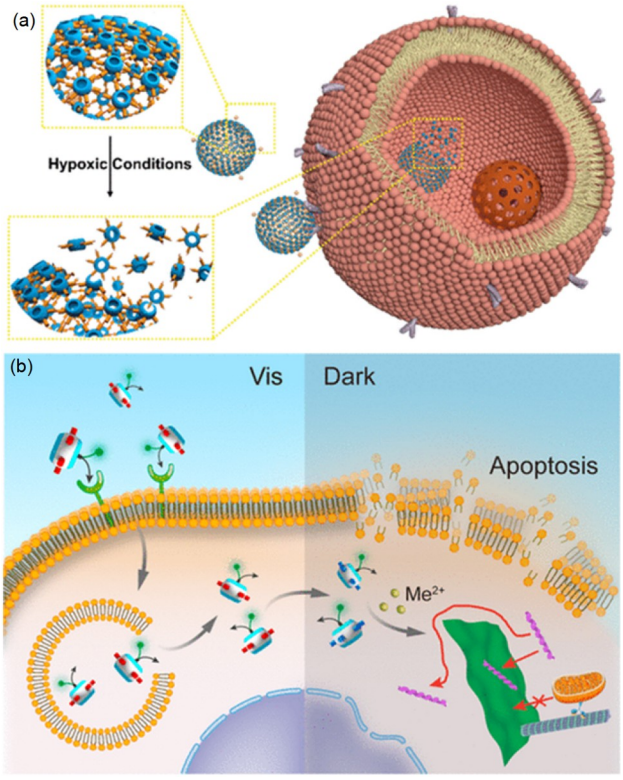


**Figure 6** (a) Schematic illustration of drug release mechanism of azobenzene-based CB[6] nanocapsules [130]. (b) Schematic illustration of CB[6]-based aggregated 2D materials for cancer therapy [132] (color online).

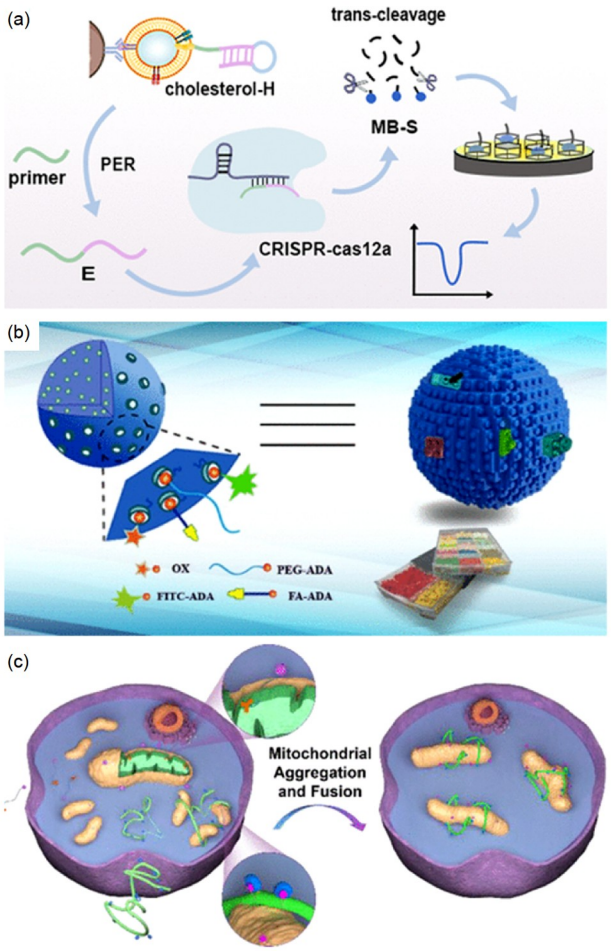


**Figure 7** (a) CB[7] on electrode for the analysis of lung cancer exosomes [133]. (b) Surface functionalization of nanoparticles based on CB[7] for drug delivery and therapy [142]. (c) Mechanism of CB[7]-based supramolecularly driven mitochondria aggregation and fusion [143] (color online).

CB[6] with multiple photochromic spiropyrane moieties could achieve photo-responsive disaggregation under visible light and aggregation in the dark in the presence of divalent metal cations (Figure 6b). In the dark, the resulting two-dimensional (2D) materials impeded cytosolic transport in HeLa cells, leading to apoptotic cell death.

### 3.3 Cucurbit[7]uril and its derivatives

#### *3.3.1 Bioimaging, sensing and detection*

Renowned for its ample cavity size (5.4 Å), CB[7] can effectively encapsulate a broad spectrum of aliphatic and aromatic molecules [117]. Furthermore, its commendable water-solubility positions it as one of the most versatile macrocycles for various biomedical applications, which has been promoted through its functionalization [120]. Modification of electrode surfaces with CB[7] has proven effective in enhancing detection sensitivity through host-guest interactions. For instance, Zhao *et al*. [133] employed CB[7] to modify electrode to facilitate the analysis of lung cancer exosomes (Figure 7a), achieving a low detection limit of 708 particles/mL. Additionally, Liang *et al*. [134] assembled CB[7] on the surface of Au nanoparticles for the electrochemical detection of amino acids. For exploiting the selective binding for insulin, Wei *et al*. [135] developed an electrochemiluminescence sensing platform by immobilizing CB[7]s on the surface of the sensing platform, which could achieve a low detection limit of 5.44 fg/mL for insulin. Encapsulation of dye molecules with subsequent release through competitive binding is a common strategy for sensing/detection, leveraging changes in the fluorescence emission of dye molecules upon CB[7] inclusion [136,137]. Zheng *et al*. [138] innovatively employed CB[7] and dye molecules as tandem assays to monitor the activity of L-DOPA decarboxylase, demonstrating the potential for L-DOPA decarboxylase deficiency diagnosis. Song *et al*. [139] selected a hydroxyphenyl benzotriazole derivative (HBT-11) to bind to CB[7]. The resulting complex, with a p$K_a$ close to neutral pH, could distinguish normal cells from cancer cells *via* different fluorescence emissions. Wang *et al*. [140] applied aggregation-induced emission (AIE) fluorophore-modified CB[7] and luminol to achieve bioluminescence

resonance energy transfer, enabling deep-tissue penetration and imaging. In another effort, Liu *et al*. [141] conducted the co-assembly of a triazine pyridinium derivative and CB[7] to enhance fluorescence emission. Additional assembly with sulfonatocalix[4]arene, hyaluronic acid, and commercial dyes further enhanced fluorescence emission, achieving two-photon NIR targeted cell imaging.

#### *3.3.2 Drug delivery and therapy*

The cavity of CB[7] is large enough to encapsulate a number of bioactive molecules [39]. Supramolecular complexation has thus been explored to modulate the photo-responsive therapeutic activity by leveraging its influence on the properties of guest molecules. In this way, Xu and Zhang *et al*. [144] have revealed the antibacterial effect of 5,10,15,20-tetrakis-(4-*N*-methylpyridyl)-porphyrin TMPyP *via* adaptable photodynamic/photothermal therapeutic processes, which enhanced biocompatibility, but preserved antibacterial activity upon CB[7] encapsulation. CB[7] can be modified with many different moieties, including AIE fluorophore [145], hyaluronic acid [146], active peptide [147], and polyethylene glycol (PEG) chains [148], for achieving various biofunctions [142,145–158]. For example, by utilizing DNA's inherent complementary binding property, Liu *et al*. [149] employed DNA-modified CB[7] to construct supramolecular DNA nanogels. Further loading with doxorubicin (DOX) and methylene blue (MB) could attain dual chemo and photodynamic therapy. Wang *et al*. [148] constructed CB[7]-based nanosystems for drug delivery and therapy. One example was involved in the generation of micelles from functionalized CB[7] (Figure 7b) [142], with CB[7] macrocycles being exposed on the surface for synergistic chemotherapy, whereas micelles formed from PEG-modified CB[7] were revealed to load Ce6 and aliphatic *N*-oxide banoxantrone (AQ4N) for enhanced therapeutic efficacy. When AIE fluorophore-functionalized CB[7] is assembled into nanoparticles, the macrocycle can encapsulate oxaliplatin (OxPt) and AQ4N to exhibit synergistic antitumor effects [145]. Wang *et al*. showed that CB[7] modified with hyaluronic acid could achieve controlled release of curcumin for psoriasis treatment [146], while CB[7] modified with Von Willebrand factor-binding peptide was found to target injured vessels for hemorrhage control [147]. Xu and Zhang *et al*. [159] also reported that conjugating camptothecin (CPT) to CB[7] could achieve self-inclusion, and CPT could be released *via* glutathione (GSH)-induced bond cleavage to realize enhanced biocompatibility and antitumor bioactivity of CPT. Wang *et al*. have further applied the modification strategy for the preparation of various nanoparticles [150–154] and liposomes [155], and to modulate the structures of membranes of macrophage, platelet, and bacteria [156–158], through which discrete biofunctions have been obtained. Zhang *et al*. [160] also explored CB[7]-based polymers for drug delivery and coated pH-sensitive materials to achieve responsive drug release under acidic conditions. When two CB[7] macrocycles are linked with a spacer containing a disulfide bond, supramolecular polymers can be constructed, which load and deliver OxPt and further realize controlled release in a reductive environment [161].

#### *3.3.3 Cellular regulation*

Supramolecular assembly serves as the foundation for biosystems and also offers the potential for cellular regulation. Based on the highly stable complexation of adamantane by CB[7], Wang *et al*. [143] combined triphenylphosphonium (TPP)-PEG-adamantane conjugate, with specific mitochondrial targeting, and CB[7]-modified hyaluronic acid to promote the aggregation and fusion of mitochondria, which may hold promise for treating diseases related to mitochondrial fission and fragmentation (Figure 7c). Liu *et al*. [162] also employed similar approach to generate multi-functionalized polymers modified with CB[7], or amantadine to anchor on cell membranes and subcellular organelles, enabling heterogeneous cell fusion and manipulation of subcellular organelle behaviors. Leveraging its excellent ability of include amino acids, CB[7] also finds use in protein modification [39]. Using this strategy, Liu *et al*. [163] reported the modification of the functional surface of proteins through encapsulation of unnatural amino acids by CB[7]. By utilizing competitive guests to bind with CB[7], controlled modulation of protein activity could be realized. This regulation strategy can also be extended to DNA. For instance, Xu *et al*. [164] introduced CB[7] as an invading ligand to DNA, with guest molecules as recognition handles into nucleobases, allowing the regulation of DNA hybridization *via* the ligand-invasion pathway. In this way, orthogonal and reversible manipulation of DNA duplex dissociation and recovery has been achieved.

### 3.4 Cucurbit[8]uril and its derivatives

#### *3.4.1 Bioimaging, sensing, and detection*

CB[8] has a cavity size of 6.9 Å that allows for accommodating two guest molecules to form ternary complexes. Despite its low water-solubility, this complexing feature positions CB[8] as a crucial element for biomedical applications because it functions well as a binder for constructing supramolecular polymers and supramolecular organic frameworks [68,165,166]. Moreover, CB[8] can also act as a direct indicator when encapsulating organic dyes for building bioimaging and biosensing systems. In this category, Liu *et al*. [167] have used CB[8] to include anthracene-

conjugated bromophenylpyridinium ANPY to produce supramolecular polymers for nucleus-targeted imaging with red phosphorescence emission (Figure 8a). Following photooxidation of the anthryl group to anthraquinone to afford AQPY, the supramolecular polymer degraded into a ternary inclusion complex, enabling lysosome-targeted imaging with green phosphorescence emission [168]. Huang *et al*. [169] also incorporated CB[8] and dye molecules into a fluorescence sensor array to detect various quaternary ammonium pesticides through competitive replacement or ternary 2:1 complex formation (Figure 8b). Zhao *et al*. [170] conducted the co-assembly of CB[8] and dixanthene derivatives to enhance optoacoustic signal strength under light irradiation. Further co-assembly with chondroitin sulfate A led to multispectral optoacoustic imaging for detecting solid tumors and ischemia/reperfusion-induced acute kidney injury *in vivo*.

Liu *et al*. [94] further developed methods to enhance bioimaging performance by integrating CB[8] with other macrocycles and polymers. One such system involved the use of CB[8], 4-bromophenyl pyridinium, sulfonated β-CD, and NiB, which enabled three-photon RTP for cancer cell imaging. This strategy can be extended to the generation of nanoparticles by incorporating CB[8], dicationic 6-bromoisoquinolinium, sulfonatocalix[4]arene, NIR fluorescence dyes, and a diarylethene molecular switch. The resulting advanced system could achieve lysosome-targeted imaging in cancer cells as well as information encryption [100], while the combination of a triphenylamine fluorophore derivative and dodecyl-modified sulfonatocalix[4]arene was found to display bright NIR light emission, which could also be applied for lysosome imaging of tumor cells as well as real-time imaging of mice [172].

### 3.4.2 *Drug delivery and therapy*

The ternary complexation of CB[8] can also be used to design supramolecular drug delivering systems. For example, Liu *et al*. [173] modified hyaluronic acid by introducing 4-bromophenylpyridium BPP units and prepared a mitochondrion-targeting peptide to enable specific mitochondrial anchoring. CB[8] was used to include BPP through 1:2 ternary complexation, which induced mitochondrial aggregation and enhanced the antitumor efficiency of cisplatin. Liu *et al*. [174] further utilized the lysosome protonation property of pyridyl-functionalized tetraphenylethylene TPE-Py to promote its binding to CB[8] in A549 lung cancer cells. Octahedron-like structures were thus produced, which could disrupt lysosome membranes and selectively suppress cancer cells. CB[8] has limited solubility in water. Li and Ma *et al*. [61] showed that introducing multiple sulfate anions

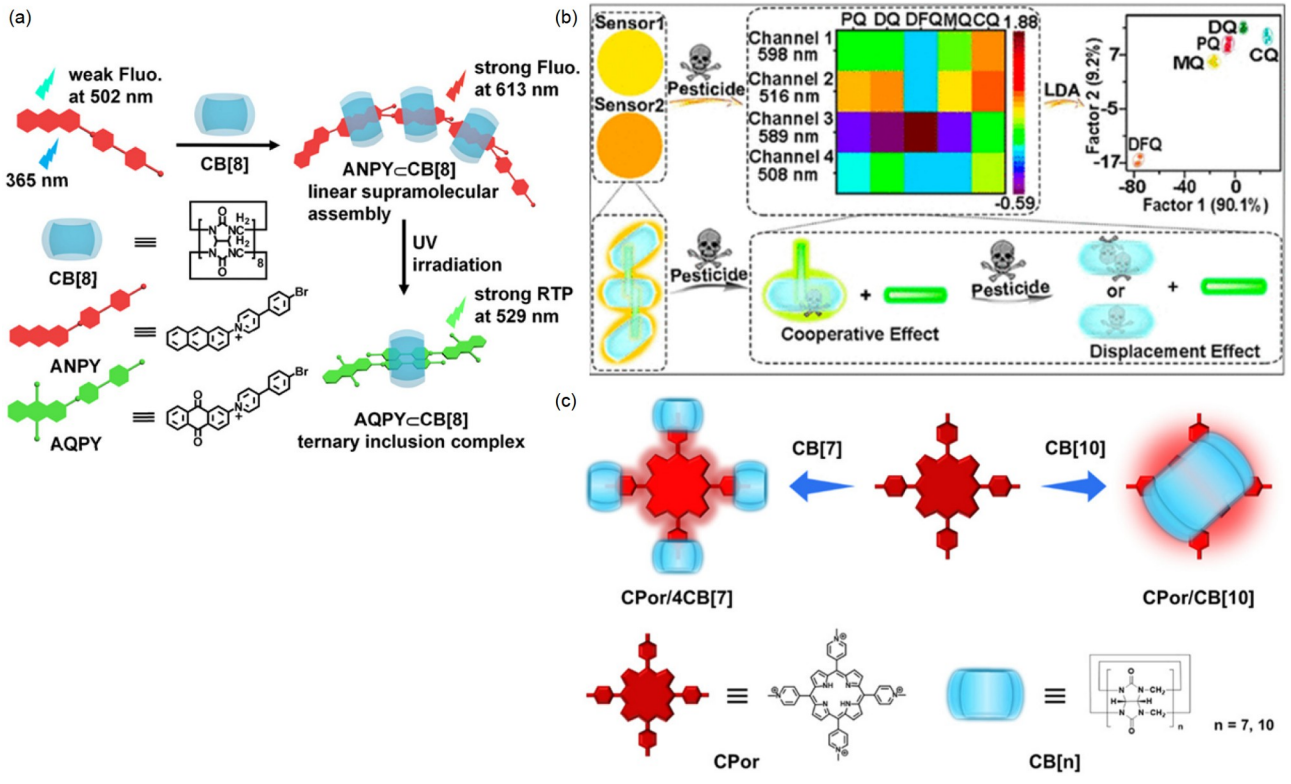


**Figure 8** (a) Phototunable conversion from red fluorescence to green phosphorescence emission in ANPY-CB[8] and AQPY-CB[8] assemblies [167]. (b) Supramolecular fluorescence sensor array for pesticides detection [169]. (c) Fabrication of supramolecular porphyrins [171] (color online).

remarkably increased its solubility and the resulting CB[8] derivatives displayed high efficacy in neutralizing the activity of neuromuscular blockers.

### 3.5 Cucurbit[10]uril, cucurbit[14]uril, and cucurbit[15]uril

#### *3.5.1 Bioimaging, sensing, and detection*

The advancement in synthetic methodology and separation technology has enabled the successful isolation of larger CB[*n*]s (*n* = 10, 13–15) [115,116,118,175]. Similar to the small analogues, CB[10] also possesses an untwisted cavity. The cavity size ranges from 9.0 to 11 Å, depending on complexation-caused deformation. The cavity is large enough to accommodate three guest molecules [176,177], while CB[14] and CB[15] have a twisted conformation, which produces two separated cavities that can host a guest molecule, respectively. Capitalizing on these distinctive binding features, Xiao *et al*. [178] utilized CB[10] and CB[15] to complex two pyridinium (PY)-anthracene-PY-conjugate guests and two PY units which the conjugate bears. In this way, a three-component supramolecular polymer with light-harvesting function and antenna effect was produced. This supramolecular polymer could function as donor to transfer energy to additional RhB acceptor, which was further applied for HeLa cells for live-cell imaging in the red channel. Xiao *et al*. [175] also showed that CB[8] could efficiently encapsulate two 4-[2-(naphthalenyl)ethenyl]pyridinium (NEP) units which were attached to a pillar[5]arene ring, forming a fluorescent supramolecular polymer. Notably, paraquat dication could insert into the stacking NEP dimer to form a sandwich trimer in the cavity of CB[10], which caused the quenching of the fluorescence of the dimer and thus was used for the detection of paraquat. Using the similar approach, Xiao *et al*. [179,180] also utilized CB[14] to construct AIE-active supramolecular polymers as bioimaging agents for detecting $Fe^{3+}$ in live HeLa cells and $Fe(CN)_6^{3-}$ in live kidney cells. Zhang *et al*. also took advantage of the large cavity of CB[10] to directly accommodate sizable cationic porphyrin (CPor) (Figure 8c) [171], which itself aggregated significantly to quench its fluorescence emission in the state of single molecule. Upon encapsulation by CB[10], to form 1:1 complex, CPor underwent de-aggregation and thus exhibited enhanced fluorescence intensity for cell imaging. CB[7] could also inhibit its aggregation, but through forming 1:4 complex.

#### *3.5.2 Supramolecular therapy*

Han *et al*. [181] utilized CB[10]-based supramolecular radicals as powerful arms to kill facultative anaerobic bacteria. For this aim, two water-soluble supramolecular complexes were formed between CB[10] and a perylene diimide derivative PSA or a tetracationic cyclophane TPE-cyc. By matching the respective redox potentials, both supramolecular complexes could be specifically reduced into corresponding supramolecular radical cations or anions by facultative anaerobic *E. coli*. The strong NIR absorption of the encapsulated radical anions and cations then acted as efficient photosensitizers (PSs) to display excellent antimicrobial activity (close to 100%) *via* photothermal therapy. Moreover, CB[10] encapsulation also increased the biocompatibility of the cyclophane.

## 4 Pillararene-based systems

### 4.1 Stimuli-responsive systems from non-functionalized pillararenes

#### *4.1.1 Supramolecular systems fabricated from amphiphilic pillararenes*

Pillararenes are a class of macrocyclic hosts that bear rigid aromatic diether units connected by methylene linkers [182,183]. The backbones can be conveniently functionalized, and the cavities are hydrophobic to include hydrophobic guests in aqueous media. Thus, in the past decade, pillararene-based host-guest chemistry has garnered considerable attention and found wide applications for the fabrication of biofunctional materials [56,184–189]. In this category, three kinds of non-functionalized supramolecular systems have been widely investigated from amphiphilic pillararenes, pillararene-based host-guest complexes and hybridized macrocycles. Typical amphiphilic pillararenes can be prepared by introducing cationic, anionic and neutral groups. Pei *et al*. [190] prepared cationic amphiphilic pillararene FCAP that bears hydrophilic ferrocenium groups, which readily self-assembled into cationic vesicles in water. Due to the redox-responsiveness of ferrocenium ions, the vesicles could conduct GSH-triggered drug/siRNA co-delivery that overcame drug resistance in cancer cells and improve the bioavailability of drugs (Figure 9a). Gao *et al*. [191] prepared a biocompatible PEG-modified amphiphilic pillar[5]arene through amide linkage, which can assemble into micelles in water. The micelles could efficiently encapsulate hydrophobic DOX with a loading capability of up to 50%. Upon encountering amide-cleaving enzymes, the amide bond was cleaved, leading to rapid dissociation of the nanoaggregates and release of DOX to target L-asparaginase-overexpressing tumor cells (Figure 9b).

#### *4.1.2 Supramolecular systems fabricated from pillararene-based host-guest complexes*

Pillararenes have hydrophobic cavity that is able to include hydrophobic guests in water, which can lead to new biofunctions [192–194]. Wang *et al*. [192] employed such kind of host-guest complexes to fabricate amphiphilic building blocks from multianionic water-soluble

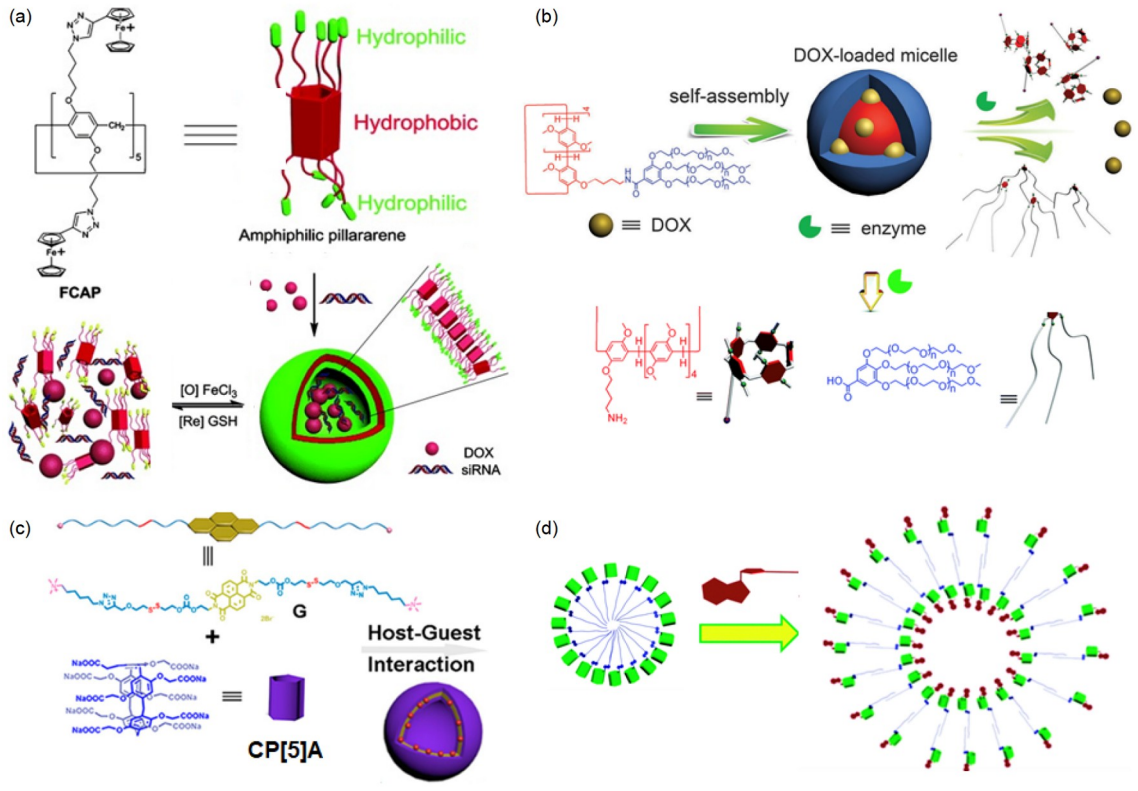


**Figure 9** Pillararene-based stimuli-responsive supramolecular systems. (a) Ferrocenium-modified amphiphilic pillararenes for drug delivery [190]. (b) Enzyme-responsive amphiphilic self-assemblies [191]. (c) Dual-responsive self-assemblies based on host-guest interaction [192]. (d) Guest-induced morphological transformation of supramolecular self-assemblies [193] (color online).

pillar[5]areneCP[5]A and disulfide bond-bearing dicationic naphthalimide G (Figure 9c), which avoid the time-consuming chemical syntheses, but exhibits distinctive properties. Especially, the incorporation of guest molecules enabled the introduction of pH and GSH dual-stimuli-responsiveness. This supra-amphiphile self-assembled into vesicles that could effectively encapsulate DOX and release the drug in acidic and GSH-overexpressed tumor microenvironment. As a result, the toxicity of DOX for normal cells was minimized, while its therapeutic efficacy against targeted tumor cells was maintained. Wang *et al*. [195] also prepared phosphate-based pillar[5,6]arenes to complex pyridinium guest for constructing controllable drug delivery platforms by self-assembling into vesicles or micelles, which could encapsulate both hydrophilic anticancer drug mitoxantrone and hydrophobic DOX. The encapsulated drugs could be efficiently released in response to stimulus of $Zn^{2+}$ or a low-pH environment. Diao *et al*. [193] prepared an amphiphilic pillar[6]arene that spontaneously self-assembled into micelles in aqueous solution (Figure 9d). The pillar[6]arene macrocycle formed stable 1:1 complex with adenosine triphosphate (ATP) through electrostatic interactions, resulting in a $>10^2$ times decrease in the critical aggregation concentration. As a result, micelles were transformed into vesicles, which were responsive to alkaline phosphatase through the hydrolysis of ATP to change back into micelles. This transformation could be used to tune controlled encapsulation and release of calcein.

### *4.1.3 Supramolecular systems fabricated from pillararene and other macrocycles*

The construction of pillararene-based hybridized self-assembled systems enables the synergistic integration of advantageous features derived from pillararenes and other macrocycles, such as the differences in cavity size and guest recognition capability. For example, to reduce the crystallinity of poly(ε-caprolactone), Li *et al*. [196] used the biodegradable hydrophobic segment of an amphiphilic pillar[5]arene to bind to β-cyclodextrin to form supramolecular pseudoblock polymer, which self-assembled into vesicles that could load DOX of up to 45.6% due to the decreased crystallinity of poly(ε-caprolactone). The supramolecular vesicles were pH-responsive and efficiently accumulated in tumor cells to enhance the antitumor efficacy of DOX. Wang *et al*. [197] further developed orthogonal host-guest recognitions and co-assembly using pillararene/β-cyclodextrin dimacrocyclic hosts to allow for simultaneous loading of two antitumor drugs. The resulting nanoparticles demonstrated synergistic effects against tumor cells within GSH-overexpressed tumor microenvironment.

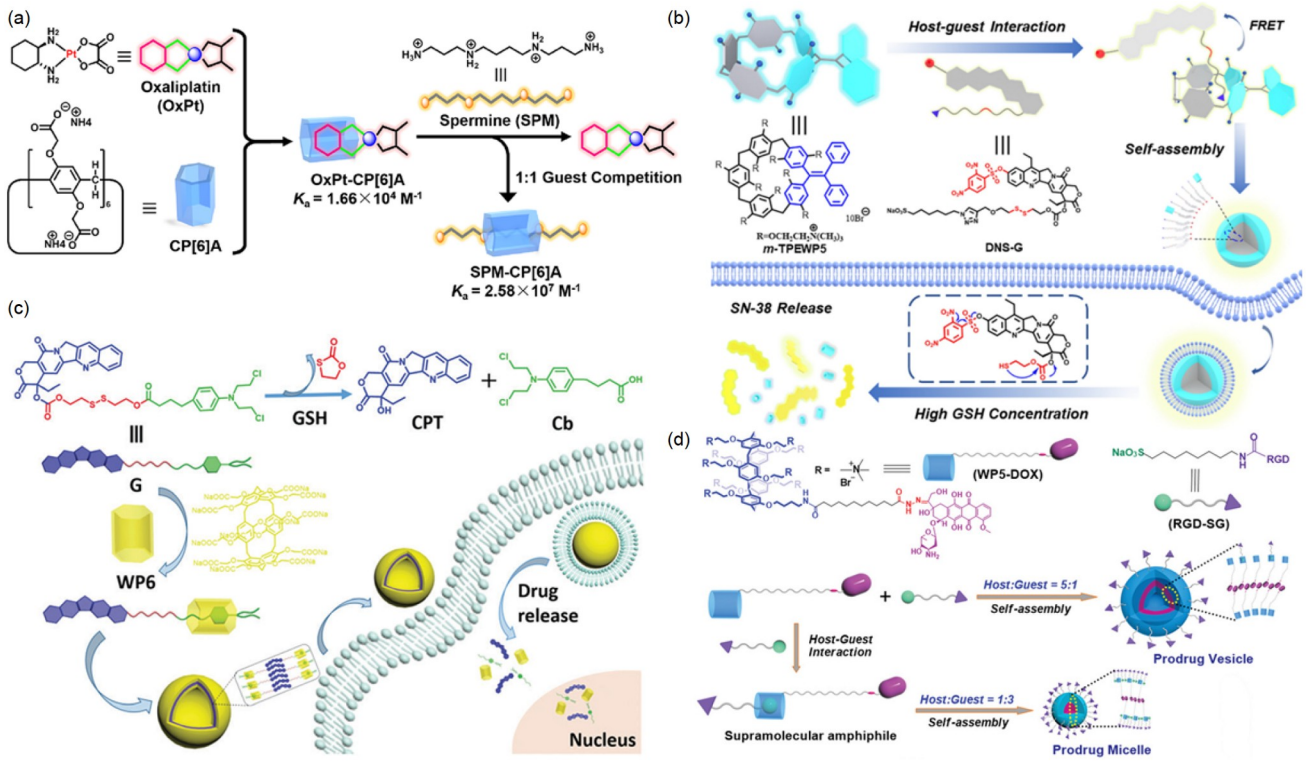


**Figure 10** Pillararene-derived supramolecular prodrugs. (a) CA[6]P-OxPt with decreased cytotoxicity and improved efficacy against colorectal cancer [199]. (b) *Meso*-TPE-functionalized pillar[5]arene-CPT prodrug with AIE [202]. (c) CPT-Cb-conjugated pillar[6]arene supramolecular prodrugs for combination chemotherapy [203]. (d) WP5-DOX supramolecular prodrug for delivery and tumor targeting by binding to RGD-SG [204] (color online).

## 4.2 Systems from functionalized pillararenes

### *4.2.1 Prodrugs*

Pillararenes have controllable cavity size and can be readily modified, thus offer useful backbones to co-assemble with various drugs to form supramolecular prodrugs as stable host-guest complexes for optimizing drug performance, improving bioavailability, reducing toxicity, and facilitating targeted delivery. The first kind of supramolecular prodrugs involve the direct encapsulation of clinically used drugs by pillararenes. For instance, Li *et al*. [198] constructed supramolecular prodrugs through the host-guest interaction between pH-responsive pillar[6]arene derivative CP[6]A and OxPt. By leveraging the differential complexation abilities of pillararenes for OxPt at different pH, controlled OxPt release could be achieved. The complexation of CP[6]A for OxPt enhanced its stability in the bloodstream and also allowed selective delivery to the tumor site. Zhang *et al*. [199] leveraged the high affinity of CP[6]A for spermine to modulate supramolecular prodrug formed by CP[6]A and OxPt. In this case, overexpressed spermine in colorectal cancer was demonstrated to facilitate the release of OxPt (Figure 10a). Yang *et al*. [200] also used this strategy to design CP[6]A derivatives for encapsulating OxPt and other drugs of different sizes. Li *et al*. [201] reported that pyridinium-functionalized pillar[6]arenes could load anionic antitumor drug pemetrexed to reduce its damage to normal cells. Upon cellular uptake of this supramolecular prodrug, pemetrexed could be selectively released from the cavity of pillar[6]arenes due to their enhanced complexation with overexpressed ATP in cancer cells.

Another strategy for the development of pillararene-derived supramolecular prodrugs is modifying drugs to allow for the utility of the host-guest complexation of pillararenes. This strategy is general for drugs that are not included by pillararenes. Supramolecular prodrugs formed in this way may be made to be amphiphilic for improving the water-solubility, biocompatibility and stability of the drugs, allowing co-loading with other drugs for combination chemotherapy, as well as realizing targeting and stimuli-responsiveness for targeted delivery and controlled release. For instance, DOX has been modified as guest molecules through hydrazone linkage and assembled with CP[6]A to form supramolecular prodrugs [205–207]. In low pH microenvironment of cancer cells, these systems can release DOX through acid-catalyzed hydrazone hydrolysis. Yao *et al*. [208] also reported a pH and reactive oxygen species (ROS) dual-responsive supramolecular polypeptide prodrug to minimize drug leakage in blood circulation and trigger drug release at tumor tissue. Negative pillar[5]arene derivatives were found to improve the stability of the supramolecular system in physiological conditions, and reversed to

positively charged in the tumor microenvironment, promoting its uptake by cancer cells. Upon irradiation with 660 nm light, Ce6 encapsulated in the system rapidly generated ROS, leading to the cleavage of thioketal linker and subsequent release of activated DOX, thereby facilitating tumor-specific drug delivery and improving its antitumor efficacy.

The above strategy has also been applied for designing the supramolecular prodrugs of CPT. For this aim, Wang *et al*. [209] constructed a GSH-responsive system through host-guest complexation between a β-*D*-galactose-functionalized water-soluble pillar[5]arene (GalP5) and a disulfide bond-containing CPT derivative. The resulting supramolecular prodrug was stable under physiological conditions, while CPT release could be triggered by GSH of high concentration in a simulated tumor environment, which effectively enhanced the biocompatibility and targeting effect of CPT. This strategy can also be used for 7-ethyl-10-hydroxy-CPT (SN-38), one of the most effective molecules among CPT derivatives, as a guest molecule to form a supramolecular prodrug system with a carboxylate pillar[5]arene [210]. Hu *et al*. [202] further expanded this design by preparing *meso*-TPE-functionalized water-soluble pillar[5]arene *m*-TPEWP5. The TPE unit displayed additional AIE effect, allowing for long-term real-time tracking and monitoring of SN-38 delivery and release (Figure 10b). Additionally, *m*-TPEWP5 could also be utilized for fabricating photoswitchable AIE-active supramolecular photosensitizer (PS) with precise control over ROS generation for antibacterial treatments [211]. The combination of multiple drugs may synergistically enhance the overall effect of chemotherapy through different anti-cancer mechanisms. For this aim, CP[6]A was used to include drugs like chlorambucil (Cb) to form host-guest complex; other drugs, such as CPT, were covalently modified with the included chlorambucil to form "drug-drug" guest molecules to realize their co-delivery (Figure 10c) [203]. Tian *et al*. [212,213] showed that similar host-guest systems could self-assemble into nano-scaled supramolecular prodrugs to enhance the effect of cancer treatment by multiple pathways, which have been applied for the construction of vesicle or micelle-type prodrugs [214–216].

The third strategy for the design of pillararene-based supramolecular prodrugs is to covalently conjugate drugs to pillararene backbones. The cavity of pillararenes can thus be used to encapsulate guest molecules with delivering and targeting functions. Through this strategy, Hu *et al*. [204] reported a stimuli-responsive tumor-targeting pillar[5]arene WP5-DOX supramolecular prodrug with WP5 including Arg-Gly-Asp-modified sulfonate (RGD-SG) guest to realize targeting function (Figure 10d). The system not only possessed high drug-loading capacity, but also exhibited good targeting ability as well as responsive drug release in acidic environment. Huang *et al*. [217] also reported a WP5-based [2]rotaxane (R1) employing TPE and triphenylphosphine (TPP) moieties as stoppers, which also displayed the functions of AIE and targeting mitochondria, respectively. By introducing DOX into R1, the resulting supramolecular prodrug constituted a dual-fluorescence-quenched Förster resonance energy transfer system. Upon hydrolysis in endo/lysosomes, the fluorescence of the system was recovered, leading to the recovery of the drug.

#### *4.2.2 Systems with targeting functions*

Introducing targeting groups can remarkably enhance the delivering efficiency, which can be performed on pillararene hosts or guest molecules. By modifying pillararenes with targeting molecules, such as galactose [209,218,219], lactose [220], mannose [221–223], and biotin [224], precise delivery of different drugs has been realized for enhancing the efficacy of cancer and bacteria treatments as well as mitigating the toxicity of the drugs delivered. For example, Pei *et al*. [219] prepared a galactose-targeting host-guest complexation PS (Figure 11a), which enabled efficient delivery and GSH-triggered release of DOX and thus enhancing the therapeutic efficacy of chemo-photodynamic combination in hypoxic tumors. Many drugs do not have fluorescence, making it difficult to monitor their delivery in real time. Pei and He *et al*. [222,223] thus constructed a supramolecular targeted delivery-fluorescence monitoring system through the self-assembly of mannose-modified pillar[5]arenes as hosts and fluorophore dicyanomethylene-4H-pyran derivatives as guests, which was applied for the targeted delivery and real-time monitoring of non-fluorescent gemcitabine and linezolid. Huang *et al*. [218] also synthesized an amphiphilic pillar[5]arene functionalized with hydrophilic galactose and hydrophobic alkyl chain, which self-assembled into nanotubes in aqueous solution. Galactose provided multivalent ligation of high affinity for carbohydrate receptors on *E. coli*, enabling effective cell adhesion for agglutinating *E. coli*. Using this approach, biotin and PEG have also been introduced onto pillar[5]arene, which could complex viologen to generate nanoparticles for targeted delivery of DOX [224].

Another approach for designing pillararene-derived targeting supramolecular systems involves modifying the guest molecules with targeting groups. Targeting moieties used include peptide [204], folic acid [225,228,229], galactose [230–232], mannose [233], biotin [234], and triphenylphosphine [217,235]. For example, Pei *et al*. [231] synthesized a tryptophan-modified pillar[5]arene to co-assemble with a galactose-containing guest to create a targeted delivery system, which not only facilitated DOX delivery but also exhibited synergistic enhancement on the anticancer effect of DOX through specific binding to DNA. Pei *et al*. [233] also fabricated supramolecular glyco-nanovesicles *via* host-guest

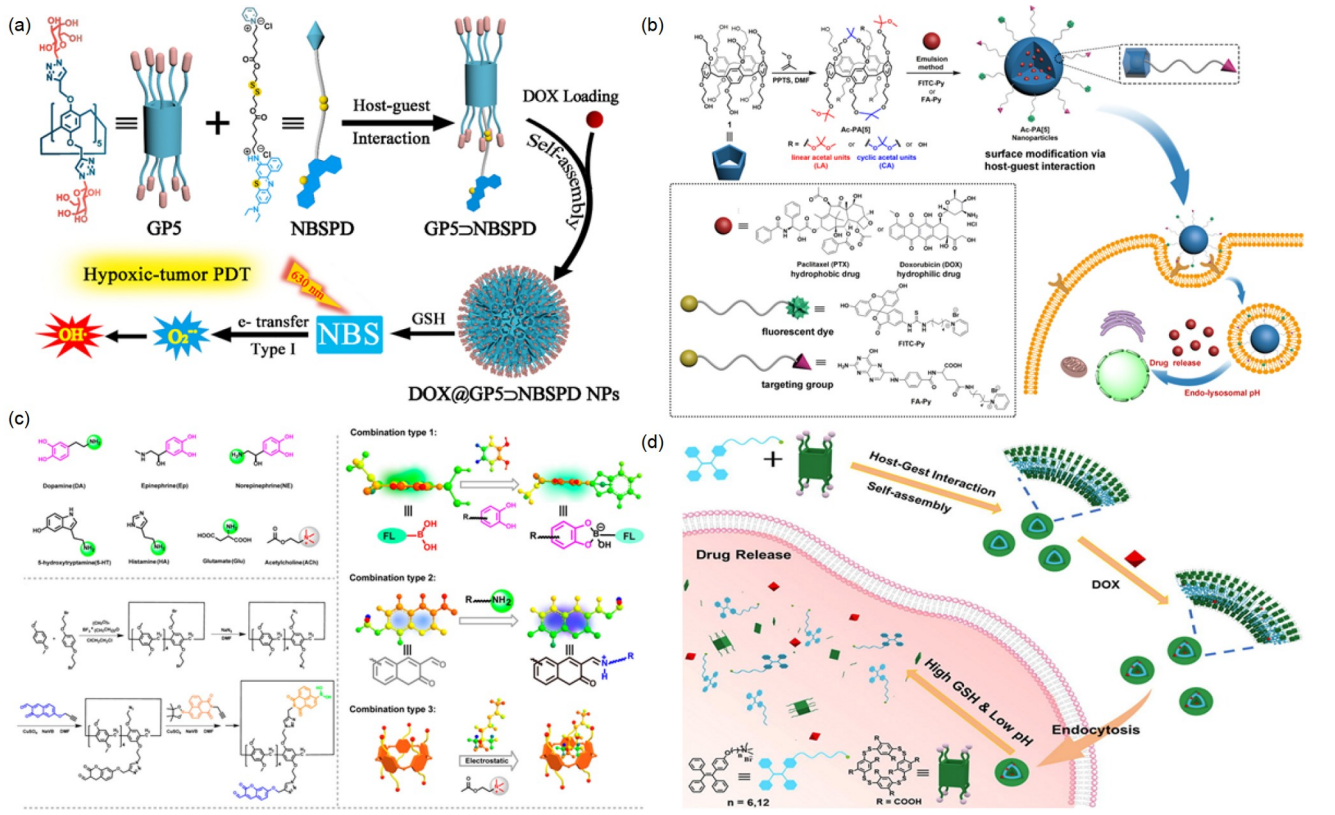


**Figure 11** Pillar[5]arene-derived supramolecular systems for targeted delivery and bioimaging. (a) Galactose-targeting system containing pyridine/NiB PS (NBSPD) for enhanced DOX loading and hypoxic-tumor therapy [219]. (b) Acetal-functionalization for pH-responsive drug delivery [225]. (c) Fluorescence array for sensing intracellular multi-neurotransmitters [226]. (d) Disulfide-connected macrocycle for dual-responsive drug release and fluorescence imaging [227] (color online).

interaction between pillar[5]arene dimer and mannose derivative for targeted drug delivery. The two pillar[5]arene macrocycles were linked by a diselenide bond to allow GSH-triggered responsiveness. Liu *et al*. [234] prepared ferrocene-bearing biotin and CPT derivatives as guests to construct supramolecular nano-prodrugs through host-guest interaction with CP[6]As. Glucose oxidase was further loaded into this system for synergistically enhancing its anti-cancer efficacy. This supramolecular prodrug demonstrated a highly efficient catalytic ability to convert glucose into hydroxyl radicals and reduce the pH value within cancer cells, thereby leading to enhanced chemodynamic therapy. Due to targeting and stimuli-responsive properties of biotin and ferrocene, it also exhibited a sensitive capacity for GSH-induced CPT release, further improving the therapy of CPT. Ma *et al*. [225] also prepared a pH-responsive acetal-functionalized pillar[5]arene derivative, which self-assembled into nanoparticles through emulsion (Figure 11b). Hydrophobic anticancer drugs paclitaxel and DOX could be loaded into the nanoparticles, which were further modified with folic acid and fluorophore derivatives as guests on the surface. In this way, a multifunctional nano-delivery host-guest system with targeting, fluorescence traceability and stimulus-responsiveness was constructed to realize real-time monitoring of targeted drug delivery and improved anticancer efficacy.

### 4.2.3 *Systems for bioimaging and diagnosis*

Multifunctional supramolecular systems constructed based on pillararenes also play important roles in cell imaging, visible drug delivery, and disease diagnosis and monitoring. Neurotransmitters are very important for neuron events and brain diseases. However, there is currently a dearth of effective probes for targeted analysis of specific neurotransmitters. Tian *et al*. [226] thus designed and synthesized a supramolecular fluorescent probe by introducing borate naphthalene and aldehyde coumarin recognition groups to a dual-functionalized fluorescent pillar[5]arene derivative (Figure 11c), enabling the identification of large-scale neurotransmitters. Imaging the kidney is imperative for assessing its functionality and monitoring the progression of renal diseases, but remains challenging due to invasiveness, radiation exposure, and high financial burden. Yang *et al*. [236] also prepared a fluorescent pillar[5]arene with ten positive charges, which allowed for selective accumulation within negatively charged filtration barrier, facilitating targeted and precise imaging of the kidney. Wang *et al*. [237] prepared a

water-soluble pillar[5]arene which could complex a protein-dependent cationic probe that possessed high binding affinity for human serum albumin (HSA). The host-guest complex thus exhibited superior HSA responsiveness and enhanced sensing selectivity, thereby favoring HSA-induced bioimaging. Liu *et al*. [227] further prepared a disulfide-connected pillar[4]arene analogue, which complexed a cationic TPE guest to fabricate a host-guest fluorescent system for advanced cellular imaging and visual drug delivery (Figure 11d). Generally, multifunctional systems constructed with different pillararenes provide powerful tools for drug delivery, diagnosis, and treatment of diseases [238–240].

### 4.2.4 *Pillararene-based hybridized systems*

Inorganic nanoparticles have been widely used as carriers for drug delivery, but may suffer from poor solubility, microphase separation as well as unsatisfactory biocompatibility. Pillararenes introduced on their surface may function as versatile anchoring points to address these drawbacks, and the resulting hybridized supramolecular systems may be used as imaging, sensing or targeting delivery agents and for achieving stimuli-responsiveness. One approach for designing such hybridized supramolecular systems is to encapsulate drugs inside the pores of mesoporous nanoparticles with free pillararenes as gate keepers. For example, Du *et al*. [241] reported that a CP[6]A-incorporated mesoporous silica nanoparticles could achieve controlled drug delivery (Figure 12a). The drug was effectively encapsulated within the nanoparticles, while CP[6]A worked as capping agent through host-guest interaction with bipyridinium on the surface of the nanoparticles. Adding acid and metal ions could detach CP[6]A from the nanoparticles, leading to controlled release of payloads. Yang *et al*. [242] constructed UiO-66-$NH_2$ metal-organic framework (MOF)-based hybridized drug delivery systems. The MOF was functionalized with quaternary ammonium, and CP[5]A was used as gatekeeper *via* host-guest complexation to afford a nanovalve. 5-Fluorouracil loaded by the MOF could be released in a controllable manner for enhanced treatment of central nervous system disease in response to acidic pH, $Zn^{2+}$ or local heating. Yang *et al*. [243] further extended this approach to hollow mesoporous silica nanoparticles by attaching CP[5]A-modified Au nanoparticles to their surface (Figure 12b). Nanoparticles obtained in this way also exhibited controlled release of the cargo with minimized premature leakage in response to high temperature as well as competitive guest such as ethylenediamine.

The combination of pillararenes with inorganic nanoparticles can also be labeled with functionalized tags. In this way, Yu *et al*. [244] developed a CP[5]A-capped CuS organic-inorganic hybrid system for combined chemodynamic and photothermal therapy of tumors (Figure 12c). Galactose derivative, together with DOX, was anchored to CP[5]A *via*

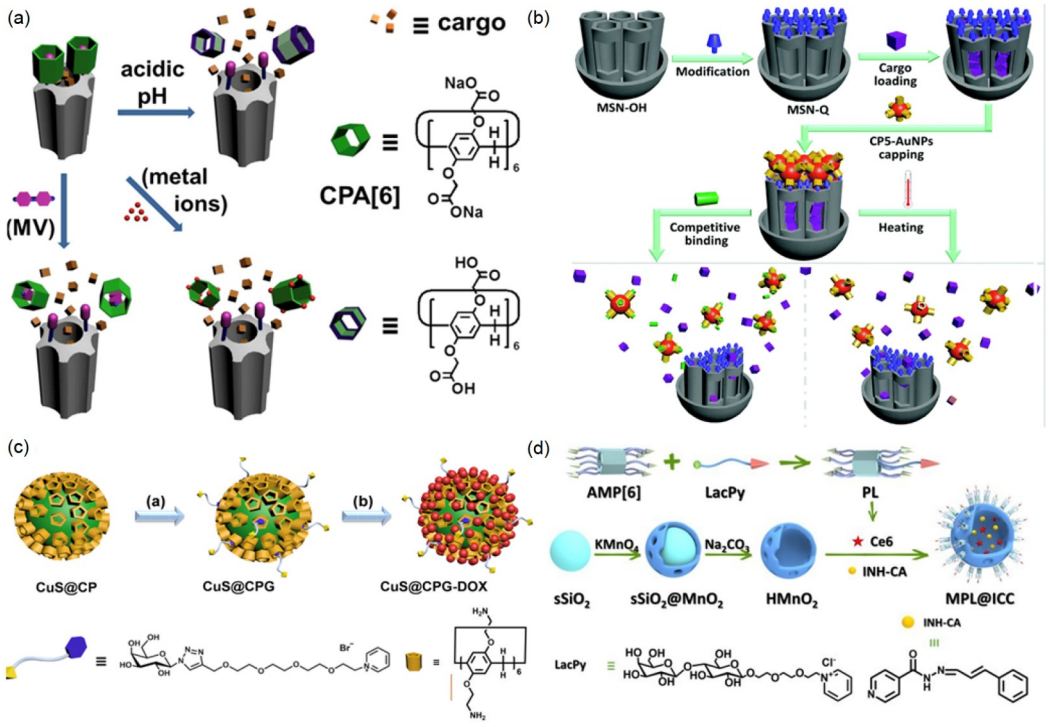


**Figure 12** Pillararene-derived hybridized supramolecular systems for drug delivery. (a) CP[6]A-incorporated silica nanoparticles for controlled drug delivery [241]. (b) Quaternary ammonium salt functionalized mesoporous silica nanoparticles gated by CP[5]A-modified Au NPs [243]. (c) Preparation of CuS@CPG–DOX *via* host-guest interactions [244]. (d) MPL@ICC nanoparticles for potentiating immunogenic death of tumor cells [245] (color online).

host-guest binding to achieve good biocompatibility and controlled DOX release in response to low pH in tumor microenvironment. Moreover, the combination of DOX-induced chemotherapy and nanoparticle-mediated photothermal therapy exhibited potent inhibition of tumor growth *in vitro* and *in vivo*. Sun *et al*. [246] further constructed CP[5]A-based core-shell upconversion nanoparticles for antitumor therapy. Again, CP[5]A was used to stabilize the hybrid nanoparticles and inhibit the release of loaded drug during delivery, while rapid drug release was achieved in the acidic microenvironment of tumor cells due to CP[5]A detachment from the nanoparticles. Moreover, the nanoparticles could convert NIR irradiation into green fluorescence for efficient bioimaging. Pei *et al*. [245] further extended the approach to an amino-bearing pillar[6]arene, which formed host-guest complex with lactose-pyridinium (Figure 12d). The complex was further used to modify $MnO_2$ nanovesicles for anti-tumor *via* immunogenic cell death. Upon entering tumor cells, $MnO_2$ could convert $H_2O_2$ to $O_2$, inducing the release of isoniazid and chlorine e6 loaded in the nanoparticles to achieve enhanced PDT. *In vivo* test showed that tumor-bearing mice could be cured without reoccurrence in more than 300 days.

## 5 Macrocycles and cages for bioapplications

### 5.1 Biphen[*n*]arenes and analogues

In addition to the above-discussed classic macrocycles, recent years have witnessed the generation of many new macrocycles and molecular cages, which provide new opportunities for developing new biofunctions. Advances related to host-guest chemistry have been achieved through the employment of biphen[*n*]arenes, naphthotubes, acyclic CB[*n*]s, and TPE-based cages. Biphen[*n*]arenes as a new family of macrocycles were created *via* modular synthetic strategy by Li *et al*. [247–252] from 2015. The diversity of size/shape/chemical environment, facile functionalization, and tunable molecular recognition properties enable their great potentials in biomedical applications. Recently, Li *et al*. [253] synthesized quaternary ammonium *per*-functionalized cationic biphen[*n*]arenes CBP4 and CBP5, which could not only effectively inhibit biofilm assembly but also eradicate intractable mature biofilms formed by both Gram-positive and Gram-negative bacterial strains with $MBEC_{50}$ value of 4.94–6.82 μM (Figure 13a). Furthermore, their inherent cavities could encapsulate antibiotic cefazolin (CFZ), synergistically enhancing biofilm eradication performance *in vitro* and improving healing efficacy on *E. coli*-infected mice models. To match medium-sized molecules, Li *et al*. [254] also custom-designed extended biphen[*n*]arenes by increasing the length of rigid monomer. One of the corresponding 2,2″,4,4″-terphen[3]arene derivatives bearing multiple sulphonatopropoxy moieties STP3 has been applied for taste masking of bitter pharmaceutical ingredients (Figure 13b). This negatively charged macrocycle also displayed strong affinity toward alkaloid drugs with $K_a$ values in the vicinity of $10^2$–$10^6$ $M^{-1}$, which was a prerequisite for avoiding bitter taste in an oral-cavity-type environment. In addition, complexation of palmatine by STP3 could retain its antibacterial activity against *S. aureus* and *E. coli*. Another 2,2″,4,4″-terphen[3]arene sulfate SATP3 was found to reverse the activity of neuromuscular blockers (Figure 13b) [65]. Benefiting from introduction of twelve sulfate ester groups, SATP3 exhibited excellent water-solubility (⩾ 10 mM) and formed 1:1 host-guest complexes with neuromuscular blockers, including rocuronium, vecuronium, pancuronium, gallamine and cisatracurium. The corresponding $K_a$ values exceeded $10^5$ $M^{-1}$. *In vitro* cytotoxicity assay and body weight change by tail vein injection proved good biocompatibility, while its reversal activity towards cisatracurium-induced muscle relaxation was demonstrated in a mouse model.

The complexation of small- or medium-sized guests by macrocyclic compounds is feasible to implement. However, the cavity size of classic macrocycles is generally less than 1 nm in diameter. Just increasing number of the monomer cannot efficiently increase the size of macrocycles due to the distortion of the backbones [257]. Because of strict constrain on cavity size, classic macrocycles cannot entirely encapsulate important biological macromolecules [103,258,259]. To achieve an effective overall complexation of peptide, Li *et al*. [255] further extended the length of rigid monomer into 1.6 nm to custom-design quaterphen[*n*]arenes WQP4 and AQP4 (Figure 13c). Tetraglycol side chains and ending carboxylate groups were attached to improve their water-solubility, cavity depth, complexation potency as well as biocompatibility. WQP4 showed strong interactions towards antimicrobial peptide pexiganan with the $K_a$ of $2.46 \times 10^5$ $M^{-1}$. Complexation of pexiganan by WQP4 could decrease its hemolysis in rabbit red blood cells. Formation of host-guest complex substantially enhanced metabolic stability of PXG. AQP4 that bears dendritic multi-carboxylate moieties was found to detoxify biotoxin LyeTxI, a 25-mer peptide in spider venom due to strong complexation ($K_a$ = $7.01 \times 10^7$ $M^{-1}$) (Figure 13c) [256].

### 5.2 Naphthotubes

Jiang *et al*. [260] constructed naphthotubes, another family of biomimetic macrocycles for host-guest studies, from naphthol precursors. Their inward-directed functional groups endow the tubes with unique recognition abilities [261]. Systematic studies were performed for the molecular recognition of amide naphthotubes (NTs), CB[7] and β-CD to drugs in water (Figure 14a) [262]. The cavities of NTs were deep enough to encapsulate both polar and nonpolar groups

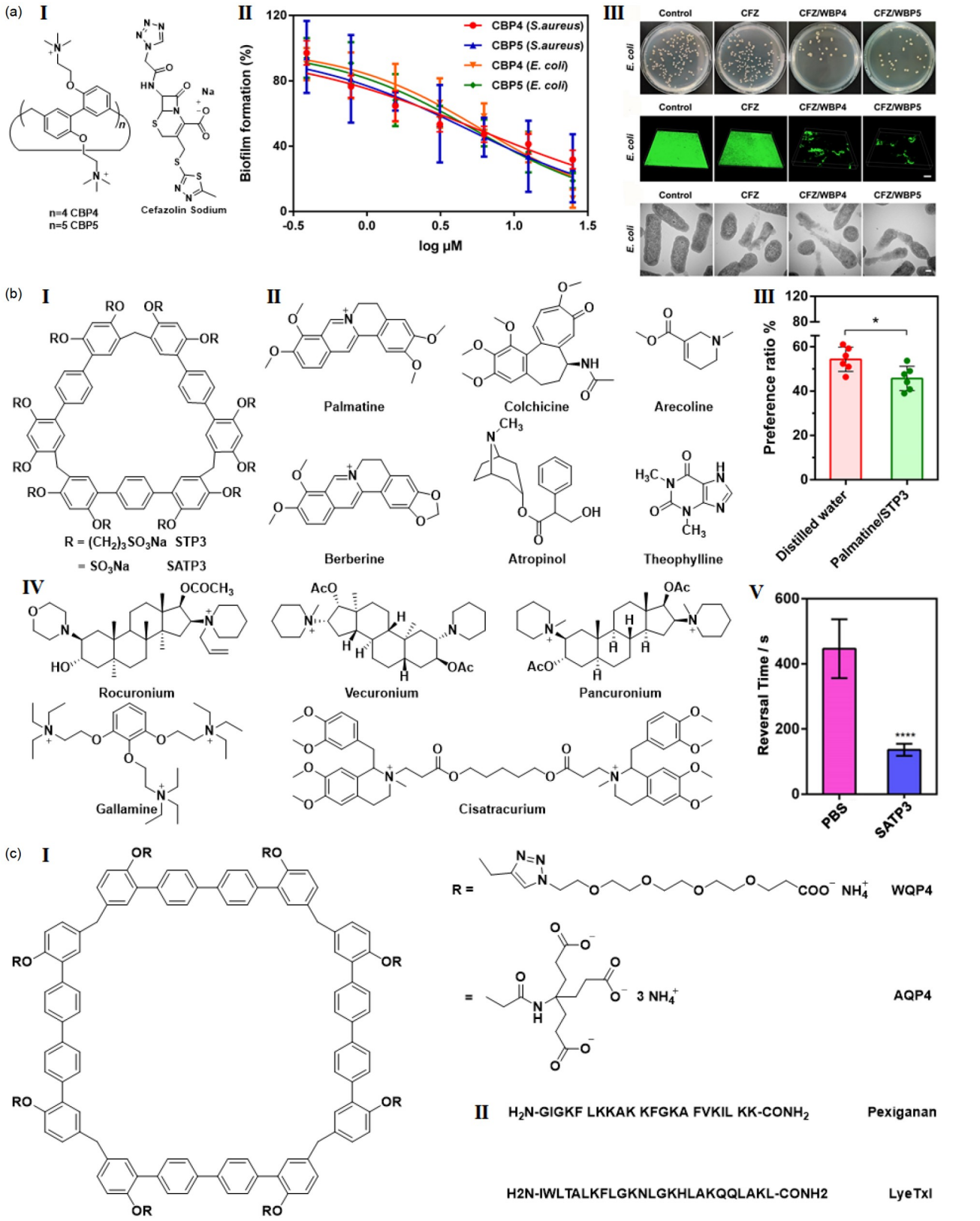


**Figure 13** (a) Structures of biphenarenes CBP4, CBP5 and cefazolin (I). Inhibition percentage of biofilm formation by macrocycles (II). Images of colony-forming units, biofilms and ultrathin sections of *E. coli* treated with various formulations (III) [253]. (b) Structures of terphenarenes STP3 and SATP3 (I) and bitter alkaloids (II). Preference ratios for palmatine/STP3 in a two-bottle preference drinking test (III). Structures of neuromuscular blockers (IV). Diagram of muscle relaxation recovery time (V) [65]. (c) Structures of quaterphen[4]arenes WQP4 and AQP4 (I). Sequences of antibacterial peptide pexiganan and spider toxin LyeTxI (II) [255,256] (color online).

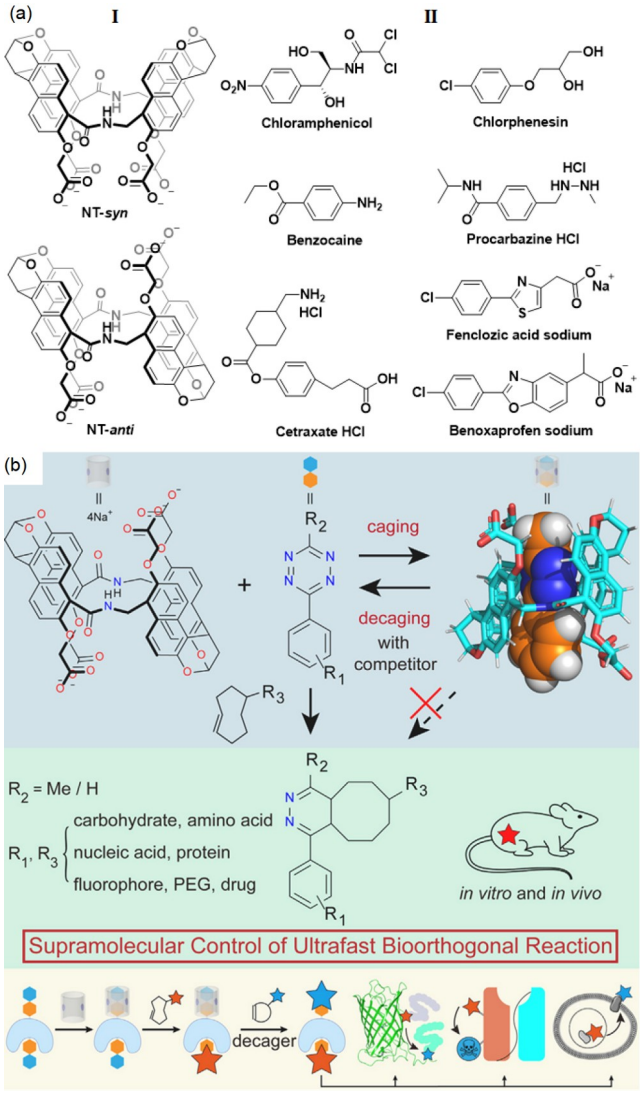


**Figure 14** (a) Structures of naphthotubes NT-*syn*, NT-*anti*, and drugs complexed [262]. (b) Diagram of reactions between Me-Tet-Ph and (*E*)-cyclooct-4-en-1-ol in the absence of NT-*anti*, and schematic illustration of supramolecular control of ultrafast bioorthogonal reaction [263] (color online).

of drugs, which was stabilized by hydrogen bonds between the polar groups and the amide protons of the hosts. Furthermore, *anti*-configured naphthotube (NT-*anti*) was applied to improve the solubility of dantrolene sodium and tepotinib in water. NT-*anti* has a solubility of up to 350 mM in water. Its solubilizing performance for poorly soluble drugs was better than that of β-cyclodextrin, a gold standard excipient. Tetrazine-mediated inverse electron demand Diels-Alder (IEDDA) reactions are widely used ultrafast bioorthogonal reactions, and convenient methods to regulate these reactions are thus of value. Liu, Jiang and co-workers [263] characterized a novel host-guest pair between NT and phenyltetrazine derivatives (Figure 14b). On the basis of this observation, a molecular-recognition strategy was developed to precisely control tetrazine-mediated IEDDA reaction with various biomolecules. NT-*anti* exhibited strong binding affinity of $10^7$ $M^{-1}$ and high selectivity to phenyltetrazine, especially for 3-methyl-6-phenyl-1,2,4,5-tetrazine (Me-Tet-Ph) and 3-phenyl-1,2,4,5-tetrazine (H-Tet-Ph). The high binding affinity allowed efficient caging effect to control the reactions. Moreover, the reactivity of phenyltetrazine group could be recovered through addition of a biocompatible competitive guest with no latency time, and the reactivity of tetrazine could also be regulated in living animals.

### 5.3 Acyclic cucurbit[*n*]urils

The complexation of acyclic cucurbit[*n*]urils (ACBs) for drugs was first reported by Isaacs *et al*. [264] in 2012. This family of acyclic hosts features an inherent "C"-shape conformation that forms a highly hydrophobic cavity for including hydrophobic drugs in water, while molecules formed by tetraglycoluril moiety display the highest complexation for hydrophobic drugs and bioactive molecules [265–267]. Their water-solubility can be modulated by introducing multiple hydrophilic side chains. Ma *et al*. [268] reported that ACB containing carboxylic moiety conjugated dextran could include anti-tumor drugs 5-fluorouracil and temozolomide to form host-guest complexes (Figure 15a), which co-assembled with polyethyleneimine (PEI) to achieve drug delivery and bioimaging. Although there were no conventional chromophores in these supramolecular systems, they exhibited enhanced unorthodox aggregation-induced luminescence in water with a quantum yield of 10%. Ma *et al*. [269] also constructed two ACB-conjugated polymers 2-MA and 2-CA based on biocompatible polymer polyallylamine as drug delivery systems (Figure 15b). The constituent ACB could encapsulate anti-tumor drugs including mitoxantrone, DOX, topotecan and irinotecan with $K_a$ values in the vicinity of $10^3$–$10^5$ $M^{-1}$. The side chains of these polymers served as pro-guests, which did not interact with ACB, while acidic microenvironments triggered their conversion to aminomethyl groups, which competitively replaced drugs *via* engulfing aminomethyl groups within ACB's cavity. Cellular uptake assays confirmed that this pro-guest strategy resulted in controlled drug release with a tunable rate, achieving targeted delivery to HeLa cells under mildly acidic conditions (pH = 6.0).

Ma *et al*. [270] further developed a supramolecular nanomedicine through host-guest interaction of ACBs for chemo-photodynamic combination therapy (Figure 15c). For this aim, CPT was used as chemotherapeutic agent and tetraphenyl porphyrin (TPP) was used as PDT PS. CPT was conjugated with TPP and methoxy poly(ethyleneglycol) to yield CPT-SS-TPP and CPT-mPEG, respectively. Supramolecular assembly of CPT-SS-TPP and CPT-mPEG was mediated by ACB to form a three-component nano-system (SNM-3). Stability and singlet oxygen generation efficiency

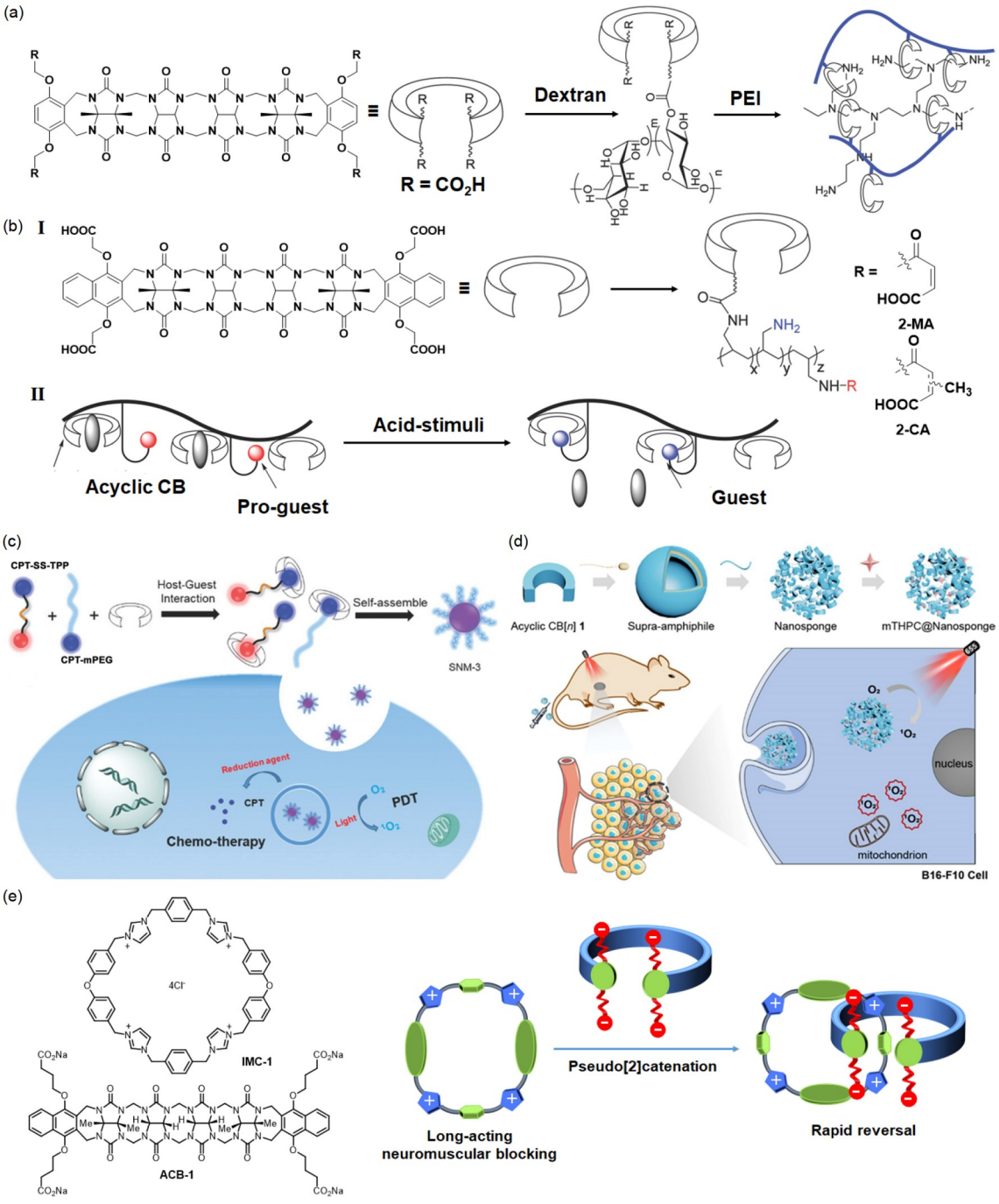


**Figure 15** (a) Synthesis of ACB-conjugated dextran and its self-assembly through host-guest interaction [268]. (b) Polymer 2-MA and 2-CA (I) and "pro-guest"-based controlled release after delivery (II) [269]. (c) The mechanism of chemo-photodynamic combination therapy [270]. (d) The fabrication of nanosponges and drug loading system [271]. (e) Structures of neuromuscular blocker IMC-1 and antagonist ACB-1 and the proposed mechanism of antagonizing IMC-1 blocking by ACB-1 [272].

of SNM-3 were significantly enhanced due to reduced aggregation-caused quenching (ACQ) and incorporation of poly(ethyleneglycol). As a result, it exhibited decreased cytotoxicity toward normal cell lines and enhanced combination therapeutic efficacy toward three human cancer cell lines (HeLa, A549, and MCF-7). Ma *et al*. [271] further used ACB to build nanosponges *via* supramolecular vesicle-templated crosslinking (Figure 15d). Such nanosponges were capable of encapsulating PDA temoporfin. When loaded with nanosponges, the PDT efficacy of temoporfin was enhanced 7.5- and 20.8-fold for HeLa and B16-F10 cancer cells, respectively, due to improved cell uptake. This ACB-based host-guest approach can also be applied to construct acid-degraded DOX prodrugs [273,274].

Anionic ACBs are able to efficiently include cationic macrocycles through interpenetrating complexation [275]. Li and co-workers [272] demonstrated that this mechanism can be applied to design a host-guest partner to realize neuromuscular blockade and antagonism activity, respectively. The partner was composed of ACB-1 as host and tetraimidazolium macrocycle IMC-1 as guest, which formed highly stable complex with $K_a$ value of over $1.3 \times 10^{10}$ $M^{-1}$ in buffer (Figure 15e). Due to possible binding multivalency, IMC-1 could reach neuromuscular blocking activity with duration of action significantly longer than that of clinically used long-acting agent pancuronium, while ACB-1 could reverse this block with recovery time shorter than that achieved by sugammadex for reversing the block of rocuronium [45], the clinically most widely used intermediate-acting blocker. Li and Ma *et al*. [276] further showed that ACB octacarboxylate derivatives could include cationic bitter compounds for effective taste masking.

### 5.4 Molecular cages

TPE derivatives as AIE luminophores have been widely explored as biofunctional materials [277–284]. Cao *et al*. [285–287] synthesized TPE-based octacationic cage oc-Cage from the reaction of two tetrapyridinium TPE moieties as central faces and four *p*-xylylene as surrounding pillars. The cage exhibited excellent fluorescence property and could recognize and detect organic dyes and biomolecules (Figure 16a), including 8-hydroxypyrene-1,3,6-trisulfonic acid trisodium salt (HPTS) and 1,3,6,8-pyrenetetrasulfonic acid tetrasodium salt (PTSA), deoxynucleotides, nucleotides (*e.g*., ATP and GTP), and DNA [8]. Furthermore, this fluorescent host-guest complexation was successfully utilized to brighten ATP-rich mitochondrion in HeLa cells. Cao *et al*. [288] also demonstrated that oc-Cage could improve the water-solubility of insoluble drugs, such as CPT, irinotecan and lenalidomide, by forming host-guest complexes in water (Figure 16b). More importantly, drugs encapsulated by the cage were more effective in killing cancer cells than drugs alone, which supported the delivery function of the cage. Moreover, drug complexes could be used to monitor drug release and track drug delivery by fluorescence microscopy *in vitro*. Cao *et al*. [289] also showed that oc-Cage could be further used to recognize and detect β-lactam antibiotics including penicillin G, carbenicillin, ampicillin, amoxicillin and methicillin by forming 1:2 host-guest complexes (Figure 16c), which led to excellent bacteriostasis potency against *Staphylococcus aureus* and methicillin-resistant *Staphylococcus aureus*. Although oc-Cage is achiral, it was revealed that it could serve as chiroptical sensor for chiral adaptive recognition with sequence specificity of di-, tetra-, and polypeptides, including amyloid β-peptide$_{1–20}$, somatostatin, and insulin (Figure 16d) [290].

## 6 Supramolecular transmembrane channels

Cell membranes are mainly composed of lipid bilayers, which separate the living cells from the environment. Chemists have long-term interests in building artificial systems to mimic the structure and function of the channel proteins in order to develop new therapeutic strategies. One of the strategies for this aim involves the use of supramolecular principles [69,291–294], some of the artificial channels developed in this way exhibit attractive bioactivity, including antimicrobial and antitumor activity [292,294–298]. For example, Hou *et al*. [299] constructed pillar[5]arene-based artificial channels Ch-1a–Ch-1d of different lengths (Figure 17a) and found that Ch-1a could be sensitive to the difference of the membrane composition of the bacterial cells and mammalian cells, causing specific insertion into the lipid bilayers of Gram-positive bacterial but not that of mammalian erythrocytes. As a result, it exhibited efficient antimicrobial activity and low hemolytic toxicity for mammalian erythrocytes. Xin *et al*. [300] prepared pillar[5]arene-gramicidin (gA) peptide hybrids Ch-2a–Ch-2c (Figure 17b) and revealed that the charge status of the gramicidin chain had a significant influence on its membrane-incorporation selectivity toward bacterial cell over mammalian cell. Positively charged Ch-2b was found to display a high antimicrobial activity against *S. aureus* and very low hemolytic toxicity.

Tumor cells can overexpress receptors for small molecular substrates, which allows for targeting these cells by conjugating the channel molecules with targeting substrates. Hou *et al*. [301] also engineered pentadecapeptide gA and prepared Gal-gA conjugate Ch-3 (Figure 17c). Due to the high affinity of galactose (Gal) for asialoglycoprotein receptor ASGPR, a lectin overexpressed on the liver cancer cell surface, it was able to target liver cancer cells and incorporated into the cell membrane to form transmembrane channels. Similar to natural gA, Ch-3 could mediate cation transmembrane transport, resulting in the disturbance of the ion homeostasis and apoptosis of the cells. Alternatively, Zeng and Ren *et al*. [302] achieved high cancer cell membrane-incorporation specificity by making use of the high-level expression of cholic acid receptors on cancer cells (Figure 17d). Cholesterol-containing artificial channel Ch-4 with a nano-sized cavity of 1.6 nm in diameter was revealed to display high anticancer activity toward liver cancer cells and low cytotoxicity to human healthy cells. The liver cancer cell-targeting behavior of the channel was proposed to be a result of overexpression of the cholic acid receptors on liver cancer cells that led to higher uptake of cholesterol-containing channel molecules.

Yang *et al*. [303] developed a different strategy for selective eradication of cancer stem cells (CSCs) with α-aminoxy

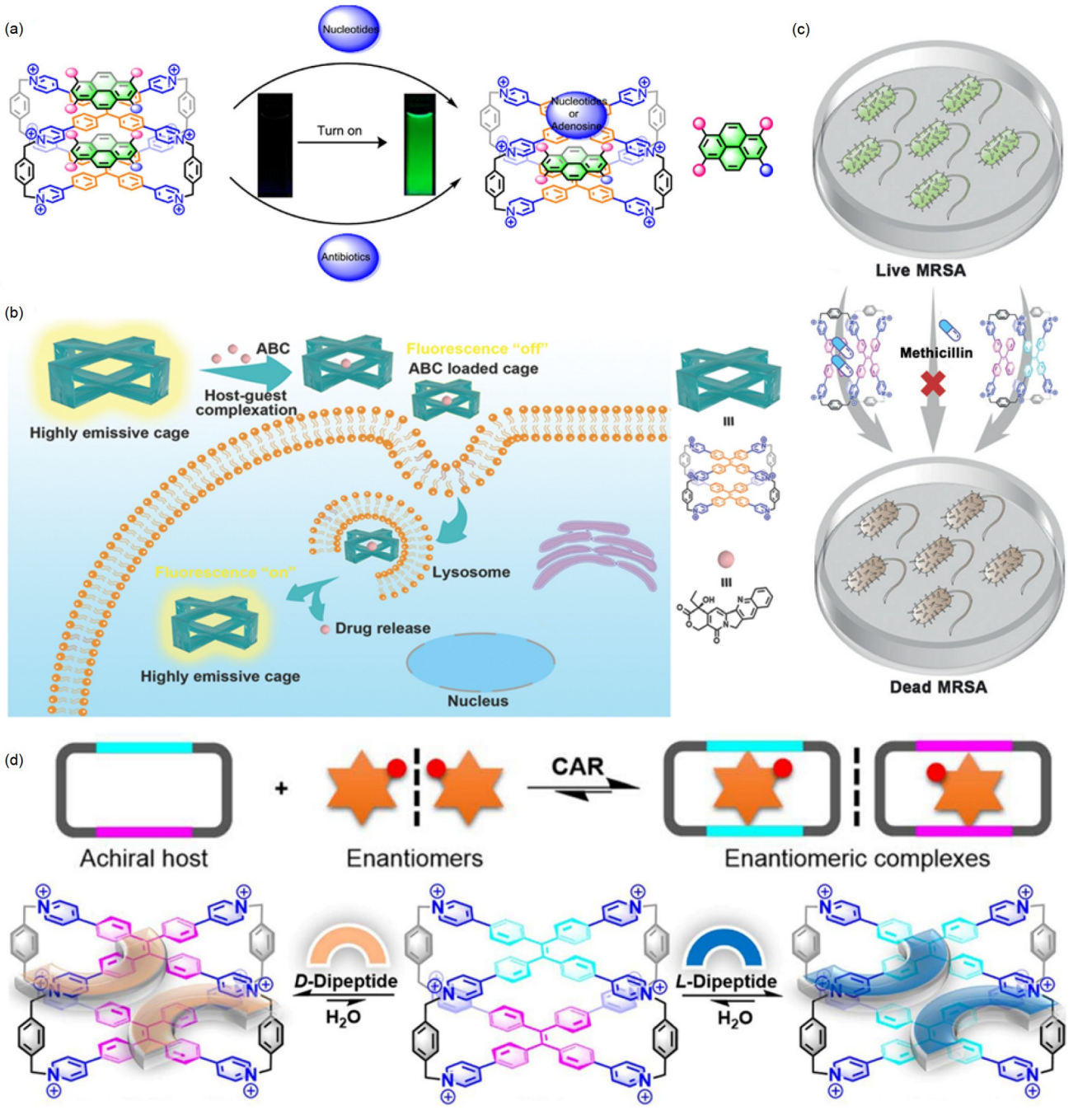


**Figure 16** Octacationic oc-Cage and its host-guest complexation and drug delivery. (a) Turn-on fluorescence *via* competitive exclusion host-guest exchange [8]. (b) Real-time fluorescence changes for monitoring drug release *in vitro* [288]. (c) Antibacterial diagram against methicillin-resistant *Staphylococcus aureus* [289]. (d) Chiral adaptive recognition for enantiomers [290] (color online).

acid derivative Ch-5 by taking advantage of the endogenous subcellular pH gradient and membrane potential across mitochondrial membranes of CSCs (Figure 17e). It was shown that in mitochondria, Ch-5 could pass through the inner mitochondrial membrane (IMM) and enter the mitochondrial matrix that possesses higher pH values. Consequently, it was deprotonated to form an anionic structure to subsequently complex $K^+$ to travel back to the intermembrane space with lower pH values. Thus, the transporter-$K^+$ complex would be re-protonated and release $K^+$. This travel cycle caused $H^+/K^+$ exchange across IMM, leading to the disruption of the ion homeostasis of mitochondria and apoptosis of CSCs. As the pH gradient and membrane potential across mitochondria membranes is an intrinsic property of CSCs due to the oxidative phosphorylation dependence, the transporter showed remarkable antitumor selectivity for CSCs over noncancer cells. Ren *et al.* [304] further constructed non-covalently stapled self-assembled artificial channels from photoactive

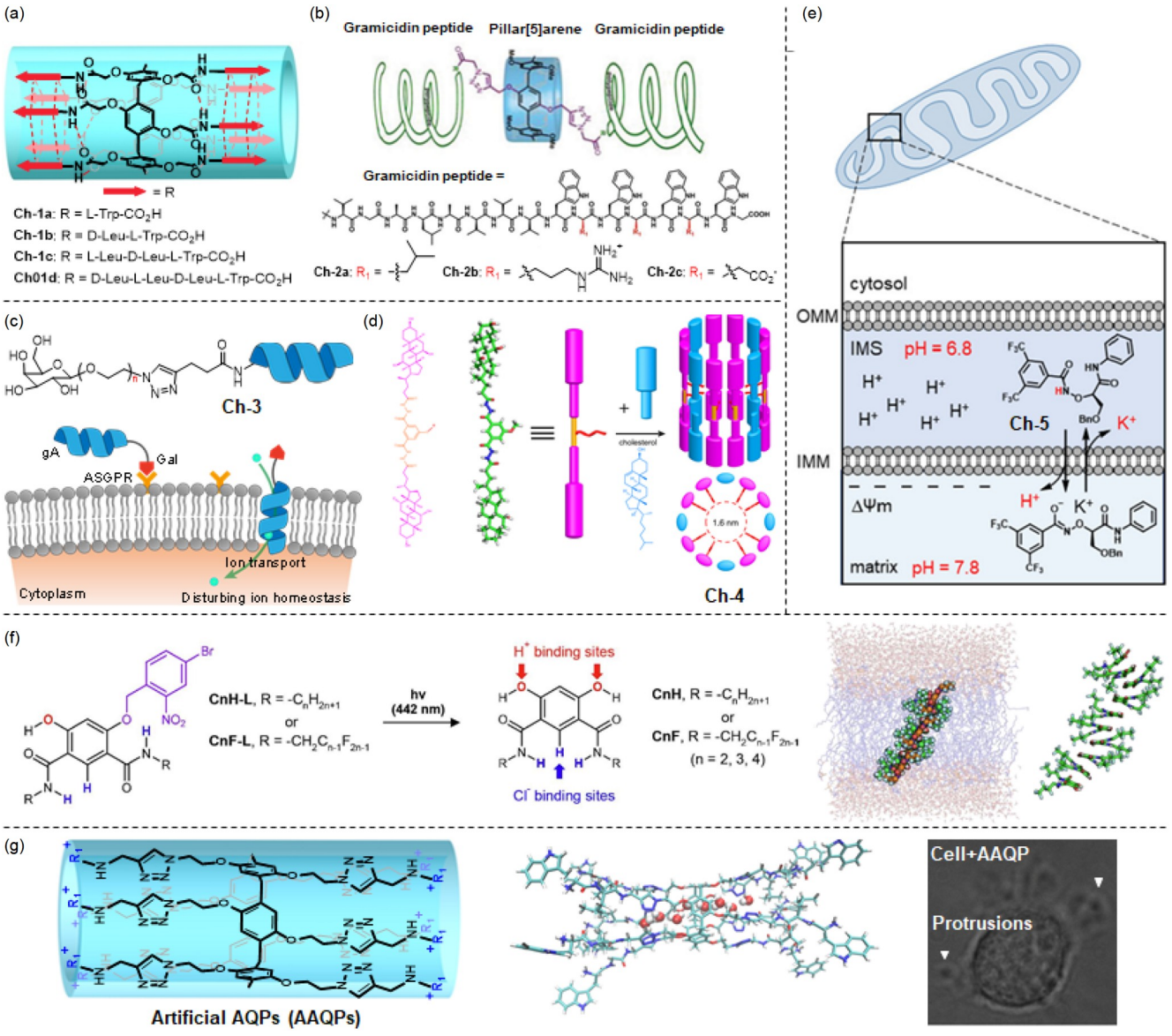


**Figure 17** Structures of bioactive supramolecular transmembrane channels. (a, b) Pillar[5]arene-based channels that bear short peptide and gramicidin chains [299,300]. (c) Galactose-modified gramicidin [301]. (d) Cholesterol-derived diacylhydrazide [302]. (e) Aminoxy amide [303]. (f) Photoactive aromatic diamide [304]. (g) Pillar[5]arene-derived artificial aquaporins [305] (color online).

CnH-L and CnF-L for achieving external stimulus (Figure 17f). Both channels exhibited co-transport of $H^+/Cl^-$ across lipid bilayer membrane. Photoirradiation caused the cleavage of the benzyl ether bond to afford CnH and CnF, which could bind to $H^+$ and $Cl^-$ simultaneously and lead to antitumor activity toward human colorectal cancer cells. Natural water channel aquaporins (AQPs) can accelerate cell migration by mediating water transmembrane transport. To mimic this process, Hou *et al*. [305] constructed artificial aquaporins (AAQPs) from pillar[5]arene that was able to work in living cell membranes with high water permeability and selectivity rivaling those of AQPs (Figure 17g). AAQPs exhibited the ability to couple with cell protrusion formation by mediating water transmembrane transport [306], which led to obvious cell shape change and migration acceleration. Remarkably, this artificial channel-facilitated cell migration could enhance *in vivo* healing of traumatic injury.

## 7 Supramolecular amphiphiles

### 7.1 Carbohydrate derivatives

The self-assembly of amphiphilic molecules in aqueous environments, driven by hydrophilic-hydrophobic interactions, has been a primary strategy for creating nanostructures such as micelles and vesicles for various bioapplications. Using

carbohydrates, peptides, and nucleic acids as hydrophilic segments, different amphiphilic monomers can be prepared to assemble nano-supramolecular carriers to realize targeting, physiological barrier penetration, and immunomodulation. The discovery of cell surface lectins has led to the innovative use of carbohydrates as hydrophilic components in designing amphiphilic molecules, which can further form supramolecular "carbohydrate clusters" to improve specific carbohydrate-related interactions. Advancements obtained are increasingly applied and studied in the field of cancer diagnostics and therapeutics, particularly for the targeted delivery of functional molecules [307,308]. Pei *et al*. [309–311] developed a series of novel amphiphilic molecules that bear hydrophilic lactose segment for targeting cell surface lectins for cancer therapy (Figure 18a). Boron-dipyrromethene (BODIPY) fluorescent dye was coupled to lactose through GSH-responsive disulfide bond. The resulting supramolecular nanoparticles were explored for combined photodynamic-photothermal therapy of liver cancer. Pei *et al*. [312] also utilized chalcogen bonding interactions to drive the self-assembly of amphiphilic monomers. For this, epidermal growth factor receptor-targeted drug gefitinib was coupled with aza-BODIPY PS through a disulfide bond to form a hydrophobic "BG" unit, and two lactose molecules were coupled *via* a disulfide bond to create a hydrophilic "L" unit. The "BG" and "L" units co-assembled into highly stable nanostructures, which were capable of HepG2 cell-targeting delivery and release of gefitinib and the PS triggered by intracellular GSH (Figure 18b). To efficiently trace the drug delivery process, NIR fluorescent dyes have been integrated into supramolecular nanocarriers. For example, Yi *et al*. [313] coupled hydrophobic DOX with NIR dye leucomethylene LMB *via* ROS-sensitive urea bond and further introduced lactose to form amphiphile Gal-MB-DOX (Figure 18c), which self-assembled into "sugar-coated bullet" nanostructures that exhibited remarkable targeting specificity towards HepG2 hepatocellular carcinoma cells. In cancer cells, the urea bond was cleaved by ROS, triggering the release and accumulation of DOX as well as the conversion of LMB into NIR dye MB and thus allowing for NIR ima-

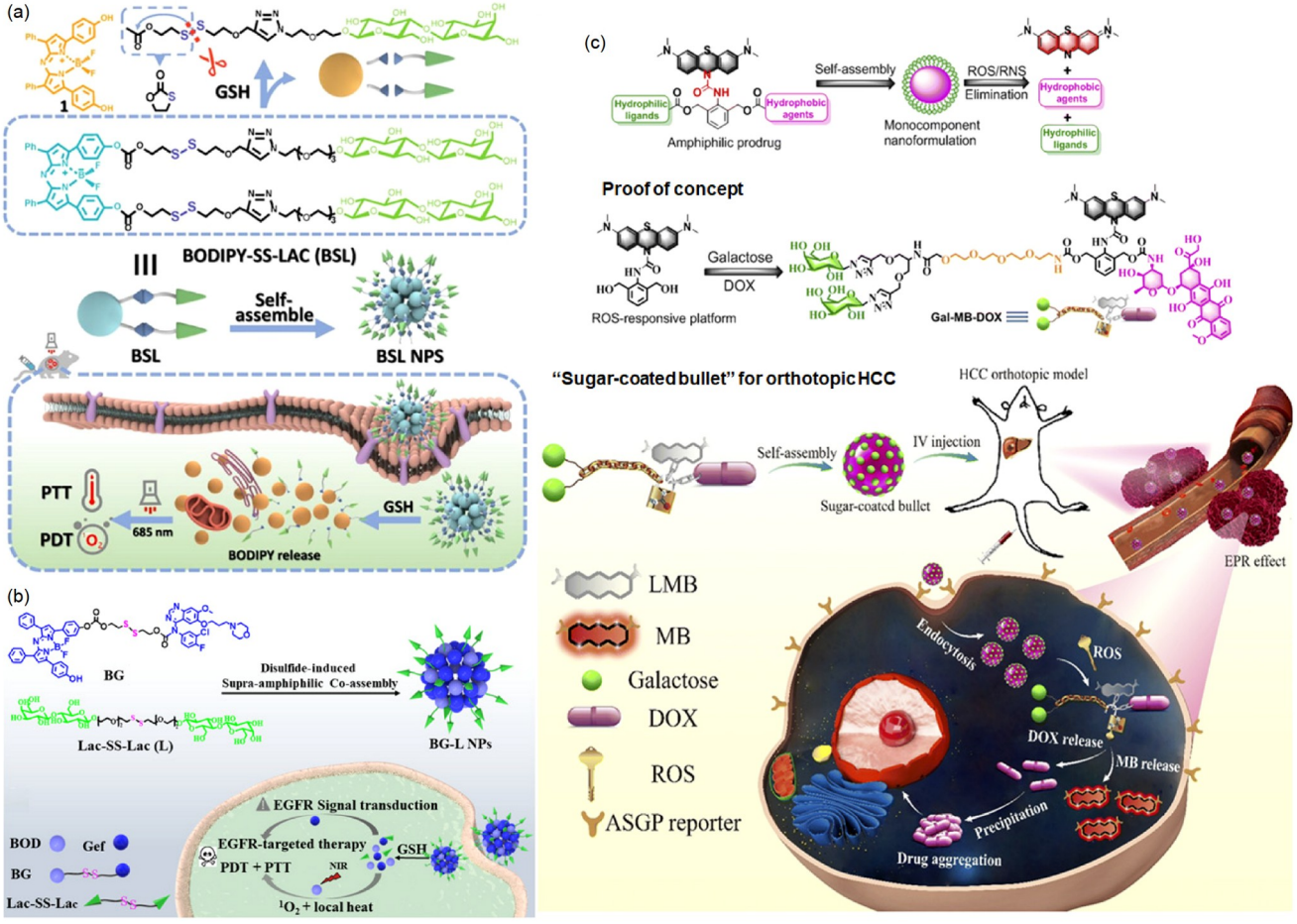


**Figure 18** Schematic illustrations of amphiphilic molecules bearing hydrophilic carbohydrates and their self-assembly and biofunctions. (a) The constitution of amphiphilic small molecule BODIPY-SS-LAC (BSL) and its self-assembly process, as well as the function mechanism of the corresponding supramolecular structure in cancer therapy [309]. (b) Supramolecular assembly strategy *via* chalcogen bonding and anti-tumor mechanism [312]. (c) Synthesis and self-assembly of Gal-MB-DOX and mechanism of drug delivery-tracing and anti-tumor [313] (color online).

ging of drug delivery and potent antitumor effect. Using different saccharides as hydrophilic targeting agents, several other amphiphilic monomers have also been developed for discrete delivery and therapeutic purposes [314–319].

### 7.2 Peptide derivatives

Peptides feature biodegradability, biosafety, customizability, and easy synthesis and modification and also allow for capabilities for various biofunctions, such as cell targeting, biological barrier penetration, immunomodulation, antibacterial, antiviral, and antioxidation. Oligopeptides containing the sequence of "arginine-glycine-aspartic acid" (RGD) can bind to integrin receptors of various cells, playing biological roles in antitumor, antithrombosis, and immune suppression by inhibiting functions of tumor cells, endothelial cells, platelets, and immune cells [320,321]. Beyond targeting capabilities, peptides can also undergo enzyme or pH-tuned conformational changes, leading to structural transformations for their self-assembled architectures as efficient supramolecular drug carriers. Using this strategy, Gong *et al*. [322] designed an amphiphilic peptide AYR with RGD as hydrophilic, enzyme-responsive end (Figure 19a). This peptide could self-aggregate into nanoparticles for encapsulating hydrophobic DOX under physiological conditions, while RGD modification improved its tumor targeting, prolonged DOX retention, and enhanced its anticancer efficacy. This design could be applied for other amphiphilic peptides for achieving enhanced anticancer activity [323]. In another effort, Yang *et al*. [324] coupled a tetrapeptide with hydrophobic anticancer drug 10-hydroxycamptothecin (HCPT) to form an amphiphile conjugate HpYss (Figure 19b), which could self-assemble to form nanoparticles under the stimulation of extracellular alkaline phosphatase (ALP), and further transform to nanofibers triggered by the intracellular GSH after cellular uptake. The nanoparticles were revealed to penetrate deeper into tumor tissues, enhancing the accumulation and retention of HCPT in tumor cells. For obtaining deeper tumor penetration, Zhu *et al*. [325] also developed a positively charged Y-shaped diacetylene lipidated peptide amphiphile, which underwent ROS-induced *in-situ* polymerization in cellular microenvironment to induce apoptosis of tumor cells and inhibit tumor metastasis. Amphiphilic dendritic peptides have been investigated as carriers for siRNA drugs [326,327]. Liu *et al*. [326] prepared amphiphilic phospholipid peptide dendrimers AmPPDs as carriers for castration-resistant prostate cancer therapy based on the gene silencing strategy (Figure 19c). The dendrimers contain natural lipid derivatives as hydrophobic tails and dendritic L-lysines as hydrophilic heads. siRNA drugs were compacted within their self-assembled structures to protect the drugs from enzymatic degradation

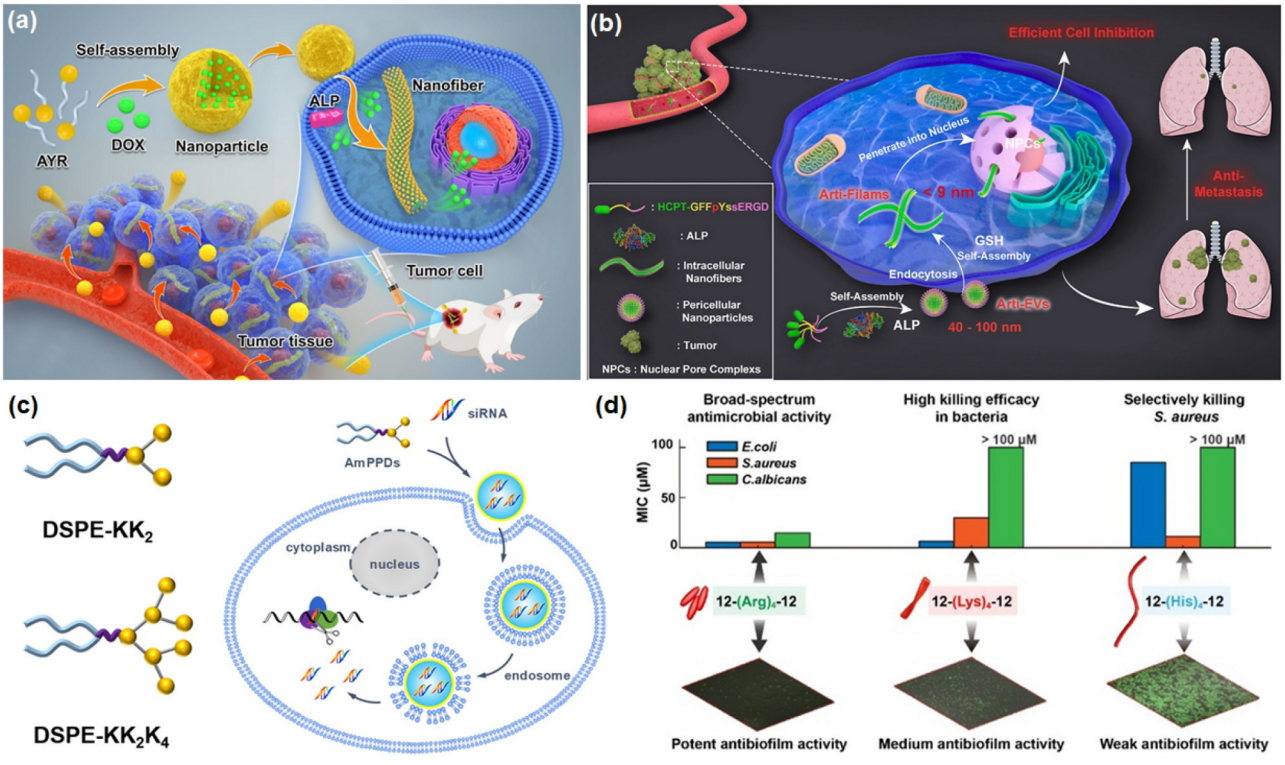


**Figure 19** Schematic illustrations of nanostructures formed by amphiphilic peptides and their function mechanisms. (a) Self-assembly of peptide AYR and morphological transformation triggered by ALP within cells [322]. (b) *In situ* sequential cellular internalization of HpYss for nucleus-targeting delivery through an organelle-mimicking cascade delivery strategy [324]. (c) Strategy for siRNA delivery using phospholipid peptide dendrimers AmPPDs with dendritic L-lysine as hydrophilic head [326]. (d) Self-assembly and antimicrobial property of gemini peptides with tetrapeptide spacers [328] (color online).

during delivery. It was found that carriers assembled with smaller dendritic peptides as the hydrophilic ends exhibited more efficient cellular uptake and intracellular siRNA release.

Another important application of amphiphilic peptide assemblies is the development of antibacterial agents [328–330]. For example, Wang *et al*. [328] prepared three gemini peptide amphiphiles with basic tetrapeptide as hydrophilic segment and dodecyl chain as hydrophobic segment (Figure 19d), which exhibited different antibacterial/antibiofilm activities. The 12-$(Arg)_4$-12 peptide assembled into short rods, which easily dissociated into monomers for membrane penetration and lysis, demonstrating broad-spectrum antibacterial activity and efficient biofilm clearance, while the relatively less polar 12-$(Lys)_4$-12 peptide formed long rods, which exhibited reduced propensity to disassemble into monomers for further membrane penetration, thus selectively killing more negatively charged bacteria and imparting moderate antibiofilm activity. The low-polarity 12-$(His)_4$-12 peptide assembled into long fibers, resulting in the weakest antibacterial and antibiofilm activities.

### 7.3 Nucleic acids and nucleotide derivatives

Nucleic acids and nucleotides are carriers of genetic information and can be used for gene expression regulation, cellular signal transduction, and immunomodulation. These functions, along with their outstanding hydrophilicity, mature synthesis, and modification techniques, have made them useful materials for constructing biofunctional supramolecular nanostructures [331–334]. For example, to address the short half-life, poor stability, and low membrane permeability of cyclic di-GMP (CDG), a stimulator of interferon genes (STING) agonist, in blood circulation, Xu *et al*. [331] combined it with cytidine-modified oleic acid molecules by base pairing to form amphiphilic dimers that could assemble into stable supramolecular nanoparticles CDG-NPs (Figure 20a). Compared with free CDG, CDG-NPs could activate STING more efficiently, and had more outstanding performance in reprogramming the immunosuppressive tumor microenvironment (TME) and enhancing the tumor immunogenicity of TME. Fu *et al*. [332] created a novel amphiphile by linking hydrophobic methotrexate and thymidylate synthase inhibitor fluorouracil (FUDR) *via* base pairing (Figure 20b), which self-assembled to afford a cancer cell mimetic nanoplatforms (M:F NPs) that could be employed for osteosarcoma treatment. Upon co-extruding with membrane materials derived from osteosarcoma cells to form cancer cell membrane-coated nanoparticles (CCNPs), it could significantly inhibit the key regulatory pathway of osteosarcoma, PI3K/AKT/mTOR. Spherical nucleic acids (SNAs) are nanostructures comprising a densely packed, highly oriented arrangement of linear nucleic acids in a three-dimensional space. Xiao *et al*. [333] synthesized amphiphilic block copolymer polystyrene-*b*-DNA (Figure 20c), which self-assembled to micelles that could cross the blood-brain barrier *via* a macrophage-mediated phagocytosis pathway. Upon loading with NIR-II fluorescent molecules, the micelles could be used for *in situ* diagnosis and imaging of glioblastoma.

## 8 Supramolecular and flexible organic frameworks

### 8.1 Supramolecular organic frameworks

In the past two decades, regular porous architectures such as metal- [335,336], covalent- [337–342], hydrogen bonded- [343,344], and halogen bonded- [345] organic frameworks have received considerable attention due to their diverse functions and applications which are mainly obtained from their efficient adsorption for many kinds of guests. However, such kinds of crystalline porous materials are typically insoluble in water. Thus, as biofunctional materials, they may have drawbacks, such as phase separation, slow decomposition and metabolism, and long-term accumulation in the body. Two-dimensional supramolecular organic frameworks have been established to exhibit regular porosity [177,346–348]. Since 2014, Li and co-workers [349] have constructed a variety of water-soluble three-dimensional (3D) diamondoid supramolecular organic frameworks (dSOFs) through the hydrophobically driven co-assembly of CB[8] and tetraphenylmethane-based tetracationic building blocks TP-a-h (Figure 21). dSOFs have intrinsic regular nanoscale porosity [68], ranging from 2.0 to 3.6 nm, which is determined by the length of the aromatic arms of the tetrahedral components. The regularity or periodicity of these 3D frameworks in aqueous media is confirmed by solution-phase X-ray scattering experiments. The X-ray diffraction analysis of one dSOF formed by a 4,4′-bipyridinium viologen-incorporated precursor also conforms the 3D porous structure [350]. Depending on the concentration of the components, dSOFs have varying sizes from 50 to 150 nm. All the dSOFs are prepared at the highest concentration of the tetrahedral components by heating the two components in a 2:1 ratio in boiling water [349,351–360]. Once formed, these frameworks could maintain their nanoscale sizes at the low concentration of 50 μM at room temperature, which indicates that they all exist in non-equilibrium state due to the high energy barrier for the decomposition of the interlocked binding pattern [361], whereas the substituents of the tetrahedral components do not have an important influence on their stability.

All the dSOFs formed by tetrahedral components that contain four 4-phenylpyridinium units produce a relatively fixed aperture of 2.1 nm. Li *et al*. [353,354,356] demon-

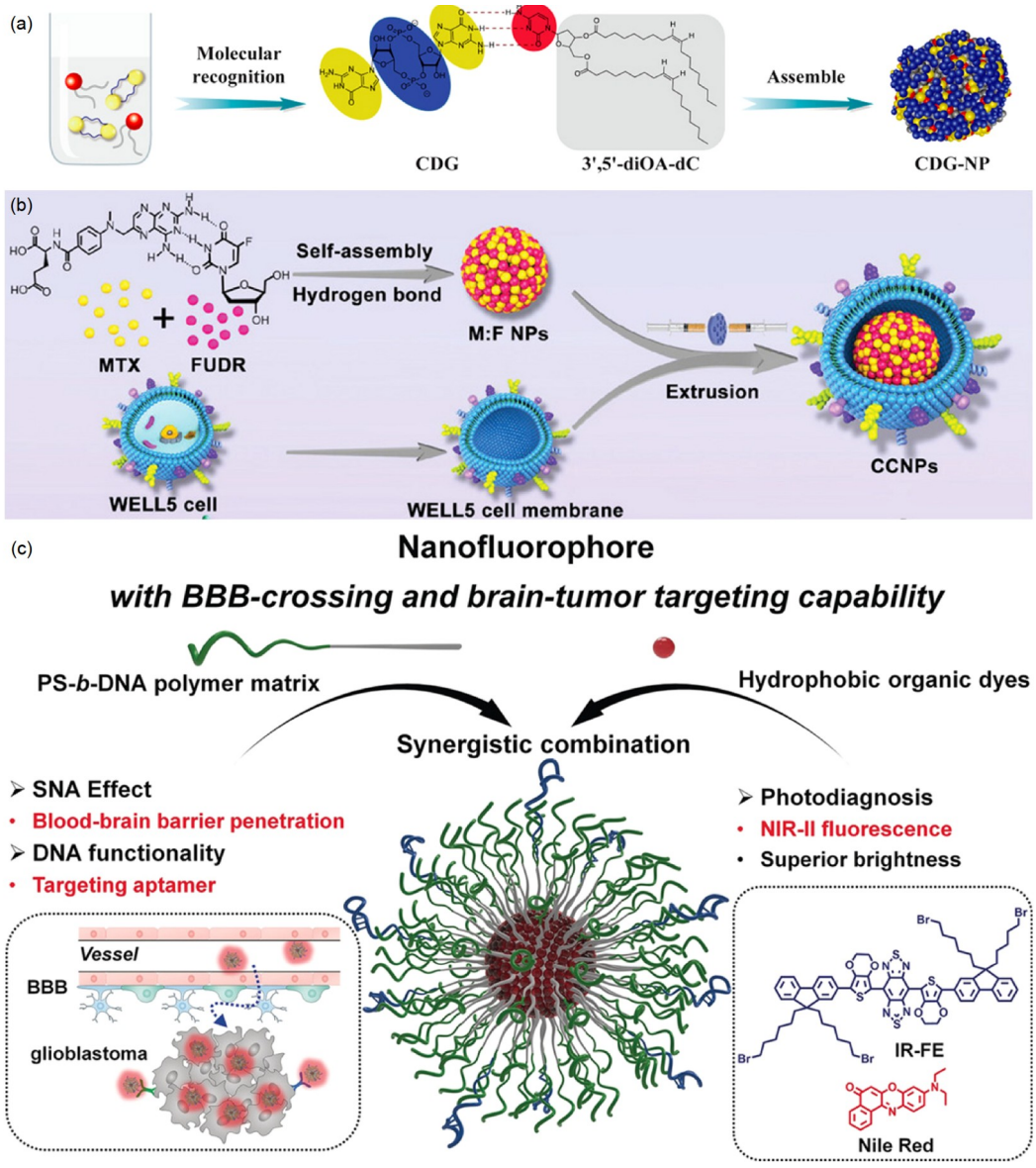


**Figure 20** Schematic representations of amphiphilic nucleic acids and nucleotides and their self-assembly behaviors. (a) Base pairing-induced combination of hydrophilic CDG and its hydrophobic partner [331]. (b) Construction of base pairing-based M:F NPs and cancer cell membrane coating process [332]. (c) Construction of organic fluorescence-emitting SNA [333] (color online).

strated that, like polycationic liposomes, these dSOFs exhibit good ability in intracellular delivery of drugs and short DNA. Moreover, the good water-solubility of SOFs also allowed them to act as solubilizing materials for hydrophobic drugs in water [362]. Li *et al*. [363] showed that the tetrahedral component TP-hdz could also be prepared through the dynamic hydrazone bond (Figure 21). This compound was stable in water and co-assembled with CB[8] to afford the corresponding dSOF-hdz, which also exhibited a good ability for intracellular delivery of DOX. In principle, the hydrazone bonding may be more easily decomposed in acidic microenvironment of cancer cells, which, however, needs to be confirmed experimentally. Temoporfin is a hydrophobic porphyrin PDA clinically applied for the treatment of skin cancers but suffers from aggregation in the body, which is harmful for its photosensitization for the generation of ROS. Ma and Li *et al*. [358] showed that temoporfin can be adsorbed by dSOF-a,b,h, leading to important improvement of its photocytotoxicity toward four different human cancer cells and tumor growth in mice.

Prodrugs have been demonstrated to be efficient in overcoming the discrete drawbacks of many drugs. One prodrug of DOX is aldoxorubicin that has been subjected to clinical trials (Figure 21) [364]. Aldoxorubicin has been proposed to undergo maleimide-thiol conjugation with albumin in blood, and this conjugation allows for its delivery by albumin to tumor sites to release doxorubicin through hydrazone hydrolysis, which is facilitated by the acidic microenvironment

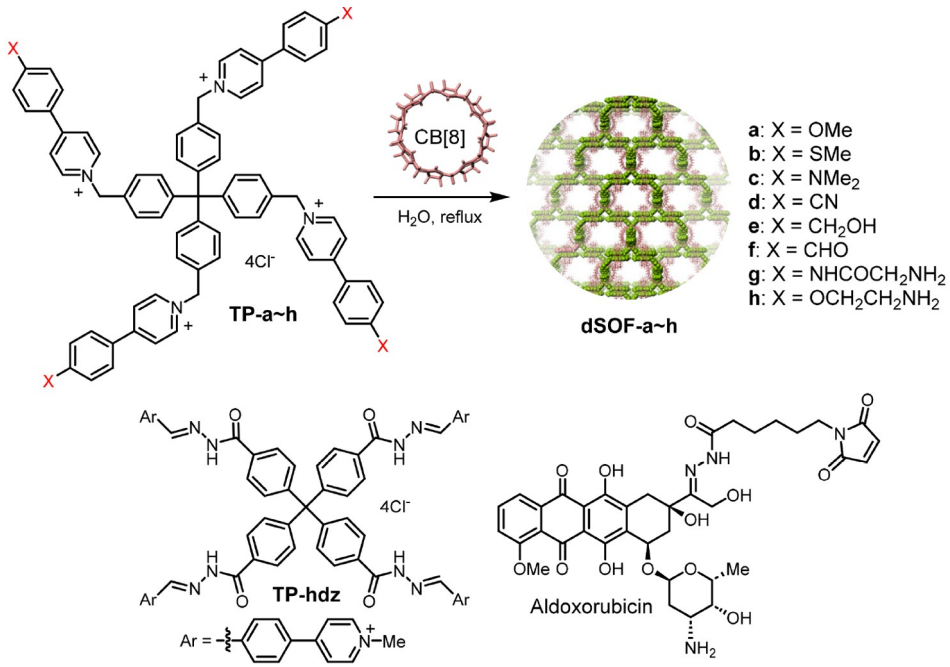


**Figure 21** The preparation of dSOF-a–dSOF-h from tetrahedral compounds TP-a–TP-h and CB[8] in water, and chemical structures of TP-hdz and aldoxorubicin (color online).

of the cancer. However, phase II clinical trials show that aldoxorubicin does not exhibit considerable efficacy enhancement. Li *et al*. [360] further modified dSOF-a and dSOF-b by introducing thiol groups to the corresponding tetrahedral component TP-h (Figure 21). Both prodrugs displayed important enhancement of the anti-cancer efficacy but did not show cardiotoxicity, which has been considered as the major superiority of aldoxorubicin over doxorubicin. The delivery of the framework has been proposed to account for the activity enhancement.

All clinically used PDAs, including photofrin, talaporfin, and hiporfin, are porphyrin derivatives that bear two or more carboxylate groups. The hydrophobicity of the porphyrin unit leads to their posttreatment aggregation in the body, which causes long-term posttreatment phototoxicity but lacks therapeutic remedies. Li *et al*. [365] studied the ability of dSOFs to restrain their posttreatment phototoxicity (Figure 22). Mouse model experiments supported that dSOF-h significantly restrained the posttreatment phototoxicity of the PDAs. Moreover, the injection of the framework did not cause a reduction of their PDT efficacy. Heparins, including unfractionated heparin (UFH) and low molecular weight heparins (LMWHs), are polysaccharides with one unit bearing two negative charges in average. They are clinically used as anticoagulants, but all have bleeding risk. Li *et al*. [359] further demonstrated that both dSOF-1 and dSOF-h could include UFH, LMWHs as well as synthetic pentasaccharide fondaparinux, which is driven by cooperative intermolecular ion-pairing electrostatic interactions. *In vitro* and *in vivo* experiments revealed that dSOF-h could fully

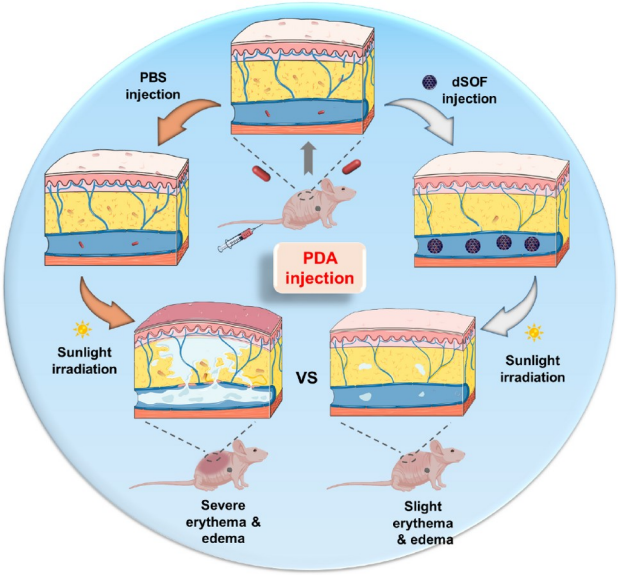


**Figure 22** Schematic illustration of the accelerated systemic clearance and reduced skin phototoxicity of PDAs *in vivo* by dSOFs [365] (color online).

neutralize UFH, LMWHs, including dalteparin, enoxaparin and nadroparin, as well as pentasaccharide fondaparinux. Similar neutralization activity can be observed for other kinds of cationic porous polymers [357]. Cao *et al*. [366] constructed two-dimensional SOFs from CB[8] and hexaphenylbenzene (HPB) for recognizing and distinguishing sequence-opposite Trp-/Phe-containing dipeptide pairs. Another strategy reported by Liu *et al*. [166] involves com-

bining CB[8] with MOFs to form metal-organic rotaxane frameworks (MORFs), which displayed highly fluorescent emission and selective detection of antibiotics such as nitrofurazone at low detection limit.

### 8.2 Flexible organic frameworks

The formation of the above dSOFs requires the tetrahedral components to be highly water-soluble due to the low water-solubility of CB[8]. As biomaterials, the intrinsic porosity of dSOFs plays an important role in adsorbing bioactive guests or drugs, whereas their periodicity might not be indispensable for the generation of biofunctions. To test this speculation, Li and co-workers [367–372] developed the so-called flexible organic frameworks (FOFs). Their preparation has been realized by making use of the multivalency principle, which allows for quantitative formation of dynamic hydrazone or disulfide bond from hydrophilic precursors in water (Figure 23a). These dynamic covalent polymers possess intrinsic porosity, while their sizes range from 20 to 100 nm depending on the concentration of the molecular precursors. FOFs formed from FP-Aa and FP-Ha–FP-Hd were found to include proteins to realize intracellular delivery [367]. FOFs obtained from the condensation of FP-Ab and FP-Ha–FP-He were revealed to include and deliver short single- and double-stranded DNA [368]. The mixture of FP-Ac and FP-Hg in 1:2 ratio gave rise to FOF-Ac/Hg that bears one more free acylhydrazine group for one FP-Hg linker (Figure 23b) [369]. This acyhydrazine could be conjugated with DOX by forming hydrazone at its C-13 keto position to afford a self-delivered FOF prodrug. The loading amount of doxorubicin can be changed by controlling the relative amount of doxorubicin. This prodrug with 8% doxorubicin loading was revealed to increase the anti-tumor activity compared with free doxorubicin. FOFs prepared from FP-Ac, FP-Ha, and FP-Hf were demonstrated to include endotoxin to significantly decrease its toxicity *in vivo* [371]. The oxidative coupling of FP-S by hydrogen peroxide leads to the formation of anionic FOF-s/s [372]. Since the backbone is generally hydrophobic, this FOF was found to include discrete neuromuscular block agents cisatracurium and rocuronium. This inclusion reduced the residual concentration of the block agents and thus reduced their block activity.

## 9 Supramolecular photodynamic therapy

### 9.1 Supramolecular approach to enhancing ROS generation efficiency of photosensitizers

PDT serves as a valuable complement to the treatment of malignant tumors and remains a prominent focus in cancer treatment research [373,374]. PDT offers various advantages, including minimal invasiveness, high spatiotemporal selectivity, and negligible drug resistance [375]. However, clinically used PSs also have several drawbacks [376], including strong aggregation, posttreatment phototoxicity, and oxygen-dependent efficacy. To address these challenges, supramolecular approach has emerged as a promising avenue for the development of new effective PSs [377], which allows for the convenient modulation of intermolecular distance and molecular orientation of PSs to regulate their aggregation state and influence their behavior in the excited state. This controllable supramolecular assembly

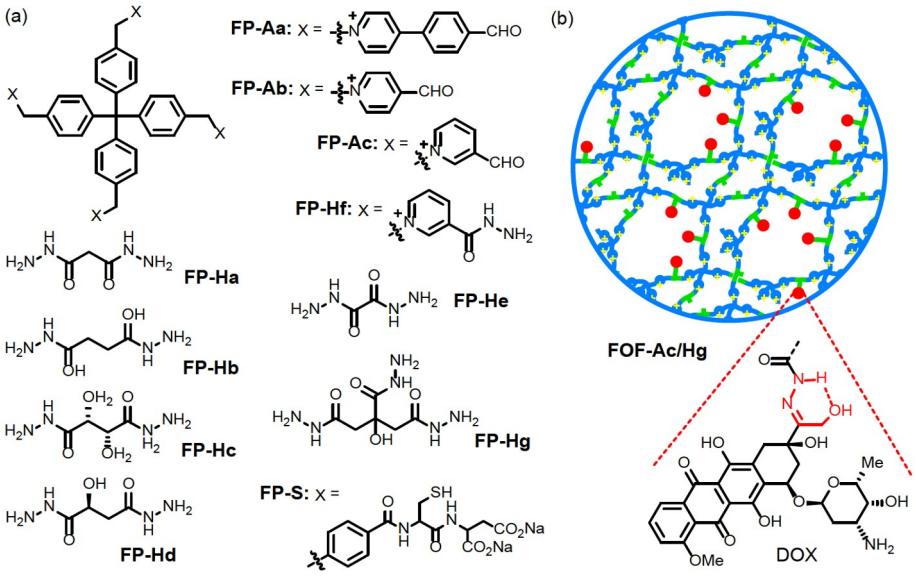


**Figure 23** (a) The structures of compounds used for the preparation of FOFs. (b) Schematic representation of FOF-Ac/Hg prepared from FP-Ac and FP-Hg (color online).

serves dual purposes—to prevent ACQ of PS activity and to enhance intersystem crossing (ISC) efficiency for the generation of triplet excited states, thereby improving the efficiency of ROS production [378]. Additionally, supramolecular assembly is dynamic and thus may be responsive to external stimuli [379–382]. To ensure that PS exhibits robust absorbance at NIR region and high quantum yield for ROS generation, PSs are often designed with conjugated and rigid structures like porphyrin [383], which however, tend to aggregate, leading to self-quenching of the excited state [384–388]. To inhibit the ACQ of PSs, Zhang *et al*. [389] developed a new supramolecular host-guest strategy. For instance, they used CB[7] to complex hydrophobic aromatic moieties attached to porphyrin to construct supramolecular PS (Figure 24a), which disrupted the close stacking of the porphyrin unit and thereby suppressed the self-quenching of its excited states, leading to improved PDT efficiency [390,391]. Wang and Cong *et al*. [392] demonstrated that other macrocycles could also be used for this purpose. For example, fluorescent hydrophilic cyclophanes AnBox·4Cl and ExAnBox·4Cl were revealed to effectively bind with hypocrellin B (HB), a pharmaceutically active natural PS for PDT (Figure 24b). The binding constants reached the level of $10^7$ $M^{-1}$, and the resulting supramolecular PSs (HB ⊂ $AnBox^{4+}$ and HB ⊂ $ExAnBox^{4+}$) displayed excellent stability, biocompatibility, and high efficiency of ROS generation, leading to outstanding PDT efficiency against cancer cells.

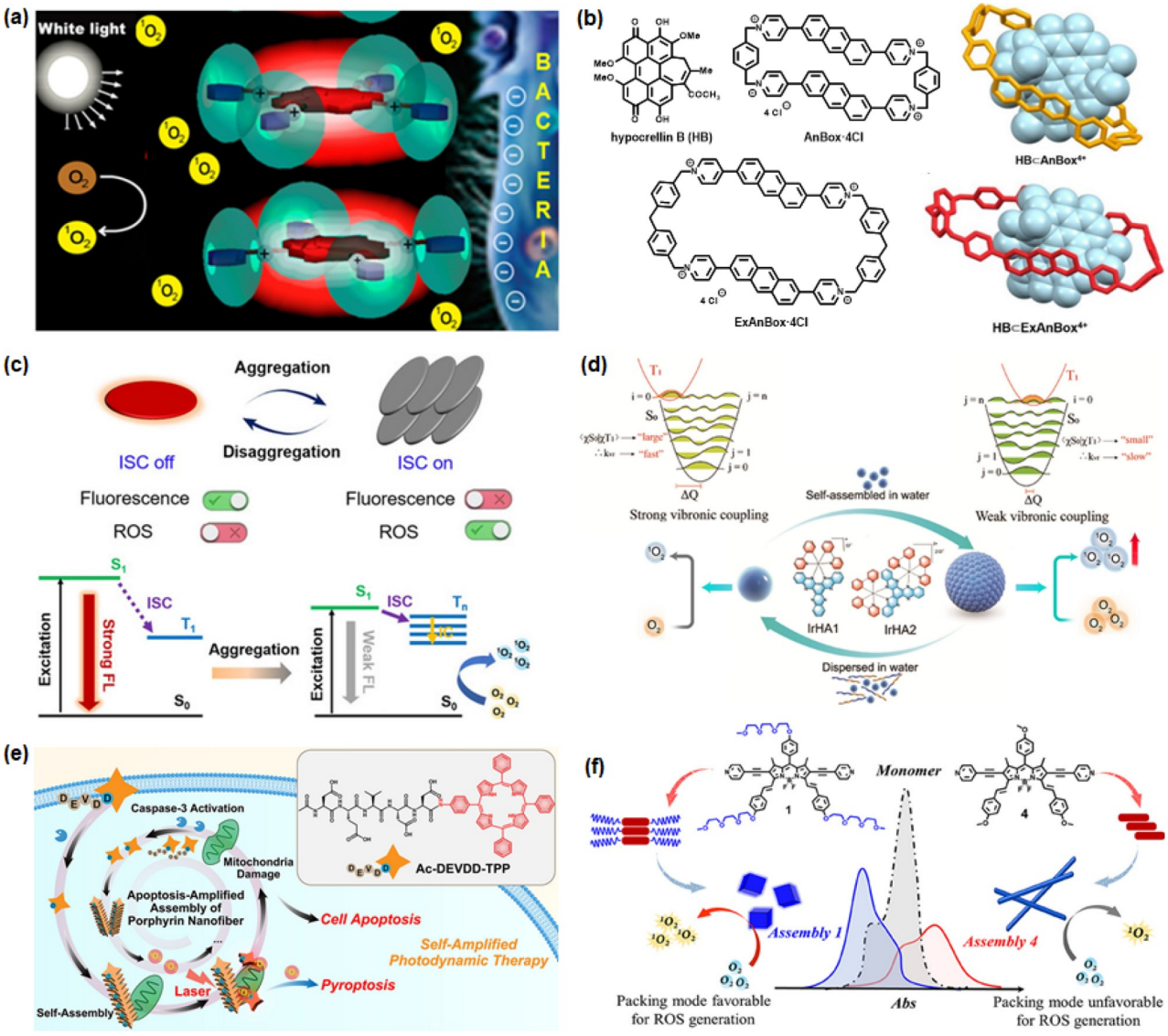


**Figure 24** Supramolecular approaches toward enhancing ROS generation efficiency. (a) Host-guest strategy using spacer to mitigate ACQ of PSs [389]. (b) Macrocycles AnBox·4Cl and ExAnBox·4Cl as receptors for PS HB [392]. (c) Assembly turning fluorophores into PSs with switching ISC on and off [393]. (d) ROS generation by photosensitizers IrHA1 and IrHA2 through the conversion from self-assembled states and dispersed states [394]. (e) Self-amplified PDT through apoptosis-amplified assembly of porphyrin nanofibers [395]. (f) Assembly of dyes: modification with TEG chains and impact on ISC processes and $^1O_2$ generation [396] (color online).

Studies on dye aggregation states reveal that some PSs do not undergo quenching upon aggregation by controlling molecular orientation to modify intermolecular orbital interactions, elevate spin-orbit coupling coefficient, and reduce singlet-triplet energy gap [397], which are combined to enhance the ISC efficiency for generating ROS. Tang *et al*. [398,399] developed PSs that featured AIE characteristics for PDT applications. These PSs do not manifest photodynamic activity in solution but exhibit remarkable photodynamic activity upon aggregation, which positions them as exemplary instances of PSs that leverage aggregation for enhanced ROS generation and photodynamic activity [400–404]. Yang, Cui, and Niu *et al*. [393] presented a practical and straightforward example for transforming fluorophores into PSs (Figure 24c). In contrast to previously reported AIE PSs, these PSs were designed through the aggregation of fluorophores without additional chemical modifications to achieve reversible switching between fluorescent dyes and heavy-atom-free PSs through aggregation and disaggregation. Notably, BODIPY derivatives exhibited bright fluorescence and generated negligible $^1O_2$ in solution. Conversely, aggregation suppressed fluorescence emission and enhanced $^1O_2$ generation, leading to excellent performance in PDT. Gou, Xia, and Xu *et al*. [394] utilized intermolecular coupling in meticulously designed PSs IrHA1 and IrHA2 to facilitate exciton delocalization (Figure 24d), which reduced exciton-vibration coupling and thereby enhanced their PDT effectiveness by obstructing the vibrational relaxation pathway. The PSs exhibited significantly improved $^1O_2$ generation efficiency due to exciton-vibration decoupling and effective suppression of vibronic couplings originating from the stretching mode of the acceptor ligand. In phototherapy, IrHA2-NPs nanoparticles exhibited remarkable biocompatibility and low dark toxicity, resulting in substantial tumor regression.

Although supramolecular assembly strategy has shown promise in enhancing ROS generation of PSs, their administration has been a challenge. *In situ* self-assembly of PSs into nano-sized structures provides a solution [405]. For instance, Liang *et al*. [395] engineered water-soluble porphyrin derivative Ac-DEVDD-TPP (Figure 24e). Following caspase-3 cleavage, a pivotal event in apoptosis, and subsequent laser irradiation, Ac-DEVDD-TPP transformed to D-TPP and further configured into porphyrin nanofibers, yielding 1.4- and 2.1-fold increase in $^1O_2$ generation *in vitro* and in cells, respectively. The resulting porphyrin nanofibers could efficiently induce cell apoptosis and pyroptosis. Compared to control Ac-DEDVD-TPP, Ac-DEVDD-TPP prompted 6.2- and 1.3-fold increase in the expression of caspase-3 in subcutaneous and orthotopic oral tumor models, respectively. PDT activity of PSs is profoundly affected by their assembly states [406]. Yang, Cui, and Niu *et al*. [396] illustrated the modulation of $^1O_2$ generation by manipulating the self-assembly of heavy-atom-free BODIPY derivatives (Figure 24f). This manipulation involved the incorporation of various tetraethylene glycol (TEG) chains on the BODIPY core. Distinct self-assembly behaviors led to significant changes in both the structures and efficiency of ISC, resulting in marked disparity in the efficiency of generating $^1O_2$, with up to 74.9-fold increase in the rate of $^1O_2$ generation. Different molecular stacking modes, which influenced the energy splitting of optically allowed transitions, were proposed to account for the great difference.

### 9.2 Supramolecular approach to controlling ROS generation efficiency of photosensitizers

Clinical translation of PDT has been hindered by its unexpected dark toxicity due to the "always on" model and low lesion specificity of PSs [407,408]. Supramolecular self-assembly provides a valuable approach to tackling this issue by controlling ROS production to facilitate the construction of "turn-on" or "turn-off" systems [25,409,410], which can effectively mitigate the dark toxicity concerns of PSs on normal tissues and organs, allowing for intelligent modulation of their performance and enhancing their specificity in lesion targeting. For example, Guo and Ding *et al*. [411] established a new host-guest strategy for constructing activatable PDT and biomarker displacement activation (BDA) (Figure 25a). In BDA, a PS is preloaded into the cavity of a macrocycle to lock its photoactivity. When encountering a biomarker overexpressed at the lesion site, the competitive inclusion of the biomarker induces the release of the PSs to trigger its photoactivity. Employing ATP as a biomarker, whose concentration in tumor tissues is $>10^4$-fold higher than that in normal tissues, guanidinium-modified calix[5]arene pentadodecyl ether GC5A-12C as carrier, and sulfonated aluminum phthalocyanine $AlPcS_4$ as PS, they achieved ATP-activated PDT for tumor ablation. $AlPcS_4$@GC5A-12C exhibited significantly lower toxicity and superior therapeutic efficacy than $AlPcS_4$. Remarkably, the principle can be expanded to bioimaging, chemotherapy, and immunotherapy for precise diagnosis and/or treatment of cancer, SARS-CoV-2, and cholestasis [412–414]. Tang, Ding, and Feng *et al*. [415] introduced a supramolecular cascade substitution strategy to adjust the dark cytotoxicity of PSs (Figure 25b). Pyridinium-functionalized TPE derivative TPE-PHO displayed pronounced dark cytotoxicity and high photo-induced ROS generation efficiency, which, however, could be weakened by the complexation of water-soluble calixarene. The resulting nano-assemblies thus exhibited enhanced biocompatibility. Competitive displacement of TPE-PHO from the calixarene cavity by 4,4′-benzidine dihydrochloride at the tumor site reinstated the dark cytotoxicity and photoactivity of TPE-PHO specifically within the tumor tissue, leading to improved PDT efficacy.

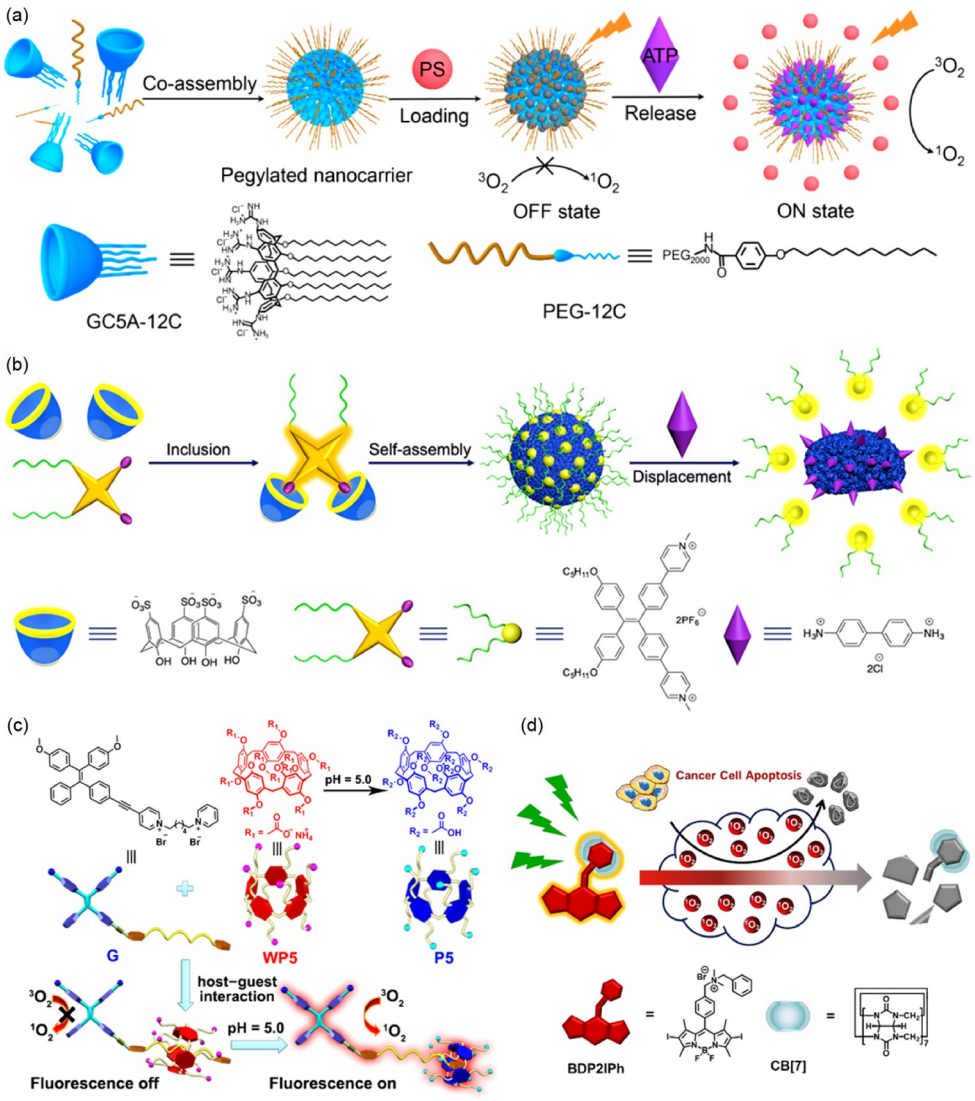


**Figure 25** Supramolecular approaches toward controlling ROS generation efficiency. (a) Pegylated GC5A-12C nanocarrier for BDA [411]. (b) Substitution-activated PS [415]. (c) Structures and cartoon representations of WP5, P5, and G [416]. (d) Self-degradable host-guest complex PS formed by BDP2IPh and CB[7] for PDT [417] (color online).

AIE-type PSs are promising materials for PDT without ACQ but also suffer from unexpected toxicity to normal tissues due to their "always-on" nature [418,419]. To address this limitation and improve PDT precision, Huang and Liu *et al*. [416] constructed a pH-activated supramolecular switchable PS based on host-guest interaction between water-soluble pillar[5]arene WP5 and AIE-PS G (Figure 25c). This complex exhibited negligible PDT activity in a neutral environment. In the acidic tumor microenvironment, WP5 was protonated to P5, leading to aggregation and subsequent $^1O_2$ generation for PDT. This pH-dependent activation allowed the complex to target tumors with minimal or no damage to normal cells. Another approach to addressing PS residual that causes damage to normal tissues involves the design of "turn-off" PSs [420,421]. For example, Zhang and Xu *et al*. [417] reported that cationic BODIPY derivative BDP2IPh co-assembled with CB[7] to form a host-guest complex through the benzyl unit (Figure 25d). The resulting supramolecular PS exhibited both improved PDT efficacy and biocompatibility. Notably, the supramolecular PS could undergo degradation triggered by ROS, ceasing the PDT activity and thus reducing its posttreatment side effects.

### 9.3 Supramolecular approaches to regulating ROS generation mechanisms of photosensitizers

Most of the reported PSs operate through the Type-II PDT mechanism, *i.e*., generating singlet oxygen *via* triplet-triplet energy transfer from excited triplet PSs to molecular oxygen [422]. This process is highly oxygen-dependent [423]. Hypoxia tumor microenvironment limits the efficacy of PDT [424], and thus great effort has been devoted to the devel-

opment of novel PDT paradigms with low or non-oxygen dependence [425–430]. Type-I PSs have been established to be able to mitigate oxygen dependence, thereby circumventing direct and rapid oxygen depletion during PDT [431–435], while supramolecular interaction between chromophores and electron-rich or -deficient building units can reduce the distance between chromophores and electron donors/acceptors [436,437], thus facilitating fast photo-induced intermolecular electron transfer and ultimately leading to ROS generation through the Type-I PDT process. Yang *et al*. [438] reported a supramolecular strategy that converted conventional Type-II PSs to Type-I PSs through host-guest interaction-enhanced electron transfer (Figure 26a). The PS comprised iodo-BODIPY, known for generating singlet oxygen through the Type-II process, and bispillar[5]arene. Their host-guest interaction reduced the distance between the substrates and the PS, enhancing photoinduced electron transfer and resulting in the production of $O_2^{-\bullet}$ through the Type-I process. This interaction suppressed the generation of singlet oxygen, as enhanced electron transfer competed with energy transfer, converting the classical Type-II PS into Type-I PS. Using this approach, Yang *et al*. [439] also constructed Type-I PDAs to achieve electron transfer from the PS to electron acceptors for PDT. Song *et al*. [440] proposed a supramolecular strategy employing bovine serum albumin (BSA) as "electron reservoir" substrate and thermally activated delayed fluorescence (TADF) PS as "electron pump" to promote the Type-I PDT process (Figure 26b). Under light irradiation, electron transfer occurred from BSA to PS, and then further to $O_2$ to generate $O_2^{\bullet-}$. The effectiveness of this supramolecular PS for Type-I PDT was demonstrated in tumor cells under hypoxic conditions.

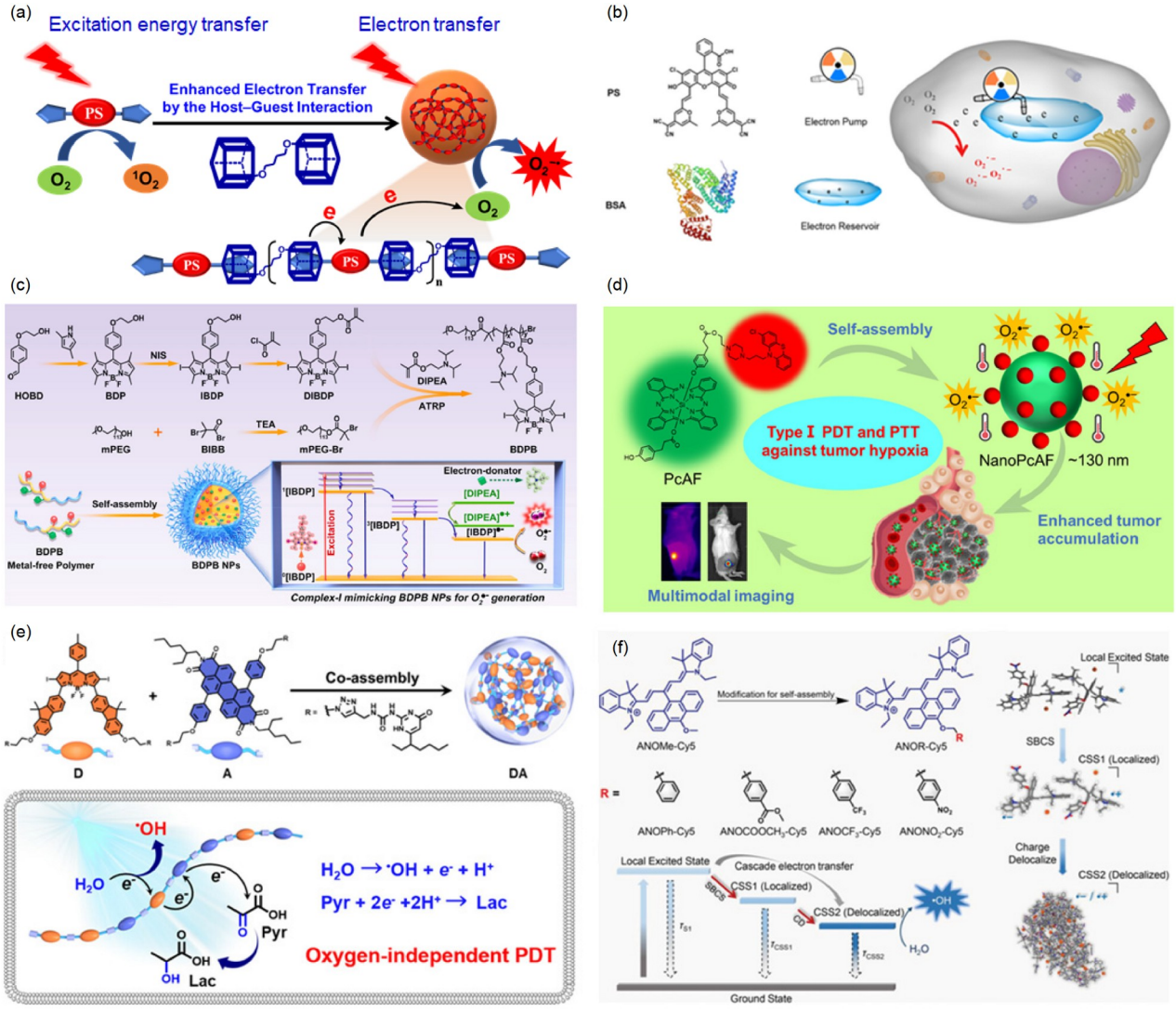


**Figure 26** Supramolecular approaches toward regulating ROS generation mechanisms. (a) Fabrication of supramolecular host-guest PS and photo-induced generation of ROS [438]. (b) Schematic illustration of PS as "electron pump" and BSA as "electron reservoir" in Type I PDT process [440]. (c) Preparation of BDPB NPs for $O_2^{\bullet-}$ generation [441]. (d) PcAF and NanoPcAF for Type-I PDT [442]. (e) DA preparation and photoinduced $^{\cdot}OH$ generation and pyruvic acid reduction [443]. (f) Chemical structure of ANOR-Cy5 and scheme of PICET-based $^{\cdot}OH$ generation [444] (color online).

Beyond introducing electron donors/acceptors through supramolecular co-assembly to enhance electron transfer is another approach, which involves direct incorporation of electron-rich/deficient units into PSs that undergo self-assembly to create nano-PSs to enhance the electron transfer process, thereby facilitating the construction of Type-I PSs. For example, Dong, Shao, and Cai *et al*. [441] prepared polymeric photosensitizer BDPB as ferroptosis inducer for starved cancer cells (Figure 26c). The polymer, composed of a BODIPY dye as PS unit and diisopropylethylamine (DIPEA) as electron-donating unit, underwent self-assembly to achieve prolonged charge separation and facilitate one-electron transfer, which resulted in the generation of $O_2^{\bullet-}$. In normal-state cancer cells, it deactivated the AMPK-mTOR signaling pathway, promoting cell repair activity and enabling survival after low-dose phototherapy. In starved cancer cells, it induced downregulation of GSH peroxidase 4 and accumulation of lipid peroxides, ultimately leading to cell death, identified as ferroptosis. Huang and Li *et al*. [442] created another Type-I nano-PS NanoPcAF (Figure 26d), which self-assembled through the axial monosubstitution of silicon (IV) phthalocyanine with perphenazine to achieve the transformation of traditional Type-II PS phthalocyanine into a Type-I PS. Under hypoxic conditions, this PS could generate 3.4 times more $O_2^{\bullet-}$ compared to the well-known PS methylene blue, and displayed a photothermal conversion efficiency 2.4 times higher than indocyanine green. This nano-PS showed significant $O_2^{\bullet-}$ generation *via* the Type-I mechanism and robust photothermal performance.

The above Type-I PSs are still $O_2$-indispensable, and the development of oxygen-independent PSs capable of generating ROS has been a challenge for PDT. To this end, Yang and Niu *et al*. [443] developed the first example of oxygen-independent supramolecular PDAs, which can generate highly toxic $^{\bullet}OH$ by directly oxidizing water (Figure 26e). The quadruple hydrogen-bonded supramolecular PDA is comprised of a BODIPY-based PS as electron donor and perylene diamide as electron acceptor. Upon light irradiation, intermolecular electron transfer and charge separation efficiently produced radical ion pairs. The ensuing cationic radicals directly oxidized water, yielding highly cytotoxic $^{\bullet}OH$, while the anionic radicals transferred electrons to pyruvic acid, completing the catalytic cycle. Noteworthy for its exceptional photocytotoxicity, this PDA demonstrated efficacy even in severe hypoxic environments and exhibited excellent *in vivo* antitumor performance in HeLa-bearing mouse model. In another work, Fan *et al*. [444] reported a nano-PS capable of generating $^{\bullet}OH$ independent of oxygen by introducing the concept of photoinduced cascade charge transfer (PICET) (Figure 26f), utilizing NIR heavy-atom-free PS ANOR-Cy5 to facilitate $^{\bullet}OH$ production. PICET, characterized by a symmetry-breaking charge separation-induced localized charge-separated state transitioning to a delocalized charge-separated state, played a vital role for $^{\bullet}OH$ generation. The hydrophobicity of ANOR-Cy5 allowed for nanoparticle formation in aqueous solution through supramolecular assembly. The resulting nano-PS exhibited a high $^{\bullet}OH$ generation yield through water oxidation. This ANOR-Cy5-based PS, owing to oxygen-independent $^{\bullet}OH$ generation and robust oxidative property, exhibited remarkably effective photoinduced anti-cancer effects even under severely hypoxic conditions.

## 10 Supramolecular photothermal therapy

Photothermal therapy (PTT) for cancer features its non-invasiveness, high controllability, precision, as well as negligible drug resistance [374,445]. As the mechanism of PTT, photothermal agents (PTAs) transform the absorbed laser energy into heat, which is independent of oxygen [446]. Hence, PTT can overcome the hypoxic environment, one of the main characteristics of solid tumors. The preferred laser used in PTT is NIR light around 700–1,700 nm [447–449]. Benefitting from less tissue absorption and scattering, the NIR light can realize deeper tissue penetration depth. The NIR range is divided into the first near-infrared (NIR-I, 700–1,000 nm) window and the second near-infrared (NIR-II, 1,000–1,700 nm) window. In comparison, NIR-II has a greater advantage in PTT because of the deeper tissue penetration and higher maximum-allowable exposure [450]. As NIR-absorbed PTAs, organic small molecules exhibit superiority in biocompatibility and biodegradability. Their self-assembly can further induce a redshift of their absorption because of the charge-transfer effect and *J*-aggregation effect [451–460]. Supramolecular free radicals refer to free radicals stabilized or activated through supramolecular approaches [460–462], which have been established as a new avenue for fabricating NIR photothermal materials. Perylene diimide (PDI) radical anions exhibit a typical red shift towards the NIR region. However, PDI radical anions are sensitive to oxygen and quenched rapidly in aqueous solution. Increasing the yield and stability of this free radical is the key link for the construction of PDI radical anions-based PTAs. To address this, Zhang *et al*. [463] reported a supramolecular strategy for the design of supramolecular PDI radical anions with significantly improved free radical yield and enhanced photothermal conversion efficiency (Figure 27a). PDI could undergo chemical reduction to generate PDI radical anion (DBA-PDI). CB[7] was utilized to encapsulate its two end groups to suppress the dimerization and quenching of PDI radical anion by forming DBA-PDI-2CB[7]. The characteristic absorption bands of the PDI radical anion at 732 and 819 nm increased significantly in intensity. The amount of PDI radical anions generated by DBA-PDI-2CB[7] complex was twice as many as the amount produced by PDI alone

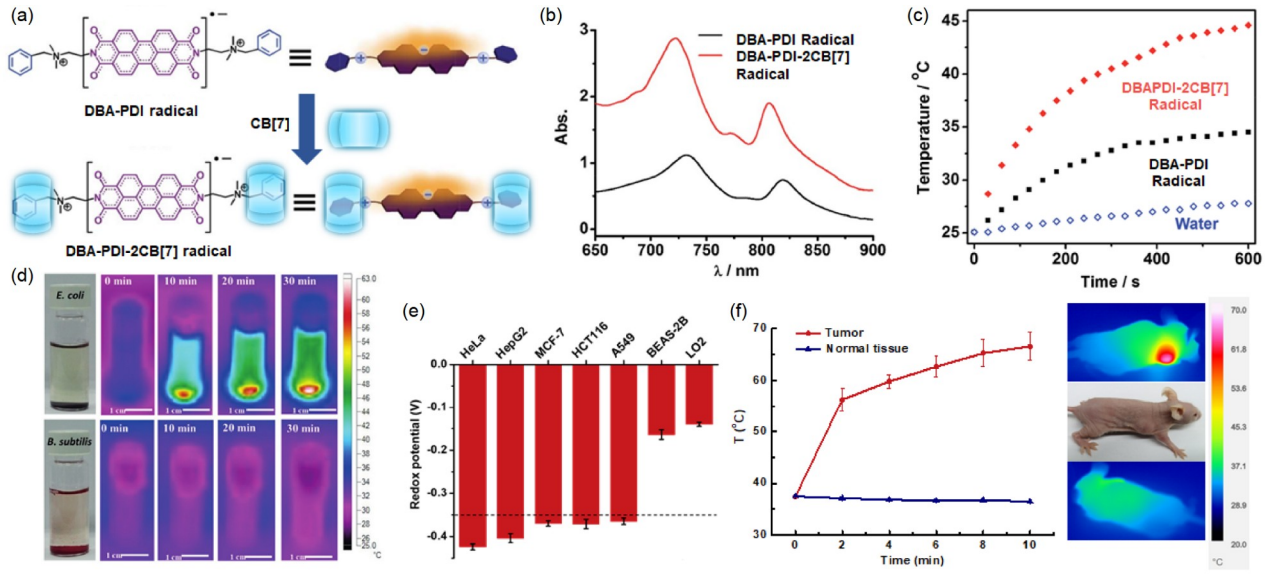


**Figure 27** Bio-reducible supramolecular radical anion for NIR PTT. (a) DBA-PDI radical and BDA-PDI-2CB[7] supramolecular radical [463]. (b) UV-vis spectra of DBA-PDI radical and DBA-PDI-2CB[7] supramolecular radical [463]. (c) Photothermal conversion of DBA-PDI radical and DBA-PDI-2CB[7] supramolecular radical under irradiation by 808 nm laser [463]. (d) Diagram of photothermal therapy for DBA-PDI-2CB[7]supramolecular radical with high selectivity towards *E. coli* over *B. subtilis* [464]. (e) Redox potentials of tumor cells under hypoxic conditions and normal cells under normoxic conditions [464]. (f) *In vivo* photothermal performances of DBA-PDI-2CB[7] supramolecular radical on HeLa tumor-bearing nude mice. Temperature changes of HeLa tumor and normal tissue *versus* irradiation time after coculturing with DBA-PDI-2CB[7] [465] (color online).

(Figure 27b) [463]. In consequence, the aqueous solution containing the DBA-PDI-2CB[7] supramolecular free radical showed a faster rate as well as a greater temperature increase than the solution containing DBA-PDI radical anion (Figure 27c) [463]. The photothermal conversion efficiency of DBA-PDI-2CB[7] supramolecular radical was determined to be 31.6%, which was much higher than that of 16.3% for DBA-PDI radical.

The redox property of PDI in aqueous solution well fits the redox microenvironment *in vivo*. Xu and Zhang *et al.* [464] developed a kind of bacterial responsive supramolecular PTAs that exhibited high selectivity towards facultative anaerobic bacteria like *E. coli* and *E. faecalis* (Figure 27d). Under NIR irradiation (808 nm), the temperature of the DBA-PDI-2CB[7] aqueous solution increased much higher in the presence of *E. coli* than *B. subtilis*. The selective antibacterial activity of the PDI-2CB[7] supramolecular radical could be realized by NIR-PTT. Moreover, the regions of various hypoxic tumors displayed strong reductive ability. The redox potentials of five kinds of tumor cells under hypoxic conditions ranged from −0.37 to −0.43 V *vs*. Ag/AgCl, which was lower than −0.35 V, the redox potential of DBA-PDI-2CB[7] to generate the radical (Figure 27e) [464]. Whereas the redox potentials of two kinds of normal cells under normoxic conditions were about −0.16 V. These results demonstrated that DBA-PDI-2CB[7] could be selectively reduced by hypoxic tumor cells. After DBA-PDI-2CB[7] was injected into the tumor and the normal tissue of mice, respectively, only the temperature of the tumor region increased remarkably after the whole body NIR irradiation (Figure 27f) [465]. Notably, the hypoxia tumor ensured the activation of DBA-PDI-2CB[7] supramolecular radicals for PTT. Furthermore, the supramolecular radical anion could be quenched by oxygen in normal tissues to turn off PTT, thereby significantly improving the biosafety of DBA-PDI-2CB[7].

Compared with the NIR-I biowindow, NIR-II light can realize larger penetration depth and maximum permissible exposure, and thus PTT at the NIR-II biowindow is drawing increasing interest. Xu and Zhang *et al.* [466] established a supramolecular radical dimer strategy using π-conjugated structure to achieve strong absorption at NIR-II biowindow (Figure 28a), which is different from the classic strategy that relies on large π-conjugates containing electron-donor/acceptor moieties. The rigid acceptor-donor-acceptor structure of *N*,*N*′-dimethylateddipyridinium thiazolo[5,4-d]thiazole ($MPT^{2+}$) could form a supramolecular dimer inside the cavity of CB[8]. The 2:1 host-guest complex $2MPT^{2+}$-CB[8] was easily fabricated with high binding constant. After $MPT^{2+}$ was reduced into radical cation $MPT^{\bullet+}$, a strong absorption at 1,004 nm appeared due to host-enhanced intermolecular charge transfer between the two $MPT^{\bullet+}$ encapsulated in CB[8]. In addition, supramolecular radical dimer $2MPT^{\bullet+}$-CB[8] showed improved stability and redox reversibility. Benefiting from the strong NIR-II absorption and high photostability, $2MPT^{\bullet+}$-CB[8] exhibited more efficient and

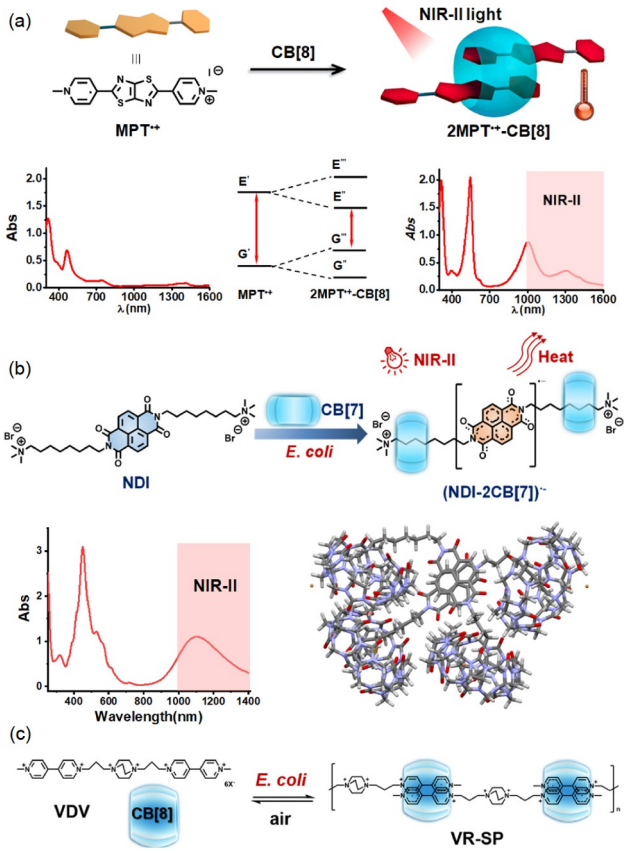


**Figure 28** Supramolecular radical dimer for efficiency NIR-II PTT. (a) $2MPT^{\bullet+}$-CB[8] system and its UV/vis-NIR absorption [466]. (b) The chemical structure, UV/vis-NIR absorption, and simulated conformation of NDI-2CB[7] supramolecular radical anion [467]. (c) Supramolecular polymerization powered by *E. coli* for NIR-II photothermal antibacterial. The figure presents chemical structure of the bifunctional monomer VDV, CB[8], and supramolecular polymer VR-SP [468] (color online).

reliable photothermal conversion than $MPT^{\bullet+}$ alone. The photothermal conversion efficiency of $2MPT^{\bullet+}$-CB[8] was as high as 54.6%. $2MPT^{\bullet+}$-CB[8] showed strong inhibition on human hepatic cancer cells through photothermal ablation even penetrating through a 5 mm thick chicken breast, thus exhibiting a great potential in deep tissue PTT.

As π-electron-deficient aromatic unit, naphthalene diimide (NDI) can be reduced to a radical anion. However, the absorption of NDI radical anion is in the visible region. Zhang *et al*. [469] reported that NDI radical anions ($NDI^{\bullet-}$) could be stabilized through CB[7] encapsulation, while Xu *et al*. [467] disclosed that the supramolecular radical anion $(NDI\text{-}2CB[7])^{\bullet-}$ could exhibit strong NIR-II absorption due to dimerization (Figure 28b), which displayed two characteristic absorption bands at 450 and 1,000–1,400 nm. The NIR-II absorption was attributed to the dimer radical. With strong reductive ability, *E. coli* could reduce NDI-2CB[7] to $(NDI\text{-}2CB[7])^{\bullet-}$. Antibacterial experiments with 1,064 nm laser indicated that $(NDI\text{-}2CB[7])^{\bullet-}$ was a highly efficient and stable NIR-II PTA. Its inhibition efficiency against *E. coli* was up to 99%. To further improve antibacterial efficiency, supramolecular free radicals could be assembled into polymeric PTA. Xu *et al*. [468] fabricated an NIR-II antibacterial PTA through *E. coli* reduction-powered *in situ* supramolecular polymerization (Figure 28c). Bifunctional monomer viologen-diazabicyclo[2.2.2]octane-viologen VDV was reduced by *E. coli* to viologen cation radical in hypoxia condition. The supramolecular dimerization of viologen cation radicals in the cavity of CB[8] was used to achieve supramolecular polymerization. The resulting supramolecular polymer VR-SP, with supramolecular dimers of viologen cation radicals integrated into the main chain, could be generated on the surface of *E. coli*. The supramolecular dimer of viologen cation radicals showed NIR absorption around 872 nm. After being incubated with *E. coli*, viologen cation radical-based supramolecular polymer (VR-SP) converted optical energy into heat more efficiently than VDV alone under NIR irradiation. The inhibition efficiency of VR-SP against *E. coli* was up to 99.9% after 12.5 min of 1,064 nm irradiation. After finishing the inhibition of *E. coli*, the supramolecular polymer could be spontaneously depolymerized into monomers by air oxidation, thereby showing an adaptive responsiveness to different biological environments.

PTT and PDT are normally implemented under different conditions for bacterial infections, while bacteria can exist in both aerobic and hypoxia atmospheres. In an oxygen environment, photosensitized ROS is efficient for therapy [470–472], while in a hypoxia environment, the photothermal conversion is the priority way for therapy. If the photoactive molecule could be switched between PS and PTA according to the corresponding circumstances, a smart antimicrobial treatment with adaptivity and specificity could be expected. To this end, Xu *et al*. [144] designed a cationic porphyrin 5,10,15,20-tetrakis-(4-*N*-methylpyridyl)-porphyrin TMPyP that could realize adaptable photodynamic/photothermal therapy processes (Figure 29a). TMPyP acted as PS in the aerobic environment and could be transformed to PTT agent with NIR absorption after being reduced by facultative anaerobes. The redox potentials of *E. coli*, *S. typhimurium*, and *E. faecalis* as facultative anaerobes were −551, −530, and −429 mV, respectively. For aerobic bacteria like *P. aeruginosa* and *B. subtilis*, the redox potential was measured to be −289 and −171 mV, respectively. Among these bacteria, the redox potentials of *E. coli* and *S. typhimurium* were clearly lower than the first one-electron reduction potential of TMPyP (−455 mV), and the redox potential of *E. faecalis* was close to that of TMPyP. Therefore, TMPyP could be reduced by these facultative anaerobes in hypoxic environment to produce phlorin, which possessed NIR absorption centered at 660 nm (Figure 29b) [144].

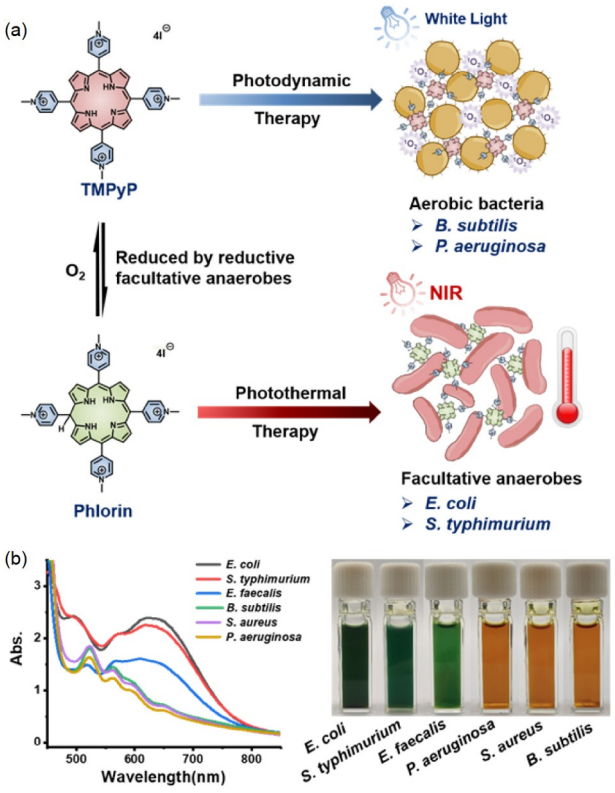


**Figure 29** Adaptable PDT and PTT for antimicrobial. (a) Schematic presentation of bacteria-responsive porphyrin TMPyP for adaptable PDT and PTT therapy. (b) UV-vis absorption spectra of TMPyP and images incubated with *E. coli*, *S. typhimurium*, *E. faecalis*, *P. aeruginosa*, *S. aureus*, and *B. subtilis* [144] (color online).

Specifically, upon incubation with *E. coli*, the mixture containing TMPyP and *E. coli* could convert light energy into heat successfully under NIR irradiation at 730 nm, leading to excellent antimicrobial activity (>99%) by PTT. In aerobic environment, TMPyP showed outstanding bacterial inhibition efficiency through white light PDT. The bacteria-responsive porphyrin for adaptable PDT and PTT may find further applications in the selective regulation of bacterial balance and non-invasive treatment of bacterial infections.

## 11 Summary and outlook

The last decade has witnessed great advances in the development of supramolecular systems for various bioapplications. In this review, we summarized the important contributions made by Chinese researchers in recent years. Clearly, the bioapplications are diverse and well feature the dynamic, reversible, and stimuli-responsive characteristics of supramolecular systems, which are usually not accessible by small molecule entities. Most of the investigations have involved the use of host-guest chemistry, which may directly enhance the activity of clinically applied drugs by improving their stability, solubility, biocompatibility or transmembrane efficiency or inhibiting their side effect or toxicity, or hold different molecular or polymeric species together to required supramolecular architectures to achieve enhanced or integrated functions for improving specific factors of drugs. In another important aspect, hydrophobically driven aggregation or self-assembly of rationally designed amphiphiles has provided an important approach to achieving enhanced activity of many drugs. In a few studies, host-guest chemistry has been applied for the design of new small molecules, partners or supramolecular drugs to reach new or better therapies. The advances clearly demonstrate the potential of supramolecular systems for preclinical studies in the future.

Currently, there are two important clinic successes of supramolecular principle. The first is the application of captisol [44], a β-cyclodextrin derivative, as an excipient or a formulating agent to increase the solubility of poorly soluble agents. The second is sugammadex [45], a γ-cyclodextrin derivative, for rapidly reversing the neuromuscular blocking activity of rocuronium and vecuronium. Both agents make use of their high affinity for the related drugs. In China, adamgammadex [473], a sugammadex analogue, has completed phase III clinical trials and is expected to receive clinical approval in the near future. There have been many supramolecular or host-guest systems that are reported to exhibit new promising biofunctions. For their preclinical development and possible clinical translation, several challenges or key questions have to be addressed or emphasized in the future. First, they must overperform or strongly complement the traditional treatments and thus display improved competitiveness. Second, for new therapies that are not clinically available, like photothermal therapy, they have to show a great market outlook to attract the support of the industry. Thus, a clear and competitive clinical scenario has to be portrayed to convince both doctors and the industry that beneficial treatment can be realized. Third, supramolecular systems are composed of two or more molecular or polymeric components. Methodologies and standards have to be developed for the assessment of their absorption, distribution, metabolism, and excretion. Fourth, a systematic assessment of biocompatibility must be performed for promising systems, which is not available for nearly all reported systems. For this aim, interdisciplinary cooperative studies should be more efficient than those performed mainly by a team in chemistry. Fifth, synthetic methodologies may need to be developed to guarantee scalable preparation of molecular and polymeric components. Finally, but not least, the dynamic and reversible features of supramolecular systems may cause uncertainty for their controlled and repeated preparations. In spite of these challenges, new breakthroughs may be expected in the coming years, not only for the development of more competitive supramolecular systems but also for the stride for preclinical and even clinical transformation.

**Conflict of interest** The authors declare no conflict of interest.


1 Pedersen CJ. *J Am Chem Soc*, 1967, 89: 7017–7036
2 Cram DJ, Cram JM. *Acc Chem Res*, 1978, 11: 8–14
3 Dong S, Zheng B, Wang F, Huang F. *Acc Chem Res*, 2014, 47: 1982–1994
4 Qu DH, Wang QC, Zhang QW, Ma X, Tian H. *Chem Rev*, 2015, 115: 7543–7588
5 Wang Y, Ping G, Li C. *Chem Commun*, 2016, 52: 9858–9872
6 Escobar L, Ballester P. *Chem Rev*, 2021, 121: 2445–2514
7 Ma YL, Sun C, Li Z, Wang Z, Wei J, Cheng Q, Zheng LS, Chang XY, Li K, Wang R, Jiang W. *CCS Chem*, 2021, 4: 1977–1989
8 Duan H, Cao F, Zhang M, Gao M, Cao L. *Chin Chem Lett*, 2022, 33: 2459–2463
9 Jia D, Zhong H, Jiang S, Yao R, Wang F. *Chin Chem Lett*, 2022, 33: 4900–4903
10 Velmurugan K, Murtaza A, Saeed A, Li J, Wang K, Zuo M, Liu Q, Hu XY. *CCS Chem*, 2022, 4: 3426–3439
11 Cheng J, Gao B, Tang H, Sun Z, Xu L, Wang L, Cao D. *Sci China Chem*, 2022, 65: 539–545
12 Liu P, Fang F, Wang H, Khashab NM. *Angew Chem Int Ed*, 2023, 62: e202218706
13 Xie M, Tong S, Wang MX. *CCS Chem*, 2022, 5: 117–123
14 Wu JR, Wu G, Yang YW. *Acc Chem Res*, 2022, 55: 3191–3204
15 Cram DJ. *Angew Chem Int Ed*, 1988, 27: 1009–1020
16 Zhu H, Chen L, Sun B, Wang M, Li H, Stoddart JF, Huang F. *Nat Rev Chem*, 2023, 7: 768–782
17 Cao L, Šekutor M, Zavalij PY, Mlinarić-Majerski K, Glaser R, Isaacs L. *Angew Chem Int Ed*, 2014, 53: 988–993
18 Shetty D, Khedkar JK, Park KM, Kim K. *Chem Soc Rev*, 2015, 44: 8747–8761
19 Liu W, Samanta SK, Smith BD, Isaacs L. *Chem Soc Rev*, 2017, 46: 2391–2403
20 Park KM, Murray J, Kim K. *Acc Chem Res*, 2017, 50: 644–646
21 Chen Z, He Q, Deng X, Peng J, Du K, Sun Y. *Chem Commun*, 2023, 59: 1907–1916
22 Ji X, Wang H, Wang H, Zhao T, Page ZA, Khashab NM, Sessler JL. *Angew Chem Int Ed*, 2020, 59: 23402–23412
23 Yeung MCL, Yam VWW. *Chem Soc Rev*, 2015, 44: 4192–4202
24 Shi Q, Wang L. *Chin J Org Chem*, 2022, 42: 1256–1257
25 Wu Q, Lei Q, Zhong HC, Ren TB, Sun Y, Zhang XB, Yuan L. *Chem Commun*, 2023, 59: 3024–3039
26 Si Y, Zhao Y, Dai W, Cui S, Sun P, Shi J, Tong B, Cai Z, Dong Y. *Chin J Chem*, 2023, 41: 1575–1582
27 Wu X, Gao L, Hu XY, Wang L. *Chem Record*, 2016, 16: 1216–1227
28 Deng CL, Murkli SL, Isaacs LD. *Chem Soc Rev*, 2020, 49: 7516–7532
29 Beatty MA, Hof F. *Chem Soc Rev*, 2021, 50: 4812–4832
30 Yin H, Bardelang D, Wang R. *Trends Chem*, 2021, 3: 1–4
31 Yu SB, Zhou W, Tian J, Ma D, Zhang DW, Li ZT. *Sci Sin Chim*, 2023, 53: 2345–2356
32 Yu G, Chen X. *Theranostics*, 2019, 9: 3041–3074
33 Yu SB, Lin F, Tian J, Yu J, Zhang DW, Li ZT. *Chem Soc Rev*, 2022, 51: 434–449
34 Li W, Xu W, Zhang S, Li J, Zhou J, Tian D, Cheng J, Li H. *J Agric Food Chem*, 2022, 70: 12746–12759
35 Maity D. *Biophys Chem*, 2023, 297: 107022
36 Inam M, Sareh Sadat MF, Chen W. *Chem Res Chin Univ*, 2023, 39: 857–861
37 Yan M, Wu S, Wang Y, Liang M, Wang M, Hu W, Yu G, Mao Z, Huang F, Zhou J. *Adv Mater*, 2023, 36: 2304249
38 Zhou J, Rao L, Yu G, Cook TR, Chen X, Huang F. *Chem Soc Rev*, 2021, 50: 2839–2891
39 Yin H, Wang R. *Israel J Chem*, 2018, 58: 188–198
40 Ma X, Zhao Y. *Chem Rev*, 2015, 115: 7794–7839
41 Geng WC, Sessler JL, Guo DS. *Chem Soc Rev*, 2020, 49: 2303–2315
42 Tian J, Lin F, Yu SB, Yu J, Tang Q, Li ZT. *Aggregate*, 2022, 3: e187
43 Liu Z, Nalluri SKM, Stoddart JF. *Chem Soc Rev*, 2017, 46: 2459–2478
44 Stella VJ, Rajewski RA. *Int J Pharm*, 2020, 583: 119396
45 Nguyen-Lee J, Moreland N, Sadoughi A, Borna R, Salehi A, Jahr JS. *Curr Anesthesiol Rep*, 2018, 8: 168–177
46 Yu H, Lin H, Xie Y, Qu M, Jiang M, Shi J, Hong H, Xu H, Li L, Liao G, Wu Z, Zhou Z. *Chin Chem Lett*, 2022, 33: 4882–4885
47 Fang G, Yang X, Chen S, Wang Q, Zhang A, Tang B. *Coord Chem Rev*, 2022, 454: 214352
48 Wang MX. *Acc Chem Res*, 2012, 45: 182–195
49 Guo DS, Liu Y. *Chem Soc Rev*, 2012, 41: 5907–5921
50 Li Y, Liu Y. *Acta Chim Sin*, 2023, 81: 928–936
51 Murray J, Kim K, Ogoshi T, Yao W, Gibb BC. *Chem Soc Rev*, 2017, 46: 2479–2496
52 Liu YH, Zhang YM, Yu HJ, Liu Y. *Angew Chem Int Ed*, 2021, 60: 3870–3880
53 Chen K, Hua ZY, Zhao JL, Redshaw C, Tao Z. *Inorg Chem Front*, 2022, 9: 2753–2809
54 Wang Z, Sun C, Yang K, Chen X, Wang R. *Angew Chem Int Ed*, 2022, 61: e202206763
55 Peng WC, Wang H, Zhang DW, Li ZT. *Chin J Org Chem*, 2022, 42: 863–870
56 Yang K, Pei Y, Wen J, Pei Z. *Chem Commun*, 2016, 52: 9316–9326
57 Li MH, Lou XY, Yang YW. *Chem Commun*, 2021, 57: 13429–13447
58 Tang R, Ye Y, Zhu S, Wang Y, Lu B, Yao Y. *Chin Chem Lett*, 2023, 34: 107734
59 Ma D, Zhang B, Hoffmann U, Sundrup MG, Eikermann M, Isaacs L. *Angew Chem Int Ed*, 2012, 51: 11358–11362
60 Schrader T, Bitan G, Klärner FG. *Chem Commun*, 2016, 52: 11318–11334
61 Liu HK, Lin F, Yu SB, Wu Y, Lu S, Liu YY, Qi QY, Cao J, Zhou W, Li X, Wang H, Zhang DW, Li ZT, Ma D. *J Med Chem*, 2022, 65: 16893–16901
62 Le MH, Taghuo K. ES, Schrader T. *Chem Commun*, 2022, 58: 2954–2966
63 Sun JD, Liu Y, Zhao Z, Yu SB, Qi QY, Zhou W, Wang H, Hu K, Zhang DW, Li ZT. *RSC Med Chem*, 2023, 14: 563–572
64 King D, Deng CL, Isaacs L. *Tetrahedron*, 2023, 145: 133607
65 Zhao Y, Chen L, Chen J, Li J, Meng Q, Sue ACH, Li C. *Chem Commun*, 2023, 59: 5858–5861
66 Chang Y, Jiao Y, Symons HE, Xu JF, Faul CFJ, Zhang X. *Chem Soc Rev*, 2019, 48: 989–1003
67 Wang J, Ding X, Guo X. *Adv Colloid Interface Sci*, 2019, 269: 187–202
68 Li ZT, Yu SB, Liu Y, Tian J, Zhang DW. *Acc Chem Res*, 2022, 55: 2316–2325
69 Si W, Xin P, Li ZT, Hou JL. *Acc Chem Res*, 2015, 48: 1612–1619
70 Park KM, Hur MY, Ghosh SK, Boraste DR, Kim S, Kim K. *Chem Commun*, 2019, 55: 10654–10664
71 Li D, Lu F, Wang J, Hu W, Cao XM, Ma X, Tian H. *J Am Chem Soc*, 2018, 140: 1916–1923
72 Zhang ZY, Xu WW, Xu WS, Niu J, Sun XH, Liu Y. *Angew Chem Int Ed*, 2020, 59: 18748–18754
73 Guo S, Dai W, Chen X, Lei Y, Shi J, Tong B, Cai Z, Dong Y. *ACS Mater Lett*, 2021, 3: 379–397
74 Hu YY, Dai XY, Dong X, Huo M, Liu Y. *Angew Chem Int Ed*, 2022, 61: e202213097
75 Zhou WL, Lin W, Chen Y, Liu Y. *Chem Sci*, 2022, 13: 7976–7989
76 Dou L, Liu Y, Hong Z, Li G, Yang Y. *Chem Rev*, 2015, 115: 12633–12665
77 Zheng Z, Li D, Liu Z, Peng HQ, Sung HHY, Kwok RTK, Williams ID, Lam JWY, Qian J, Tang BZ. *Adv Mater*, 2019, 31: 1904799
78 Shen FF, Chen Y, Xu X, Yu HJ, Wang H, Liu Y. *Small*, 2021, 17: 2101185
79 Zhang T, Ma X, Tian H. *Chem Sci*, 2020, 11: 482–487
80 Li Y, Dong Y, Cheng L, Qin C, Nian H, Zhang H, Yu Y, Cao L. *J Am*

*Chem Soc*, 2019, 141: 8412–8415
81 Fan C, Wei L, Niu T, Rao M, Cheng G, Chruma JJ, Wu W, Yang C. *J Am Chem Soc*, 2019, 141: 15070–15077
82 Liu Z, Liu Y. *Chem Soc Rev*, 2022, 51: 4786–4827
83 Wang C, Ma XK, Guo P, Jiang C, Liu YH, Liu G, Xu X, Liu Y. *Adv Sci*, 2022, 9: 2103041
84 Ma X, Wang J, Tian H. *Acc Chem Res*, 2019, 52: 738–748
85 Zhang T, Ma X, Wu H, Zhu L, Zhao Y, Tian H. *Angew Chem Int Ed*, 2020, 59: 11206–11216
86 Xu DA, Zhou QY, Dai X, Ma XK, Zhang YM, Xu X, Liu Y. *Chin Chem Lett*, 2022, 33: 851–854
87 Ma XK, Zhang W, Liu Z, Zhang H, Zhang B, Liu Y. *Adv Mater*, 2021, 33: 2007476
88 Zhou WL, Chen Y, Yu Q, Zhang H, Liu ZX, Dai XY, Li JJ, Liu Y. *Nat Commun*, 2020, 11: 4655
89 Chen Y, Zhang YM, Liu Y. *Israel J Chem*, 2011, 51: 515–524
90 Zhao J, Zhang YM, Sun HL, Chang XY, Liu Y. *Chem Eur J*, 2014, 20: 15108–15115
91 Zhao W, He Z, Tang BZ. *Nat Rev Mater*, 2020, 5: 869–885
92 Huo M, Dai XY, Liu Y. *Small*, 2022, 18: 2104514
93 Dai XY, Huo M, Dong X, Hu YY, Liu Y. *Adv Mater*, 2022, 34: 2203534
94 Shen FF, Liu Z, Yu HJ, Wang H, Xu X, Liu Y. *Adv Opt Mater*, 2022, 10: 2200245
95 Huo M, Dai XY, Liu Y. *Angew Chem Int Ed*, 2021, 60: 27171–27177
96 Huo M, Dai XY, Liu Y. *Adv Sci*, 2022, 9: 2201523
97 Li P, Chen Y, Liu Y. *Chin Chem Lett*, 2019, 30: 1190–1197
98 Liu G, Xu X, Dai X, Jiang C, Zhou Y, Lu L, Liu Y. *Mater Horiz*, 2021, 8: 2494–2502
99 Zhang R, Chen Y, Chen L, Zhang Y, Liu Y. *Adv Opt Mater*, 2023, 11: 2300101
100 Wang HJ, Xing WW, Zhang HY, Xu WW, Liu Y. *Adv Opt Mater*, 2022, 10: 2201178
101 Dai XY, Hu YY, Sun Y, Huo M, Dong X, Liu Y. *Adv Sci*, 2022, 9: 2200524
102 Chen XM, Chen Y, Yu Q, Gu BH, Liu Y. *Angew Chem Int Ed*, 2018, 57: 12519–12523
103 Xu Z, Jia S, Wang W, Yuan Z, Jan Ravoo B, Guo DS. *Nat Chem*, 2018, 11: 86–93
104 Wang H, Xu XX, Pan YC, Yan YX, Hu XY, Chen RW, Ravoo BJ, Guo DS, Zhang T. *Adv Mater*, 2021, 33: 2006483
105 Pan YC, Tian JH, Guo DS. *Acc Chem Res*, 2023, 56: 3626–3639
106 Tian JH, Hu XY, Hu ZY, Tian HW, Li JJ, Pan YC, Li HB, Guo DS. *Nat Commun*, 2022, 13: 4293
107 Hu XY, Hu ZY, Tian JH, Shi L, Ding F, Li HB, Guo DS. *Chem Commun*, 2022, 58: 13198–13201
108 Pan YC, Wang H, Xu X, Tian HW, Zhao H, Hu XY, Zhao Y, Liu Y, Ding G, Meng Q, Ravoo BJ, Zhang T, Guo DS. *CCS Chem*, 2021, 3: 2485–2497
109 Pan YC, Yue YX, Hu XY, Li HB, Guo DS. *Adv Mater*, 2021, 33: 2104310
110 Zhang Z, Yue YX, Xu L, Wang Y, Geng WC, Li JJ, Kong XL, Zhao X, Zheng Y, Zhao Y, Shi L, Guo DS, Liu Y. *Adv Mater*, 2021, 33: 2007719
111 Zhang TX, Zhang ZZ, Yue YX, Hu XY, Huang F, Shi L, Liu Y, Guo DS. *Adv Mater*, 2020, 32: 1908435
112 Yue YX, Zhang Z, Wang ZH, Ma R, Chen MM, Ding F, Li HB, Li JJ, Shi L, Liu Y, Guo DS. *Small Struct*, 2022, 3: 2200067
113 Geng WC, Jia S, Zheng Z, Li Z, Ding D, Guo DS. *Angew Chem Int Ed*, 2019, 58: 2377–2381
114 Li S, Ma R, Hu XY, Li HB, Geng WC, Kong X, Zhang C, Guo DS. *Adv Mater*, 2022, 34: 2203765
115 Liu S, Zavalij PY, Isaacs L. *J Am Chem Soc*, 2005, 127: 16798–16799
116 Cheng XJ, Liang LL, Chen K, Ji NN, Xiao X, Zhang JX, Zhang YQ, Xue SF, Zhu QJ, Ni XL, Tao Z. *Angew Chem Int Ed*, 2013, 52: 7252–7255
117 Barrow SJ, Kasera S, Rowland MJ, del Barrio J, Scherman OA. *Chem Rev*, 2015, 115: 12320–12406
118 Li Q, Qiu SC, Zhang J, Chen K, Huang Y, Xiao X, Zhang Y, Li F, Zhang YQ, Xue SF, Zhu QJ, Tao Z, Lindoy LF, Wei G. *Org Lett*, 2016, 18: 4020–4023
119 Kim J, Jung IS, Kim SY, Lee E, Kang JK, Sakamoto S, Yamaguchi K, Kim K. *J Am Chem Soc*, 2000, 122: 540–541
120 Yin H, Cheng Q, Bardelang D, Wang R. *JACS Au*, 2023, 3: 2356–2377
121 Sun XR, Yang HP, Zhang W, Zhang S, Hu JH, Liu M, Zeng X, Li Q, Redshaw C, Tao Z, Xiao X. *ACS Appl Mater Interfaces*, 2023, 15: 4668–4676
122 Guo J, Shi L, Liu M. *New J Chem*, 2021, 45: 18221–18228
123 Guo J, Han X, Wang S, Liu M, Liu L, Wang P. *Anal Methods*, 2022, 14: 2642–2648
124 Wang Y, Ding L, Yu H, Liang F. *Chin Chem Lett*, 2022, 33: 283–287
125 Zhang S, Tian Y, Liu M, Hong-Meng T, Li CR, Zeng X, Xiao X, Redshaw C. *Mater Chem Front*, 2022, 6: 973–980
126 Liu M, Cen R, Lu JH, Meng TH, Li CR, Redshaw C, Prior TJ, Tao Z, Xiao X. *Mater Chem Front*, 2022, 6: 2859–2868
127 Liu C, Xia Y, Tao Z, Ni XL. *Chin Chem Lett*, 2022, 33: 1529–1532
128 Kim S, Yun G, Khan S, Kim J, Murray J, Lee YM, Kim WJ, Lee G, Kim S, Shetty D, Kang JH, Kim JY, Park KM, Kim K. *Mater Horiz*, 2017, 4: 450–455
129 Sun C, Zhang H, Yue L, Li S, Cheng Q, Wang R. *ACS Appl Mater Interfaces*, 2019, 11: 22925–22931
130 Sun C, Yue L, Cheng Q, Wang Z, Wang R. *ACS Mater Lett*, 2020, 2: 266–271
131 Sun C, Wang Z, Yue L, Huang Q, Lu S, Wang R. *J Mater Chem B*, 2020, 8: 8878–8883
132 Hou D, Xu Y, Yan J, Zeng Q, Wang Z, Chen Y. *ACS Nano*, 2023, 17: 3055–3063
133 Sha L, Bo B, Yang F, Li J, Cao Y, Zhao J. *Anal Chem*, 2022, 94: 8748–8755
134 Liu S, Zhang H, Wang Y, Zeng Y, Chatterjee S, Liang F. *Chin Chem Lett*, 2023, 34: 107712
135 Zhang X, Du Y, Feng R, Ren X, Wu T, Jia Y, Zhang N, Li F, Wei Q, Ju H. *Biosens Bioelectron*, 2023, 227: 115170
136 Yin H, Chen L, Yang B, Bardelang D, Wang C, Lee SMY, Wang R. *Org Biomol Chem*, 2017, 15: 4336–4343
137 Yin H, Dumur F, Niu Y, Ayhan MM, Grauby O, Liu W, Wang C, Siri D, Rosas R, Tonetto A, Gigmes D, Wang R, Bardelang D, Ouari O. *ACS Appl Mater Interfaces*, 2017, 9: 33220–33228
138 Ren S, Geng WC, Cui X, Wu B, Zheng Z. *ChemistrySelect*, 2023, 8: e202203646
139 Xu P, Zhou S, Druzhinin SI, Schönherr H, Song B. *Dyes Pig*, 2023, 217: 111366
140 Chen J, Huang Q, Wang Q, Ding Y, Lu S, Wang LH, Li S, Wang R. *ACS Appl Nano Mater*, 2022, 5: 5993–6000
141 Zhao X, Zhou X, Xing WW, Liu Y. *Chem Commun*, 2023, 59: 11516–11519
142 Sun C, Zhang H, Li S, Zhang X, Cheng Q, Ding Y, Wang LH, Wang R. *ACS Appl Mater Interfaces*, 2018, 10: 25090–25098
143 Sun C, Wang Z, Yue L, Huang Q, Cheng Q, Wang R. *J Am Chem Soc*, 2020, 142: 16523–16527
144 Hu H, Wang H, Yang Y, Xu JF, Zhang X. *Angew Chem Int Ed*, 2022, 61: e202200799
145 Chen J, Li S, Wang Z, Pan Y, Wei J, Lu S, Zhang QW, Wang LH, Wang R. *Chem Sci*, 2021, 12: 7727–7734
146 Ding YF, Wei J, Quan X, Gu W, Xi L, Zheng Y, Zhao Y, Luo J, Li S, Mok GSP, Wang R. *Carbohydrate Polyms*, 2022, 296: 119968
147 Ding YF, Huang Q, Quan X, Cheng Q, Li S, Zhao Y, Mok GSP, Wang R. *Acta Biomater*, 2022, 149: 248–257
148 Huang X, Chen T, Mu N, Lam HW, Sun C, Yue L, Cheng Q, Gao C, Yuan Z, Wang R. *Acta Biomater*, 2021, 131: 483–492
149 Yang H, Duan Z, Liu F, Zhao Z, Liu S. *ACS Macro Lett*, 2023, 12: 295–301

150 Yue L, Sun C, Cheng Q, Ding Y, Wei J, Wang R. *Chem Commun*, 2019, 55: 13506–13509
151 Yue L, Sun C, Kwong CHT, Wang R. *J Mater Chem B*, 2020, 8: 2749–2753
152 Xie B, Zhao H, Shui M, Ding Y-, Sun C, Wang Z, Gao C, Chen G, Wang R. *Small*, 2022, 18: 2201971
153 He K, Ding YF, Zhao Z, Liu B, Nie W, Luo X, Yu HZ, Liu J, Wang R. *Adv Funct Mater*, 2024, 34: 2309949
154 Gao C, Huang Q, Liu C, Kwong CHT, Yue L, Wan JB, Lee SMY, Wang R. *Nat Commun*, 2020, 11: 2622
155 Cheng Q, Yang Z, Quan X, Ding Y, Li J, Wang Z, Zhao Y, Chen X, Wang R. *Theranostics*, 2023, 13: 611–620
156 Gao C, Cheng Q, Li J, Chen J, Wang Q, Wei J, Huang Q, Lee SMY, Gu D, Wang R. *Adv Funct Mater*, 2021, 31: 2102440
157 Ding YF, Wang Z, Kwong CHT, Zhao Y, Mok GSP, Yu HZ, Wang R. *J Control Release*, 2023, 360: 82–92
158 Xie B, Zhao H, Zhang R, Ding Y, Gao C, He Y, Wang R. *J Control Release*, 2023, 357: 371–378
159 Wu H, Xia T, Qi F, Mei S, Xia Y, Xu JF, Zhang X. *CCS Chem*, 2022, 5: 823–829
160 Wang H, Wu H, Yi Y, Xue KF, Xu JF, Wang H, Zhao Y, Zhang X. *CCS Chem*, 2021, 3: 1413–1425
161 Wu H, Wang H, Qi F, Xia T, Xia Y, Xu JF, Zhang X. *ACS Appl Mater Interfaces*, 2021, 13: 33962–33968
162 Huang F, Liu J, Liu Y. *Chem Sci*, 2022, 13: 8885–8894
163 Cao W, Qin X, Wang Y, Dai Z, Dai X, Wang H, Xuan W, Zhang Y, Liu Y, Liu T. *Angew Chem Int Ed*, 2021, 60: 11196–11200
164 Xiao L, Wang LL, Wu CQ, Li H, Zhang QL, Wang Y, Xu L. *Nat Commun*, 2022, 13: 5936
165 Yang L, Tan X, Wang Z, Zhang X. *Chem Rev*, 2015, 115: 7196–7239
166 Wu W, Xu Y, Wang S, Pang Q, Liu S. *Chem Commun*, 2023, 59: 5890–5893
167 Wang C, Liu YH, Liu Y. *Small*, 2022, 18: 2201821
168 Yu HJ, Zhou Q, Dai X, Shen FF, Zhang YM, Xu X, Liu Y. *J Am Chem Soc*, 2021, 143: 13887–13894
169 Wei KN, Yang RP, Huang SZ, Tao Z, Tang Q, Huang Y. *J Agric Food Chem*, 2023, 71: 9549–9557
170 Wu Y, Sun L, Chen X, Liu J, Ouyang J, Zhang X, Guo Y, Chen Y, Yuan W, Wang D, He T, Zeng F, Chen H, Wu S, Zhao Y. *Nat Commun*, 2023, 14: 3918
171 Wang H, Yang Y, Yuan B, Ni XL, Xu JF, Zhang X. *ACS Appl Mater Interfaces*, 2021, 13: 2269–2276
172 Wang HJ, Zheng MM, Xing WW, Li YX, Wang YY, Zhu H, Zhang YM, Yu Q, Liu Y. *Chem Sci*, 2023, 14: 8401–8407
173 Dai XY, Zhang B, Yu Q, Liu Y. *J Med Chem*, 2022, 65: 7363–7370
174 Wu X, Liu M, Niu J, Liu Q, Jiang X, Zheng Y, Qian Y, Zhang YM, Shen J, Liu Y. *Chem Sci*, 2023, 14: 1724–1731
175 Luo Y, Zhang W, Zhao J, Yang MX, Ren Q, Redshaw C, Tao Z, Xiao X. *Chin Chem Lett*, 2023, 34: 107780
176 Liu F, Chowdhury S, Rosas R, Monnier V, Charles L, Karoui H, Gigmes D, Ouari O, Chevallier F, Bucher C, Kermagoret A, Liu S, Bardelang D. *Org Lett*, 2021, 23: 5283–5287
177 Zhang PQ, Li Q, Wang ZK, Tang QX, Liu PP, Li WH, Yang GY, Yang B, Ma D, Li ZT. *Chin Chem Lett*, 2023, 34: 107632
178 Zhang W, Luo Y, Jia MH, Ni XL, Tao Z, Xiao CD, Xiao X. *Sens Actuat B-Chem*, 2022, 366: 132006
179 Zhang W, Luo Y, Zhao J, Lin WH, Ni XL, Tao Z, Xiao X, Xiao CD. *Sens Actuat B-Chem*, 2022, 354: 131189
180 Zhang W, Yang L, Luo Y, Xiao H, Yang H, Ni X, Tao Z, Xiao X. *Sens Actuat B-Chem*, 2023, 379: 133255
181 Wu D, Zhang Z, Li X, Han J, Hu Q, Yu Y, Mao Z. *J Control Release*, 2023, 354: 626–634
182 Ogoshi T, Kanai S, Fujinami S, Yamagishi T, Nakamoto Y. *J Am Chem Soc*, 2008, 130: 5022–5023
183 Tao HQ, Cao DR, Liu LZ, Kou YH, Wang LY, Meier H. *Sci China Chem*, 2012, 55: 223–228
184 Xue M, Yang Y, Chi X, Zhang Z, Huang F. *Acc Chem Res*, 2012, 45: 1294–1308
185 Yu HM, Yu XY, Chen Y. *Chin Chem Lett*, 2023, 34: 108037
186 Tang ZD, Sun XM, Huang TT, Liu J, Shi B, Yao H, Zhang YM, Wei TB, Lin Q. *Chin Chem Lett*, 2023, 34: 107698
187 Li Z, Shen Z, Pei Y, Chao S, Pei Z. *Chem Commun*, 2023, 59: 989–1005
188 Lu B, Xia J, Huang Y, Yao Y. *Chem Commun*, 2023, 59: 12091–12099
189 Yang Q, Xu W, Cheng M, Zhang S, Kovaleva EG, Liang F, Tian D, Liu J, Abdelhameed RM, Cheng J, Li H. *Chem Commun*, 2022, 58: 3255–3269
190 Chang Y, Yang K, Wei P, Huang S, Pei Y, Zhao W, Pei Z. *Angew Chem Int Ed*, 2014, 53: 13126–13130
191 Gao L, Zheng B, Chen W, Schalley CA. *Chem Commun*, 2015, 51: 14901–14904
192 Liu X, Jia K, Wang Y, Shao W, Yao C, Peng L, Zhang D, Hu XY, Wang L. *ACS Appl Mater Interfaces*, 2017, 9: 4843–4850
193 Zhou J, Chen M, Diao G. *Chem Commun*, 2014, 50: 11954–11956
194 Hu XY, Jia K, Cao Y, Li Y, Qin S, Zhou F, Lin C, Zhang D, Wang L. *Chem Eur J*, 2015, 21: 1208–1220
195 Hu XY, Liu X, Zhang W, Qin S, Yao C, Li Y, Cao D, Peng L, Wang L. *Chem Mater*, 2016, 28: 3778–3788
196 He J, Chen J, Lin S, Niu D, Hao J, Jia X, Li N, Gu J, Li Y, Shi J. *Biomacromolecules*, 2018, 19: 2923–2930
197 Yin Y, Sun P, Dong H, Chen Y, Chen S, Wang L. *Chin Chem Lett*, 2023, 34: 108594
198 Li B, Meng Z, Li Q, Huang X, Kang Z, Dong H, Chen J, Sun J, Dong Y, Li J, Jia X, Sessler JL, Meng Q, Li C. *Chem Sci*, 2017, 8: 4458–4464
199 Hao Q, Chen Y, Huang Z, Xu JF, Sun Z, Zhang X. *ACS Appl Mater Interfaces*, 2018, 10: 5365–5372
200 Yang J, Dai D, Ma L, Yang YW. *Chin Chem Lett*, 2021, 32: 729–734
201 Chen J, Zhang Y, Zhang Y, Zhao L, Chen L, Chai Y, Meng Z, Jia X, Meng Q, Li C. *Chin Chem Lett*, 2021, 32: 3034–3038
202 Tian X, Zuo M, Niu P, Velmurugan K, Wang K, Zhao Y, Wang L, Hu XY. *ACS Appl Mater Interfaces*, 2021, 13: 37466–37474
203 Shao W, Liu X, Sun G, Hu XY, Zhu JJ, Wang L. *Chem Commun*, 2018, 54: 9462–9465
204 Hu XY, Gao L, Mosel S, Ehlers M, Zellermann E, Jiang H, Knauer SK, Wang L, Schmuck C. *Small*, 2018, 14: 1803952
205 Cao Y, Zou X, Xiong S, Li Y, Shen Y, Hu X, Wang L. *Chin J Chem*, 2015, 33: 329–334
206 Wang Y, Du J, Wang Y, Jin Q, Ji J. *Chem Commun*, 2015, 51: 2999–3002
207 Cao Y, Li Y, Hu XY, Zou X, Xiong S, Lin C, Wang L. *Chem Mater*, 2015, 27: 1110–1119
208 Ding Y, Wang C, Ma Y, Zhu L, Lu B, Wang Y, Wang J, Chen T, Dong CM, Yao Y. *Acta Biomater*, 2022, 143: 381–391
209 Liu X, Shao W, Zheng Y, Yao C, Peng L, Zhang D, Hu XY, Wang L. *Chem Commun*, 2017, 53: 8596–8599
210 Sun G, He Z, Hao M, Xu Z, Hu XY, Zhu JJ, Wang L. *Chem Commun*, 2019, 55: 10892–10895
211 Tian X, Li S, Velmurugan K, Bai Z, Liu Q, Wang K, Zuo M, Hu XY. *Mater Chem Front*, 2023, 7: 2484–2492
212 Bai Y, Li X, Li M, Shang Q, Yang J, Fan L, Tian W. *J Mater Chem B*, 2022, 10: 4952–4958
213 Bai Y, Liu C, Yang J, Liu C, Shang Q, Tian W. *Colloids Surfs B-Biointerfaces*, 2022, 217: 112606
214 Chao S, Lv X, Ma N, Shen Z, Zhang F, Pei Y, Pei Z. *Chem Commun*, 2020, 56: 8861–8864
215 Chen J, Zhang Y, Meng Z, Guo L, Yuan X, Zhang Y, Chai Y, Sessler JL, Meng Q, Li C. *Chem Sci*, 2020, 11: 6275–6282
216 Sun G, Zuo M, Xu Z, Wang K, Wang L, Hu XY. *ACS Appl Bio Mater*, 2022, 5: 3320–3328
217 Yu G, Wu D, Li Y, Zhang Z, Shao L, Zhou J, Hu Q, Tang G, Huang F. *Chem Sci*, 2016, 7: 3017–3024
218 Yu G, Ma Y, Han C, Yao Y, Tang G, Mao Z, Gao C, Huang F. *J Am*

*Chem Soc*, 2013, 135: 10310–10313
219 Chao S, Shen Z, Pei Y, Lv Y, Chen X, Ren J, Yang K, Pei Z. *Chem Commun*, 2021, 57: 7625–7628
220 Li J, Lv X, Li J, Jin W, Chen Z, Wen Y, Pei Z, Pei Y. *Org Chem Front*, 2023, 10: 1927–1935
221 Peng H, Xie B, Yang X, Dai J, Wei G, He Y. *Chem Commun*, 2020, 56: 8115–8118
222 Peng H, Xie B, Cen X, Dai J, Dai Y, Yang X, He Y. *Mater Chem Front*, 2022, 6: 360–367
223 Chao S, Huang P, Shen Z, Pei Y, Lv Y, Lu Y, Pei Z. *Org Chem Front*, 2023, 10: 3491–3497
224 Yu G, Yu W, Shao L, Zhang Z, Chi X, Mao Z, Gao C, Huang F. *Adv Funct Mater*, 2016, 26: 8999–9008
225 Lan S, Liu Y, Shi K, Ma D. *ACS Appl Bio Mater*, 2020, 3: 2325–2333
226 Mei Y, Zhang QW, Gu Q, Liu Z, He X, Tian Y. *J Am Chem Soc*, 2022, 144: 2351–2359
227 Tang M, Liu YH, Xu XM, Zhang YM, Liu Y. *BioOrg Medicinal Chem*, 2022, 57: 116649
228 Yu G, Zhou J, Shen J, Tang G, Huang F. *Chem Sci*, 2016, 7: 4073–4078
229 Wang J, Wang D, Cen M, Jing D, Bei J, Huang Y, Zhang J, Lu B, Wang Y, Yao Y. *J Nanobiotechnol*, 2022, 20: 33
230 Chang Y, Hou C, Ren J, Xin X, Pei Y, Lu Y, Cao S, Pei Z. *Chem Commun*, 2016, 52: 9578–9581
231 Yang K, Chang Y, Wen J, Lu Y, Pei Y, Cao S, Wang F, Pei Z. *Chem Mater*, 2016, 28: 1990–1993
232 Lu Y, Hou C, Ren J, Yang K, Chang Y, Pei Y, Dong H, Pei Z. *Int J Nanomed*, 2019, Volume 14: 3525–3532
233 Wang Y, Jin M, Chen Z, Hu X, Pu L, Pei Z, Pei Y. *Chem Commun*, 2020, 56: 10642–10645
234 Liu X, Liu J, Meng C, Zhu P, Liu X, Qian J, Ling S, Zhang Y, Ling Y. *ACS Appl Mater Interfaces*, 2021, 13: 53574–53585
235 Yang X, Wu B, Zhou J, Lu H, Zhang H, Huang F, Wang H. *Nano Lett*, 2022, 22: 7588–7596
236 Yang X, Xiao H, He J, Yang L, Tao Z, Xiao X, Li Q, Yang H. *Sens Actuat B-Chem*, 2023, 392: 134065
237 Fan JW, Xu SH, Han Y, Yan CG, Wang Q. *Dyes Pig*, 2023, 220: 111776
238 Zhou J, Hua B, Shao L, Feng H, Yu G. *Chem Commun*, 2016, 52: 5749–5752
239 Liu D, Du J, Qi S, Li M, Wang J, Liu M, Du X, Wang X, Ren B, Wu D, Shen J. *Mater Chem Front*, 2021, 5: 1418–1427
240 Chen T, Wang J, Tang R, Huang Y, Zhao Q, Yao Y. *Chin Chem Lett*, 2023, 34: 108088
241 Huang X, Du X. *ACS Appl Mater Interfaces*, 2014, 6: 20430–20436
242 Tan LL, Song N, Zhang SXA, Li H, Wang B, Yang YW. *J Mater Chem B*, 2016, 4: 135–140
243 Wang X, Tan LL, Li X, Song N, Li Z, Hu JN, Cheng YM, Wang Y, Yang YW. *Chem Commun*, 2016, 52: 13775–13778
244 Li QL, Sun Y, Ren L, Wang X, Wang C, Li L, Yang YW, Yu X, Yu J. *ACS Appl Mater Interfaces*, 2018, 10: 29314–29324
245 Li J, Hu B, Chen Z, Li J, Jin W, Wang Y, Wan Y, Lv Y, Pei Y, Liu H, Pei Z. *Chem Sci*, 2024, 15: 765–777
246 Li H, Wei R, Yan GH, Sun J, Li C, Wang H, Shi L, Capobianco JA, Sun L. *ACS Appl Mater Interfaces*, 2018, 10: 4910–4920
247 Chen H, Fan J, Hu X, Ma J, Wang S, Li J, Yu Y, Jia X, Li C. *Chem Sci*, 2015, 6: 197–202
248 Li B, Wang B, Huang X, Dai L, Cui L, Li J, Jia X, Li C. *Angew Chem Int Ed*, 2019, 58: 3885–3889
249 Xu K, Zhang Z-, Yu C, Wang B, Dong M, Zeng X, Gou R, Cui L, Li C. *Angew Chem Int Ed*, 2020, 59: 7214–7218
250 Xu K, Li B, Yao S, Li Z, Lu Y, Dong M, Qiu J, Luo L, Li C. *Angew Chem Int Ed*, 2022, 61: e202203016
251 Li S, Zhang ZY, Lv JF, Li L, Li J, Li C. *J Mater Chem A*, 2023, 11: 4957–4962
252 Zhang ZY, Li C. *Acc Chem Res*, 2022, 55: 916–929
253 Du X, Ma M, Zhang Y, Yu X, Chen L, Zhang H, Meng Z, Jia X, Chen J, Meng Q, Li C. *Angew Chem Int Ed*, 2023, 62: e202301857
254 Chen J, Chen L, Zhang Y, Zhao L, Dong M, Meng Z, Meng Q, Li C. *Chem Commun*, 2022, 58: 3370–3373
255 Chen J, Meng Q, Zhang Y, Dong M, Zhao L, Zhang Y, Chen L, Chai Y, Meng Z, Wang C, Jia X, Li C. *Angew Chem Int Ed*, 2021, 60: 11288–11293
256 Zhao L, Chen J, Tian L, Zhang Y, Chen L, Du X, Ma M, Li J, Meng Q, Li C. *Adv Healthcare Mater*, 2022, 11: 2200270
257 Hu XB, Chen Z, Chen L, Zhang L, Hou JL, Li ZT. *Chem Commun*, 2012, 48: 10999
258 Lee JW, Shin MH, Mobley W, Urbach AR, Kim HI. *J Am Chem Soc*, 2015, 137: 15322–15329
259 Chen L, Meng Z, Tian L, Zhang Y, Zhao L, Du X, Ma M, Zhang H, Chen J, Meng Q. *Org Biomol Chem*, 2022, 20: 2222–2226
260 Huang GB, Wang SH, Ke H, Yang LP, Jiang W. *J Am Chem Soc*, 2016, 138: 14550–14553
261 Yang LP, Wang X, Yao H, Jiang W. *Acc Chem Res*, 2020, 53: 198–208
262 Ma YL, Quan M, Lin XL, Cheng Q, Yao H, Yang XR, Li MS, Liu WE, Bai LM, Wang R, Jiang W. *CCS Chem*, 2021, 3: 1078–1092
263 Cao W, Wang H, Quan M, Li Y, Su Y, Li Y, Jiang W, Liu T. *Chem*, 2023, 9: 2881–2901
264 Ma D, Hettiarachchi G, Nguyen D, Zhang B, Wittenberg JB, Zavalij PY, Briken V, Isaacs L. *Nat Chem*, 2012, 4: 503–510
265 Liu H, Guo YJ. *J Incl Phenom Macrocycl Chem*, 2022, 102: 723–733
266 Zhou J, Zhang R, Lv P, Zhang S, Zhang Y, Yang J, Yang B. *Int J Pharm*, 2022, 626: 122190
267 Lin J, Yang L, Liao X, Gao C, Yang B. *J Incl Phenom Macrocycl Chem*, 2019, 95: 159–168
268 Chen J, Liu Y, Mao D, Ma D. *Chem Commun*, 2017, 53: 8739–8742
269 Jiang S, Lan S, Mao D, Yang X, Shi K, Ma D. *Chem Commun*, 2018, 54: 9486–9489
270 Mao W, Liao Y, Ma D. *Chem Commun*, 2020, 56: 4192–4195
271 Zhao Z, Yang J, Liu Y, Wang S, Zhou W, Li ZT, Zhang DW, Ma D. *J Mater Chem B*, 2023, 11: 9027–9034
272 Wu Y, Yang J, Zhuang SY, Yu SB, Zong Y, Liu YY, Wu G, Qi QY, Wang H, Tian J, Zhou W, Ma D, Zhang DW, Li ZT. *J Med Chem*, 2024
273 Mao W, Mao D, Yang F, Ma D. *Chem Eur J*, 2019, 25: 2272–2280
274 Jiang S, Mao W, Mao D, Li ZT, Ma D. *Chin Chem Lett*, 2022, 33: 881–884
275 Lu X, Samanta SK, Zavalij PY, Isaacs L. *Angew Chem Int Ed*, 2018, 57: 8073–8078
276 Peng WC, Lei Z, Lin QH, Wu Y, Yang JY, Wang H, Zhou W, Zhang DW, Li ZT, Ma D. *ChemPlusChem*, 2023, 88: e202300465
277 Balachandran YL, Jiang X. *CCS Chem*, 2021, 4: 420–436
278 Mei J, Leung NLC, Kwok RTK, Lam JWY, Tang BZ. *Chem Rev*, 2015, 115: 11718–11940
279 Qu R, Zhen X, Jiang X. *CCS Chem*, 2021, 4: 401–419
280 Song BL Zhang XH Qiao ZY, Wang H. *CCS Chem*, 2021, 4: 437-455
281 Feng Y, Wang N, Ju H. *Sci China Chem*, 2022, 65: 2417–2436
282 Ding W, Cheng B, Wang M, Dou Q, Li S, Zhang P, Luo Q. *Chin J Org Chem*, 2022, 42: 363–383
283 Chen S, Xu J, Li Y, Peng B, Luo L, Feng H, Chen Z, Wang Z. *Chin J Org Chem*, 2022, 42: 1651–1666
284 Gui Y, Chen K, Sun Y, Tan Y, Luo W, Zhu D, Xiong Y, Yan D, Wang D, Tang BZ. *Chin J Chem*, 2023, 41: 1249–1259
285 Duan H, Li Y, Li Q, Wang P, Liu X, Cheng L, Yu Y, Cao L. *Angew Chem Int Ed*, 2020, 59: 10101–10110
286 Cheng L, Liu K, Duan Y, Duan H, Li Y, Gao M, Cao L. *CCS Chem*, 2021, 3: 2749–2763
287 Cheng L, Tian P, Li Q, Li A, Cao L. *CCS Chem*, 2022, 4: 2914–2920
288 Duan Y, Wang J, Cheng L, Duan H, Tian P, Zhang Y, Cao L. *Org Biomol Chem*, 2022, 20: 3998–4005
289 Dong Y, Cheng L, Duan Y, Xu H, Dong R, Guo B, Cao L. *Synlett*, 2023, 35: 109–112

290 Cheng L, Tian P, Duan H, Li Q, Song X, Li A, Cao L. *Chem Sci*, 2023, 14: 833–842
291 Shen J, Ren C, Zeng H. *Acc Chem Res*, 2022, 55: 1148–1159
292 Luo Y, Zhu C, Zhang T, Yan T, Liu J. *Chem Res Chin Univ*, 2023, 39: 3–12
293 Min J, Zhang C, Qi S, Wang L, Dong Z. *Chem Res Chin Univ*, 2022, 38: 803–808
294 Qi S, Tian J, Zhang J, Zhang L, Zhang C, Lin Z, Min J, Mao S, Dong Z. *CCS Chem*, 2021, 4: 1850–1857
295 Yan T, Zheng X, Liu S, Zou Y, Liu J. *Sci China Chem*, 2022, 65: 1265–1278
296 Li YW, Fu YH, Hou JL. *Chin J Chem*, 2022, 40: 1293–1297
297 Yuan L, Jiang P, Hu J, Zeng H, Huo Y, Li Z, Zeng H. *Chin Chem Lett*, 2022, 33: 2026–2030
298 Ma H, Ye R, Jin L, Zhou S, Ren C, Ren H, Shen J, Zeng H. *Chin Chem Lett*, 2023, 34: 108355
299 Zhang M, Zhu PP, Xin P, Si W, Li ZT, Hou JL. *Angew Chem Int Ed*, 2017, 56: 2999–3003
300 Xin P, Zhao L, Mao L, Xu L, Hou S, Kong H, Fang H, Zhu H, Jiang T, Chen CP. *Chem Commun*, 2020, 56: 13796–13799
301 Haoyang WW, Xiao Q, Ye Z, Fu Y, Zhang DW, Li J, Xiao L, Li ZT, Hou JL. *Chem Commun*, 2021, 57: 1097–1100
302 Shen J, Gu Y, Ke L, Zhang Q, Cao Y, Lin Y, Wu Z, Wu C, Mu Y, Wu YL, Ren C, Zeng H. *Nat Commun*, 2022, 13: 5985
303 Shen FF, Dai SY, Wong NK, Deng S, Wong AST, Yang D. *J Am Chem Soc*, 2020, 142: 10769–10779
304 Zhong Q, Cao Y, Xie X, Wu Y, Chen Z, Zhang Q, Jia C, Wu Z, Xin P, Yan X, Zeng Z, Ren C. *Angew Chem Int Ed*, 2024, 63: e202314666
305 Yan ZJ, Wang D, Ye Z, Fan T, Wu G, Deng L, Yang L, Li B, Liu J, Ma T, Dong C, Li ZT, Xiao L, Wang Y, Wang W, Hou JL. *J Am Chem Soc*, 2020, 142: 15638–15643
306 Xiao Q, Fan T, Wang Y, Li ZT, Hou JL, Wang Y. *CCS Chem*, 2023, 5: 1745–1752
307 Cao S, Pei Z, Xu Y, Pei Y. *Chem Mater*, 2016, 28: 4501–4506
308 Hou C, Ma N, Shen Z, Chi G, Chao S, Pei Y, Chen L, Lu Y, Pei Z. *IJN*, 2020, Volume 15: 10417–10424
309 Feng W, Lv Y, Chen Z, Wang F, Wang Y, Pei Y, Jin W, Shi C, Wang Y, Qu Y, Ji W, Pu L, Liu XW, Pei Z. *Chem Eng J*, 2021, 417: 129178
310 Feng W, Zhang S, Wan Y, Chen Z, Qu Y, Li J, James TD, Pei Z, Pei Y. *ACS Appl Mater Interfaces*, 2022, 14: 20749–20761
311 Ma K, Shi J, Pei Y, Pei Z. *J Colloid Interface Sci*, 2022, 609: 353–363
312 Jin W, Chen Z, Yang S, Qu Y, Pei Y, Pei Z. *Chem Commun*, 2022, 58: 12584–12587
313 Liu F, Liu L, Liu D, Wei P, Feng W, Yi T. *Chem Sci*, 2022, 13: 10815–10823
314 Li J, Wang Y, Pei Z, Pei Y. *Chem Commun*, 2022, 58: 3338–3341
315 Xu Y, Qian L, Fang M, Liu Y, Xu ZJ, Ge X, Zhang Z, Liu ZP, Lou H. *Eur J Med Chem*, 2023, 259: 115693
316 Huo M, Wang H, Li L, Tong Y, Hu C, Gu Y, Liu J, Yin T. *J Control Release*, 2021, 336: 89–104
317 Tong KC, Wan PK, Lok CN, Che CM. *Chem Sci*, 2021, 12: 15229–15238
318 Li Y, Yuan X, Yu J, Fan Y, He T, Lu S, Li X, Qiu H, Yin S. *ACS Appl Bio Mater*, 2020, 3: 8061–8068
319 Xu Y, Liang N, Liu J, Gong X, Yan P, Sun S. *Carbohydrate Polyms*, 2022, 290: 119509
320 Xia X, Yang X, Huang P, Yan D. *ACS Appl Mater Interfaces*, 2020, 12: 18301–18308
321 Chen L, Deng J, Yu A, Hu Y, Jin B, Du P, Zhou J, Lei L, Wang Y, Vakal S, Li X. *Bioactive Mater*, 2022, 10: 420–429
322 Gong Z, Zhou B, Liu X, Cao J, Hong Z, Wang J, Sun X, Yuan X, Tan H, Ji H, Bai J. *ACS Appl Mater Interfaces*, 2021, 13: 55913–55927
323 Hong Z, Sun X, Sun X, Cao J, Yang Z, Pan Z, Yu T, Dong J, Zhou B, Bai J. *Mater Sci Eng-C*, 2021, 129: 112389
324 Zhan J, Wang Y, Ma S, Qin Q, Wang L, Cai Y, Yang Z. *Bioactive Mater*, 2022, 9: 120–133
325 Lv N, Ma T, Qin H, Yang ZR, Wu Y, Li D, Tao J, Jiang H, Zhu J. *Sci China Mater*, 2022, 65: 2861–2870
326 Dong Y, Chen Y, Zhu D, Shi K, Ma C, Zhang W, Rocchi P, Jiang L, Liu X. *J Control Release*, 2020, 322: 416–425
327 Wu Y, Zhong D, Li Y, Wu H, Zhang H, Mao H, Yang J, Luo K, Gong Q, Gu Z. *Nanoscale*, 2021, 13: 4887–4898
328 Qi R, Zhang N, Zhang P, Zhao H, Liu J, Cui J, Xiang J, Han Y, Wang S, Wang Y. *ACS Appl Mater Interfaces*, 2020, 12: 17220–17229
329 Huang R, Yu QH, Yao XD, Liu WL, Cheng YJ, Ma YH, Zhang AQ, Qin SY. *ACS Appl Mater Interfaces*, 2022, 14: 159–171
330 Peng F, Chen Y, Liu J, Xing Z, Fan J, Zhang W, Qiu F. *J Colloid Interface Sci*, 2021, 591: 314–325
331 Xu L, Deng H, Wu L, Wang D, Shi L, Qian Q, Huang X, Zhu L, Gao X, Yang J, Su Y, Feng J, Zhu X. *ACS Nano*, 2023, 17: 10090–10103
332 Fu Y, He G, Liu Z, Wang J, Li M, Zhang Z, Bao Q, Wen J, Zhu X, Zhang C, Zhang W. *Small*, 2022, 18: 2202337
333 Xiao F, Lin L, Chao Z, Shao C, Chen Z, Wei Z, Lu J, Huang Y, Li L, Liu Q, Liang Y, Tian L. *Angew Chem Int Ed*, 2020, 59: 9702–9710
334 Li Y, Liu Y, Ren Y, Su L, Li A, An Y, Rotello V, Zhang Z, Wang Y, Liu Y, Liu S, Liu J, Laman JD, Shi L, van der Mei HC, Busscher HJ. *Adv Funct Mater*, 2020, 30: 2004942
335 Diercks CS, Kalmutzki MJ, Diercks NJ, Yaghi OM. *ACS Cent Sci*, 2018, 4: 1457–1464
336 Wang Q, Sun J, Wei D. *Chin J Chem*, 2022, 40: 1359–1385
337 Waller PJ, Gándara F, Yaghi OM. *Acc Chem Res*, 2015, 48: 3053–3063
338 Hao Q, Tao Y, Ding X, Yang Y, Feng J, Wang RL, Chen XM, Chen GL, Li X, OuYang H, Hu XL, Tian J, Han BH, Zhu G, Wang W, Zhang F, Tan B, Li ZT, Wang D, Wan LJ. *Sci China Chem*, 2023, 66: 620–682
339 Wang L, Wang D. *Chem Res Chin Univ*, 2022, 38: 265–274
340 Guo L, Zhang J, Huang Q, Zhou W, Jin S. *Chin Chem Lett*, 2022, 33: 2856–2866
341 Lin G, Mal A, Wang X, Zhou X, Gui B, Wang C. *Sci China Chem*, 2023, 66: 2977–2985
342 Xu Y, Ren G, Zhang D, Sun L, Zhao Y. *Chin J Chem*, 2023, 41: 3447–3472
343 Lin RB, He Y, Li P, Wang H, Zhou W, Chen B. *Chem Soc Rev*, 2019, 48: 1362–1389
344 Gao X, Lu W, Wang Y, Song X, Wang C, Kirlikovali KO, Li P. *Sci China Chem*, 2022, 65: 2077–2095
345 Xia N, Zhao J, Gong G, Dong H, Li H, Wang J, Wang L, Chen S. *Sci China Chem*, 2023, 66: 3169–3177
346 Zhang KD, Tian J, Hanifi D, Zhang Y, Sue ACH, Zhou TY, Zhang L, Zhao X, Liu Y, Li ZT. *J Am Chem Soc*, 2013, 135: 17913–17918
347 Li Y, Yan C, Li Q, Cao L. *Sci China Chem*, 2022, 65: 1279–1285
348 Yin ZJ, Jiang SY, Liu N, Qi QY, Wu ZQ, Zhan TG, Zhao X. *CCS Chem*, 2021, 4: 141–150
349 Tian J, Zhou TY, Zhang SC, Aloni S, Altoe MV, Xie SH, Wang H, Zhang DW, Zhao X, Liu Y, Li ZT. *Nat Commun*, 2014, 5: 5574
350 Yang B, Zhang JW, Yu SB, Wang ZK, Zhang PQ, Yang XD, Qi QY, Yang GY, Ma D, Li ZT. *Sci China Chem*, 2021, 64: 1228–1234
351 Tian J, Xu ZY, Zhang DW, Wang H, Xie SH, Xu DW, Ren YH, Wang H, Liu Y, Li ZT. *Nat Commun*, 2016, 7: 11580
352 Wu YP, Yang B, Tian J, Yu SB, Wang H, Zhang DW, Liu Y, Li ZT. *Chem Commun*, 2017, 53: 13367–13370
353 Tian J, Yao C, Yang WL, Zhang L, Zhang DW, Wang H, Zhang F, Liu Y, Li ZT. *Chin Chem Lett*, 2017, 28: 798–806
354 Yao C, Tian J, Wang H, Zhang DW, Liu Y, Zhang F, Li ZT. *Chin Chem Lett*, 2017, 28: 893–899
355 Yan M, Liu XB, Gao ZZ, Wu YP, Hou JL, Wang H, Zhang DW, Liu Y, Li ZT. *Org Chem Front*, 2019, 6: 1698–1704
356 Yang B, Zhang XD, Li J, Tian J, Wu YP, Yu FX, Wang R, Wang H, Zhang DW, Liu Y, Zhou L, Li ZT. *CCS Chem*, 2019, 1: 156–165
357 Gao ZZ, Wang ZK, Wei L, Yin G, Tian J, Liu CZ, Wang H, Zhang

DW, Zhang YB, Li X, Liu Y, Li ZT. *ACS Appl Mater Interfaces*, 2020, 12: 1404–1411
358 Xu ZY, Mao W, Zhao Z, Wang ZK, Liu YY, Wu Y, Wang H, Zhang DW, Li ZT, Ma D. *J Mater Chem B*, 2022, 10: 899–908
359 Lin F, Yu SB, Liu YY, Liu CZ, Lu S, Cao J, Qi QY, Zhou W, Li X, Liu Y, Tian J, Li ZT. *Adv Mater*, 2022, 34: e2200549
360 Liu YY, Wang ZK, Yu SB, Liu Y, Wang H, Zhou W, Li ZT, Zhang DW. *J Mater Chem B*, 2022, 10: 4163–4171
361 Sorrenti A, Leira-Iglesias J, Markvoort AJ, de Greef TFA, Hermans TM. *Chem Soc Rev*, 2017, 46: 5476–5490
362 Wang ZK, Xu ZY, Li JJ, Yu SB, Wang H, Guo DS, Zhang DW, Li ZT. *Chin J Org Chem*, 2022, 42: 2235
363 Zhang YC, Zeng PY, Ma ZQ, Xu ZY, Wang ZK, Guo B, Yang F, Li ZT. *Drug Deliver*, 2022, 29: 128–137
364 Cranmer LD. *Onco Targets Ther*, 2019, 12: 2047–2062
365 Liu Y, Liu CZ, Wang ZK, Zhou W, Wang H, Zhang YC, Zhang DW, Ma D, Li ZT. *Biomaterials*, 2022, 284: 121467
366 Li Y, Li Q, Miao X, Qin C, Chu D, Cao L. *Angew Chem Int Ed*, 2021, 60: 6744–6751
367 Lin JL, Wang ZK, Xu ZY, Wei L, Zhang YC, Wang H, Zhang DW, Zhou W, Zhang YB, Liu Y, Li ZT. *J Am Chem Soc*, 2020, 142: 3577–3582
368 Wang ZK, Lin JL, Zhang YC, Yang CW, Zhao YK, Leng ZW, Wang H, Zhang DW, Zhu J, Li ZT. *Mater Chem Front*, 2021, 5: 869–875
369 Xu ZY, Liu HK, Wu Y, Zhang YC, Zhou W, Wang H, Zhang DW, Ma D, Li ZT. *ACS Appl Bio Mater*, 2021, 4: 4591–4597
370 Zong Y, Xu YY, Wu Y, Liu Y, Li Q, Lin F, Yu SB, Wang H, Zhou W, Sun XW, Zhang DW, Li ZT. *J Mater Chem B*, 2022, 10: 3268–3276
371 Sun JD, Li Q, Haoyang WW, Zhang DW, Wang H, Zhou W, Ma D, Hou JL, Li ZT. *Mol Pharm*, 2022, 19: 953–962
372 Wu Y, Liu YY, Liu HK, Yu SB, Lin F, Zhou W, Wang H, Zhang DW, Li ZT, Ma D. *Chem Sci*, 2022, 13: 9243–9248
373 Otvagin VF, Kuzmina NS, Kudriashova ES, Nyuchev AV, Gavryushin AE, Fedorov AY. *J Med Chem*, 2022, 65: 1695–1734
374 Overchuk M, Weersink RA, Wilson BC, Zheng G. *ACS Nano*, 2023, 17: 7979–8003
375 Ran B, Wang Z, Cai W, Ran L, Xia W, Liu W, Peng X. *J Am Chem Soc*, 2021, 143: 17891–17909
376 Allison RR, Sibata CH. *Photodiagnosis Photodynamic Ther*, 2010, 7: 61–75
377 Zhu H, Li Q, Khalil-Cruz LE, Khashab NM, Yu G, Huang F. *Sci China Chem*, 2021, 64: 688–700
378 Tu L, Li C, Xiong X, Hyeon Kim J, Li Q, Mei L, Li J, Liu S, Seung Kim J, Sun Y. *Angew Chem Int Ed*, 2023, 62: e202301560
379 Meng LB, Zhang W, Li D, Li Y, Hu XY, Wang L, Li G. *Chem Commun*, 2015, 51: 14381–14384
380 Zheng BD, Ye J, Zhang XQ, Zhang N, Xiao MT. *Coord Chem Rev*, 2021, 447: 214155
381 Tang B, Xu W, Xu JF, Zhang X. *Angew Chem Int Ed*, 2021, 60: 9384–9388
382 Cai B, Song H, Brnovic A, Pavliuk MV, Hammarström L, Tian H. *J Am Chem Soc*, 2023, 145: 18687–18692
383 Gu Y, Lai H, Chen ZY, Zhu Y, Sun Z, Lai X, Wang H, Wei Z, Chen L, Huang L, Zhang Y, He F, Tian L. *Angew Chem Int Ed*, 2023, 62: e202303476
384 Jin J, Zhu Y, Zhang Z, Zhang W. *Angew Chem Int Ed*, 2018, 57: 16354–16358
385 Xing R, Zou Q, Yuan C, Zhao L, Chang R, Yan X. *Adv Mater*, 2019, 31: 1900822
386 Pang E, Zhao S, Wang B, Niu G, Song X, Lan M. *Coord Chem Rev*, 2022, 472: 214780
387 Zhang Z, Ma L, Fang F, Hou Y, Lu C, Mu C, Zhang Y, Liu H, Gao K, Wang M, Zhang Z, Li X, Zhang M. *JACS Au*, 2022, 2: 1479–1487
388 Li YX, Liu Y, Wang H, Li ZT, Zhang DW. *ACS Appl Bio Mater*, 2022, 5: 881–888
389 Liu K, Liu Y, Yao Y, Yuan H, Wang S, Wang Z, Zhang X. *Angew Chem Int Ed*, 2013, 52: 8285–8289
390 Liu Y, Huang Z, Liu K, Kelgtermans H, Dehaen W, Wang Z, Zhang X. *Polym Chem*, 2014, 5: 53–56
391 Li WJ, Hu Z, Xu L, Wang XQ, Wang W, Yin GQ, Zhang DY, Sun Z, Li X, Sun H, Yang HB. *J Am Chem Soc*, 2020, 142: 16748–16756
392 Zheng X, Lei SN, Gao Z, Dong X, Xiao H, Liu W, Tung CH, Wu LZ, Wang P, Cong H. *Chem Sci*, 2023, 14: 3523–3530
393 Kang YF, Chen WK, Teng KX, Wang LY, Xu XC, Niu LY, Cui G, Yang QZ. *CCS Chem*, 2022, 4: 3516–3528
394 Zhao J, Gao Y, Huang R, Chi C, Sun Y, Xu G, Xia XH, Gou S. *J Am Chem Soc*, 2023, 145: 11633–11642
395 Liu X, Zhan W, Gao G, Jiang Q, Zhang X, Zhang H, Sun X, Han W, Wu FG, Liang G. *J Am Chem Soc*, 2023, 145: 7918–7930
396 Zhang D, Peng LY, Teng KX, Niu LY, Cui G, Yang QZ. *ACS Mater Lett*, 2023, 5: 180–188
397 Kenry , Liu B. *Acc Mater Res*, 2022, 3: 721–734
398 Dai J, Wu X, Ding S, Lou X, Xia F, Wang S, Hong Y. *J Med Chem*, 2020, 63: 1996–2012
399 Zhang Z, Kang M, Tan H, Song N, Li M, Xiao P, Yan D, Zhang L, Wang D, Tang BZ. *Chem Soc Rev*, 2022, 51: 1983–2030
400 Zhu W, Li Y, Guo S, Guo WJ, Peng T, Li H, Liu B, Peng HQ, Tang BZ. *Nat Commun*, 2022, 13: 7046
401 Zhao H, Xu J, Feng C, Ren J, Bao L, Zhao Y, Tao W, Zhao Y, Yang X. *Adv Mater*, 2022, 34: 2106390
402 Wei K, Wu Y, Zheng X, Ma G, Ji C, Yin M. *Adv Funct Mater*, 2023, 33: 2305187
403 Ji C, Gao Q, Dong X, Yin W, Gu Z, Gan Z, Zhao Y, Yin M. *Angew Chem Int Ed*, 2018, 57: 11384–11388
404 Liu BK, Zheng J, Wang H, Niu LY, Yang QZ. *Mater Chem Front*, 2023, 7: 5879–5890
405 Zhou XQ, Wang P, Ramu V, Zhang L, Jiang S, Li X, Abyar S, Papadopoulou P, Shao Y, Bretin L, Siegler MA, Buda F, Kros A, Fan J, Peng X, Sun W, Bonnet S. *Nat Chem*, 2023, 15: 980–987
406 Zhang D, Teng KX, Zhao L, Niu LY, Yang QZ. *Adv Mater*, 2023, 35: 2209789
407 Teng KX, Niu LY, Kang YF, Yang QZ. *Chem Sci*, 2020, 11: 9703–9711
408 Tam LKB, Chu JCH, He L, Yang C, Han KC, Cheung PCK, Ng DKP, Lo PC. *J Am Chem Soc*, 2023, 145: 7361–7375
409 Zhang D, Xiong MC, Niu LY, Yang QZ. *Chem Commun*, 2022, 58: 10060–10063
410 Wang S, Zhao Z, Yao J, Jiang S, Li ZT, Ma D. *Chin Chem Lett*, 2023, 34: 107805
411 Gao J, Li J, Geng WC, Chen FY, Duan X, Zheng Z, Ding D, Guo DS. *J Am Chem Soc*, 2018, 140: 4945–4953
412 Hu XY, Gao J, Chen FY, Guo DS. *J Control Release*, 2020, 324: 124–133
413 Huang Q, Hu ZY, Guo S, Guo DS, Wang R. *Supramol Mater*, 2022, 1: 100020
414 Wu JJ, Chen FY, Han BB, Zhang HQ, Zhao L, Zhang ZR, Li JJ, Zhang BD, Zhang YN, Yue YX, Hu HG, Li WH, Zhang B, Chen YX, Guo DS, Li YM. *CCS Chem*, 2023, 5: 885–901
415 Feng HT, Li Y, Duan X, Wang X, Qi C, Lam JWY, Ding D, Tang BZ. *J Am Chem Soc*, 2020, 142: 15966–15974
416 Shao L, Pan Y, Hua B, Xu S, Yu G, Wang M, Liu B, Huang F. *Angew Chem Int Ed*, 2020, 59: 11779–11783
417 Yuan B, Wu H, Wang H, Tang B, Xu JF, Zhang X. *Angew Chem Int Ed*, 2021, 60: 706–710
418 Huang B, Wang P, Ouyang Y, Pang R, Liu S, Hong C, Ma S, Gao Y, Tian J, Zhang W. *ACS Appl Mater Interfaces*, 2020, 12: 41038–41046
419 Min X, Yi F, Han XL, Li M, Gao Q, Liang X, Chen Z, Sun Y, Liu Y. *Chem Eng J*, 2022, 432: 134327
420 Tian J, Li B, Zhang F, Yao Z, Song W, Tang Y, Ping Y, Liu B. *Angew Chem Int Ed*, 2023, 62: e202307288
421 Gao J, Yang H, Lu Y, Shi Q, Xu S, Wu W, Hu F, Liu B. *Chem Mater*, 2023, 35: 1229–1237

422 Chen W, Zhang Y, Yi HB, Wang F, Chu X, Jiang JH. *Angew Chem Int Ed*, 2023, 62: e202300162
423 Li J, Zhuang Z, Zhao Z, Tang BZ. *View*, 2022, 3: 20200121
424 Li M, Xia J, Tian R, Wang J, Fan J, Du J, Long S, Song X, Foley JW, Peng X. *J Am Chem Soc*, 2018, 140: 14851–14859
425 Pham TC, Nguyen VN, Choi Y, Lee S, Yoon J. *Chem Rev*, 2021, 121: 13454–13619
426 Chen H, Wan Y, Cui X, Li S, Lee CS. *Adv Healthcare Mater*, 2021, 10: e2101607
427 Yang G, Ni JS, Li Y, Zha M, Tu Y, Li K. *Angew Chem Int Ed*, 2021, 60: 5386–5393
428 Shen Z, Zheng S, Fang Y, Zhang G, Zhu C, Liu S, Hu J. *Angew Chem Int Ed*, 2023, 62: e202219153
429 Chao S, Shen Z, Li B, Pei Y, Pei Z. *Chem Commun*, 2023, 59: 3455–3458
430 Peng J, Du K, Sun J, Yang X, Wang X, Zhang X, Song G, Feng F. *Angew Chem Int Ed*, 2023, 62: e202214991
431 Wang YY, Liu YC, Sun H, Guo DS. *Coord Chem Rev*, 2019, 395: 46–62
432 Huang H, Banerjee S, Qiu K, Zhang P, Blacque O, Malcomson T, Paterson MJ, Clarkson GJ, Staniforth M, Stavros VG, Gasser G, Chao H, Sadler PJ. *Nat Chem*, 2019, 11: 1041–1048
433 Teng KX, Chen WK, Niu LY, Fang WH, Cui G, Yang QZ. *Angew Chem Int Ed*, 2021, 60: 19912–19920
434 Chen D, Xu Q, Wang W, Shao J, Huang W, Dong X. *Small*, 2021, 17: e2006742
435 Castano AP, Demidova TN, Hamblin MR. *Photodiagnosis Photodynamic Ther*, 2004, 1: 279–293
436 Ding H, Yu H, Dong Y, Tian R, Huang G, Boothman DA, Sumer BD, Gao J. *J Control Release*, 2011, 156: 276–280
437 Teng KX, An ZP, Niu LY, Yang QZ. *ACS Mater Lett*, 2024, 6: 290–297
438 Teng KX, Niu LY, Yang QZ. *Chem Sci*, 2022, 13: 5951–5956
439 Teng KX, Niu LY, Xie N, Yang QZ. *Nat Commun*, 2022, 13: 6179
440 Chen W, Wang Z, Tian M, Hong G, Wu Y, Sui M, Chen M, An J, Song F, Peng X. *J Am Chem Soc*, 2023, 145: 8130–8140
441 Chen D, Liang C, Qu X, Zhang T, Mou X, Cai Y, Wang W, Shao J, Dong X. *Biomaterials*, 2023, 292: 121944
442 Zhao YY, Zhang L, Chen Z, Zheng BY, Ke M, Li X, Huang JD. *J Am Chem Soc*, 2021, 143: 13980–13989
443 Teng KX, Niu LY, Yang QZ. *J Am Chem Soc*, 2023, 145: 4081–4087
444 Zhao X, He S, Wang J, Ding J, Zong S, Li G, Sun W, Du J, Fan J, Peng X. *Adv Mater*, 2023, 35: 2305163
445 Gao P, Wang H, Cheng Y. *Chin Chem Lett*, 2022, 33: 575–586
446 Jung HS, Verwilst P, Sharma A, Shin J, Sessler JL, Kim JS. *Chem Soc Rev*, 2018, 47: 2280–2297
447 Xi D, Xiao M, Cao J, Zhao L, Xu N, Long S, Fan J, Shao K, Sun W, Yan X, Peng X. *Adv Mater*, 2020, 32: 1907855
448 Chu Y, Liao S, Liao H, Lu Y, Geng X, Wu D, Pei J, Wang Y. *CCS Chem*, 2022, 4: 3002–3013
449 Xia X, Wang R, Hu Y, Yao Q, Long S, Sun W, Fan J, Peng X. *Sci China Chem*, 2022, 65: 821–828
450 Cao Y, Dou JH, Zhao N, Zhang S, Zheng YQ, Zhang JP, Wang JY, Pei J, Wang Y. *Chem Mater*, 2017, 29: 718–725
451 Huang Y, Wang Z, Chen Z, Zhang Q. *Angew Chem Int Ed*, 2019, 58: 9696–9711
452 Sun C, Zhao M, Zhu X, Pei P, Zhang F. *CCS Chem*, 2022, 4: 476–486
453 Wang Y, Zhu W, Du W, Liu X, Zhang X, Dong H, Hu W. *Angew Chem Int Ed*, 2018, 57: 3963–3967
454 Wang Z, Zhen X, Upputuri PK, Jiang Y, Lau J, Pramanik M, Pu K, Xing B. *ACS Nano*, 2019, 13: 5816–5825
455 Ou C, Na W, Ge W, Huang H, Gao F, Zhong L, Zhao Y, Dong X. *Angew Chem Int Ed*, 2021, 60: 8157–8163
456 Wen X, Chen YT, He J, Wang B, Ye X, Guo Y, Ni S, Chen S, Phillips DL, Dang L, Li MD. *Sol RRL*, 2023, 7: 2300262
457 Zou Q, Abbas M, Zhao L, Li S, Shen G, Yan X. *J Am Chem Soc*, 2017, 139: 1921–1927
458 Zhao L, Liu Y, Chang R, Xing R, Yan X. *Adv Funct Mater*, 2019, 29: 1806877
459 Zhao L, Liu Y, Xing R, Yan X. *Angew Chem Int Ed*, 2020, 59: 3793–3801
460 Chang R, Zou Q, Zhao L, Liu Y, Xing R, Yan X. *Adv Mater*, 2022, 34: 2200139
461 Wang Y, Yang T, Ke H, Zhu A, Wang Y, Wang J, Shen J, Liu G, Chen C, Zhao Y, Chen H. *Adv Mater*, 2015, 27: 3874–3882
462 Guo Z, He H, Zhang Y, Rao J, Yang T, Li T, Wang L, Shi M, Wang M, Qiu S, Song X, Ke H, Chen H. *Adv Mater*, 2021, 33: 2004225
463 Jiao Y, Liu K, Wang G, Wang Y, Zhang X. *Chem Sci*, 2015, 6: 3975–3980
464 Yang Y, He P, Wang Y, Bai H, Wang S, Xu JF, Zhang X. *Angew Chem Int Ed*, 2017, 56: 16239–16242
465 Wang H, Xue KF, Yang Y, Hu H, Xu JF, Zhang X. *J Am Chem Soc*, 2022, 144: 2360–2367
466 Tang B, Li WL, Chang Y, Yuan B, Wu Y, Zhang MT, Xu JF, Li J, Zhang X. *Angew Chem Int Ed*, 2019, 58: 15526–15531
467 Hu H, Zhang YY, Ma H, Yang Y, Mei S, Li J, Xu JF, Zhang X. *Angew Chem Int Ed*, 2023, 62: e202308513
468 Yin Z, Yang Y, Yang J, Song G, Hu H, Zheng P, Xu JF. *CCS Chem*, 2022, 4: 3285–3295
469 Song Q, Li F, Wang Z, Zhang X. *Chem Sci*, 2015, 6: 3342–3346
470 Ma H, Long S, Cao J, Xu F, Zhou P, Zeng G, Zhou X, Shi C, Sun W, Du J, Han K, Fan J, Peng X. *Chem Sci*, 2021, 12: 13809–13816
471 Ma H, Lu Y, Huang Z, Long S, Cao J, Zhang Z, Zhou X, Shi C, Sun W, Du J, Fan J, Peng X. *J Am Chem Soc*, 2022, 144: 3477–3486
472 Gao Y, Chen X, Li M, Zhang L, Zhu J. *CCS Chem*, 2023, 5: 624–632
473 Zhang Y, Jiang Y, Lei Q, Li C, Jin S, Wang Q, Huang Y, Li Y, Hong Y, Wang S, Lin H, Li H, Ou Y, Zou X, Sun Q, Guo Q, Chen Z, Min S, Qi Y, Jie Q, Liu J, Liu B, Zhang W. *Br J Anaesthes*, 2024, 132: 45–52